Responses to comments from Referee #1

MANUSCRIPT: acp-2018-944

TITLE: From weak to intense downslope winds: origin, interaction with boundary-layer turbulence and impact on CO_2 variability

AUTHORS: Jon A. Arrillaga, Carlos Yagüe, Carlos Román-Cascón, Mariano Sastre, Maria Antonia Jiménez, Gregorio Maqueda and Jordi Vilà-Guerau de Arellano

---

MAIN CHANGES IN THE MANUSCRIPT:

o Title.

o Abstract and motivating aspects.

o Denomination: katabatic → downslope.

o Further information about data postprocessing in Sect. 2.2.

o New Sect. 4 in the revised manuscript: analysis of the heat and momentum budgets, profiles and the estimation of the jet-maximum height for three representative events.

o Summary and conclusions.

o Appendix A (footprint estimation) and B (assessment of the thermal profile).

o Removed figures (numbers from the old manuscript): Fig. 7, Fig. 10, Fig. 11 and Fig. 12.

o Merged figures (numbers from the old manuscript): Figs. 4 and 5, Figs. 8 and 9.

o New figures (numbers in the revised manuscript): Fig. 7, Fig. 8, Fig. 9, Fig. 10, Fig. A1 and Fig. B1.

o Slightly modified figures (numbers in the revised manuscript): Fig. 1 and Fig. 11.

o Wording and English review.

Judgement:

I think that obtained results may be useful for further understanding of the katabatic flows and manuscript is suitable for publication in the ACP, however not before a major revision. I recommend acceptance with major revisions although most of the comments are not that major and related to lack of clarity. My specific comments are listed below.

We thank Referee #1 for his/her review about the manuscript and for highlighting its suitability for publication in ACP. Responses to the specific comments are given point-by-point below, and the changes undertaken in the manuscript can be checked up both from the revised manuscript and the tracked-changes version of the manuscript provided.

Revision issues:

1. Although it is appropriate to refer readers to other papers for the details of the field campaign and instrumentations, more info is needed in this paper than is currently provided (see my remarks detailed below).

As suggested by this referee, we have included further information in the new manuscript regarding instrumentation, data post-processing and corrections. Specifications about each of the posed queries are provided below.

2. Data (post) processing. Data processing is only briefly mentioned (p. 5). More info is needed in this paper for the details of the turbulent flux measurements than is currently provided. A reader (in order to acknowledge the results) would want to know: 1) how the filtering was done (block average, high-pass, other?), 2) what data-quality control checks were used, 3) how the wind stress (or momentum flux, friction velocity) was computed in Fig. 11? Based only on the longitudinal (or downstream) $< u'w' >$ wind stress component or both longitudinal and lateral (or crosswind) $< v'w' >$ stress components? Why?

The referee is right when stating that the data processing and corrections were briefly mentioned. Following his/her query, we have included further information about the filtering, data quality control checks and correction of the turbulent fluxes, as well as minor manual checks, in the new manuscript (Page 5 Lines 22-34, and Page 6 Lines 1-6).
Regarding the calculation of the friction velocity, since the double rotation (and not the triple rotation) has been applied to the sonic coordinate system (as specified in the new manuscript), the friction velocity was calculated considering both the longitudinal- and lateral-stress components.

3. Large errors in the measurement of the turbulent fluxes can result from relatively small errors in the alignment of a sonic anemometer due to the cross contamination of velocities (i.e. fluctuations in the longitudinal wind speed components appear as vertical velocity fluctuations, and vice versa). To avoid these

errors rotation of the anemometers' axes is needed to place the measured wind components in a streamline coordinate system. The most common method is a double rotation of the anemometer coordinate system to compute the longitudinal, lateral, and vertical velocity components (Kaimal and Finnigan, 1994, section 6.6). Was this done?

We agree that rotation of the sonic-anemometer axes is needed to prevent errors in the estimation of the turbulent parameters. Indeed, the double-rotation method was applied to compute the longitudinal, lateral and vertical velocity components. It has now been specified in the new manuscript (Lines 32-34 on Page 5).

4. Since the sonic anemometer measures the so-called 'sonic' virtual temperature (which is close to the virtual temperature) the moisture correction in the sonic anemometer signal is necessary to obtain the correct value of temperature itself and sensible heat flux (e.g. Kaimal and Finnigan, 1994). Authors reported the sensible heat flux (Figure 9). To value the present results the authors should either show that the moisture corrections and their impact on the results are small, or (if otherwise) apply moisture corrections to the sonic temperature following Schotanus et al. (1983) based on the data collected by the Campbell fast-response open path infrared gas analyzer listed in Table 1.

Moisture corrections were applied to the sonic temperature following Schotanus et al. (1983) to derive the air temperature and sensible-heat flux. In fact, all the parameters based on the fast-temperature measurements shown in the figures along the manuscript have undergone this correction. It is described in the Easyflux DL software (Campbell Scientific, 2017) and now explained in the new manuscript (Line 34 on Page 5 to Line 2 on Page 6).
The effect of applying both moisture and Webb corrections (linked with next query by Referee#1) to the calculation of respectively the sensible and latent heat fluxes, is shown below in Fig. I for a selected downslope event within the analysed period.

References:

Cambell Scientific: EasyFlux DL Eddy-Covariance CR3000 Datalogger Program, `https://s.campbellsci.com/documents/us/product-brochures/b_easyflux-dl.pdf`*, 2017*

Schotanus P., Nieuwstadt F.T.M., De Bruin H.A.R. (1983) Temperature measurement with a sonic anemometer and its application to heat and moisture fluxes. Boundary-Layer Meteorol. 26(1): 81–93. DOI:`10.1007/BF00164332`
.

5. Authors say nothing about the Webb correction (also referred as WPL or Webb effect after the paper by Webb et al. [1980]). This correction must be taken into account when the turbulent fluxes of minor constituents such as carbon dioxide or, in some cases, water vapor are measured (Webb et al. 1980).

The referee is right that nothing about the WPL correction was mentioned in the manuscript,

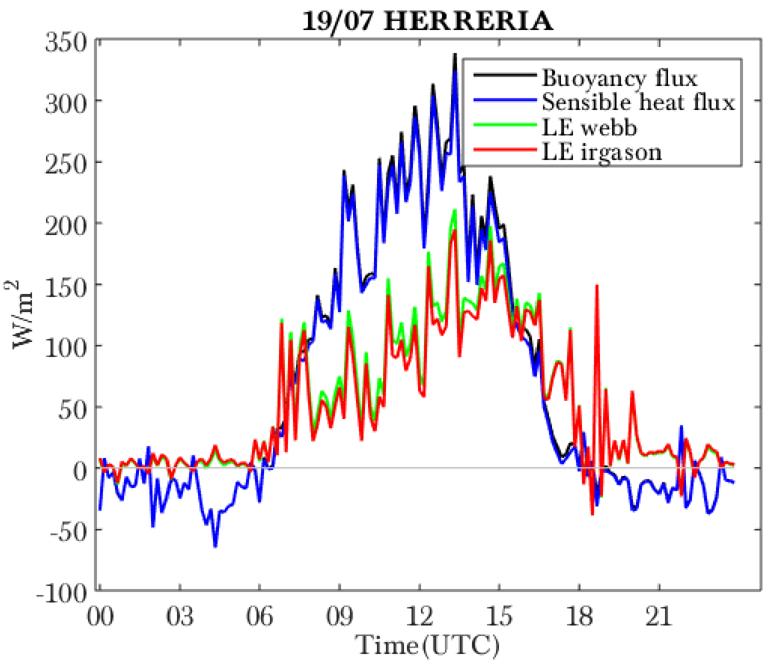

Figure I: Buoyancy flux, sensible heat flux (after moisture correction) and the latent-heat flux before and after the Webb correction on July 19 2017 in La Herrería.

although it had been considered to correct latent-heat and CO_2 turbulent fluxes. It is mentioned now in the new manuscript (Line 2 on Page 6) so that the reader will know that this correction has been applied. As an illustrative proof, Fig. II compares the CO_2 turbulent fluxes before and after applying this correction for the same downslope event from Fig. I. It can be observed how the Webb correction is considerably important during daytime.

6. In a slope-following coordinate system, the horizontal (along the slope) heat (buoyancy) flux contributes to the net buoyancy term and, therefore, the Monin-Obukhov stability parameter z/L (see page 11 and Fig. 10) contains this additional term (e.g., see Grachev et al. 2016, their Eq. (3) and references therein). Authors say nothing about this issue for calculation z/L which is very important point for katabatic flows.

We thank the referee for this interesting and important aspect, but given the issues with the horizontal heat fluxes, the challenging application of the MOST theory stressed by Referee#2, and the fact that the calculated stability parameters are not strictly needed for the conclusions drawn in this study, we have removed former Fig. 10 from the old manuscript.

Minor and editorial/technical comments:

I. Page 5, Line 8. Replace CO^2 by CO_2.

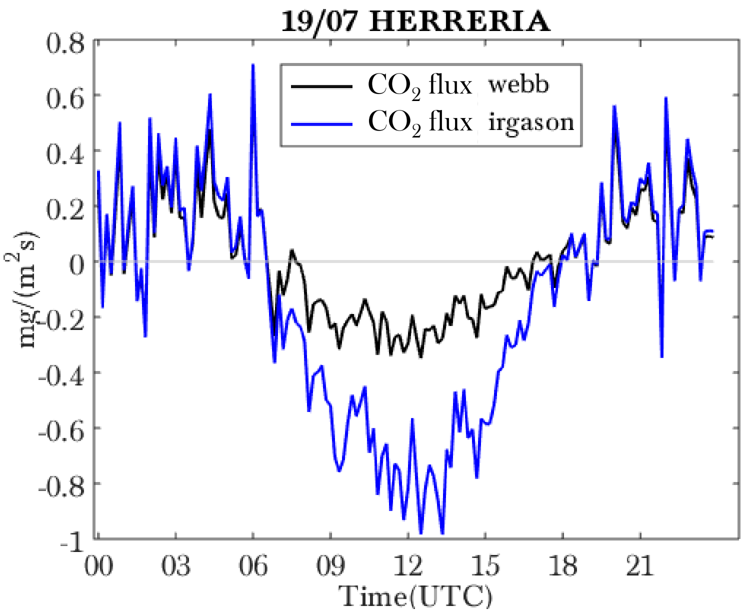

Figure II: CO_2 turbulent fluxes before and after the WPL correction on July 19 2017 in La Herrería.

Corrected, thank you.

II. Page 11, Line 28. I suggest to provide a definition of the Monin-Obukhov stability parameter (z/L) and the bulk Richardson number (R_B) for a layman reader.

We thank Referee#1 for this suggestion, but for the reasons given in the response to Query 6 above, those definitions are not necessary anymore in the new version.

III. Page 12, Lines 2-9. I would like also to see here a discussion on difficulties and controversy of interpretation associated with the critical Richardson number (e.g., Grachev et al. 2013 and references therein).

For the reasons explained in the preceding comment, that discussion is not needed anymore.

References: Replace 'Boundary Layer Meteorol.' by 'Boundary-Layer Meteorol.' (dash is missed).

Corrected, thank you.

Page 19, Line 1. Please correct Silvana's name: Di Sabatino S. instead Sabatino, S.D.

Corrected, thank you.

Page 20, Line 9. Please correct reference Pardyjak et al. as follows: Pardyjak E.R., Fernando H.J.S., Hunt J.C.R, Grachev A.A., Anderson J.A. (2009) A case study of the development of nocturnal slope flows in a wide open valley and associated air quality implications. Meteorologische Zeitschrift, 18(1), 85–100. DOI: 10.1127/0941-2948/2009/362

Accordingly corrected, thank you.

Responses to comments from Referee #2

MANUSCRIPT: acp-2018-944

TITLE: From weak to intense downslope winds: origin, interaction with boundary-layer turbulence and impact on CO_2 variability

AUTHORS: Jon A. Arrillaga, Carlos Yagüe, Carlos Román-Cascón, Mariano Sastre, Maria Antonia Jiménez, Gregorio Maqueda and Jordi Vilà-Guerau de Arellano

---

MAIN CHANGES IN THE MANUSCRIPT:

o Title.

o Abstract and motivating aspects.

o Denomination: katabatic → downslope.

o Further information about data postprocessing in Sect. 2.2.

o New Sect. 4 in the revised manuscript: analysis of the heat and momentum budgets, profiles and the estimation of the jet-maximum height for three representative events.

o Summary and conclusions.

o Appendix A (footprint estimation) and B (assessment of the thermal profile).

o Removed figures (numbers from the old manuscript): Fig. 7, Fig. 10, Fig. 11 and Fig. 12.

o Merged figures (numbers from the old manuscript): Figs. 4 and 5, Figs. 8 and 9.

o New figures (numbers in the revised manuscript): Fig. 7, Fig. 8, Fig. 9, Fig. 10, Fig. A1 and Fig. B1.

o Slightly modified figures (numbers in the revised manuscript): Fig. 1 and Fig. 11.

o Wording and English review.

General comments:

The authors study downslope flows at a site close to the Guadarrama Mountain Range by means of mean and turbulence measurements at a 10 m tower. The authors use an algorithm to identify periods with low synoptic forcing and katabatic flows, and then separate the periods into those with weak, intermediate and strong katabatic flows. Finally, they study the conditions under which each of these occurs and the associated boundary layer structure and CO2. The study shows some interesting, though not surprising results on the correlation between the strong wind episodes that lead to weakly stable stratification, and weak wind episodes that lead to very stable stratification. Still, the study has major gaps and in general lacks a thorough analysis of physical processes and associated budgets needed to substantiate the explanations which are at the moment sometimes given without a thorough proof (see specific comments below on whether this flows are katabatic at all and what their origin is given that katabatic flows cannot develop in unstable stratification, on the need to look at budgets, or for example the text connected with Figure 3). Also, there is a lack of thorough understanding of the nature of these flows (both in terms of the driving mechanisms and the interaction with turbulence) and the fact that the location of the jet maximum is a vital information that is lacking from the entire study, if indeed this flows are shown to be katabatic. If the turbulence data are collected from above the jet maximum, then it is turbulence that is not connected with the ground and therefore is not expected to show standard boundary layer characteristics (such as MOST etc). Where the jet maximum within the tower depth for each averaging period is needs to be added in the discussion of all the results and all the discussions and conclusions adjusted accordingly. For a more in depth study of the turbulence characteristics of katabatic flows Grachev et al. (2016) paper gives excellent information.

We thank Referee #2 for his/her useful suggestions and comments about the manuscript. We have considered all the major points and modified the manuscript accordingly. First, and directly associated with the concern about the nature of katabatic flows in this study, we have decided to change the way we refer to them to the generic "downslope flows" (Zardi and Whiteman, 2013)). The algorithm ensures that they are to some extent thermally-driven, but since some of them have a dynamical input, we have decided to denominate them, as a whole, downslope flows. Some of them, in any case, behave as pure katabatic flows as it is indicated in the new manuscript. Moreover, the physical processes underlying the formation and development of the downslope flows have been more deeply explored. For that, the heat and momentum budgets have been calculated and investigated for the individual cases. Additionally, a moderate downslope flow has been added to the analysis of individual representative events. For these events, the interaction with turbulence, their dynamical and thermal characteristics, as well as the location of the jet maximum have been explored. Please notice that Sects. 4.2 and 5.1 have been eliminated from the old manuscript and new sections have been added in the new manuscript (Sect. 4, Appendix A and B). The responses to the specific queries from the referee, are provided point-by-point below. The modifications undertaken in the manuscript can be checked up both from the revised manuscript and the tracked-changes version provided.

Specific major comments:

1. Turbulence data processing. As already mentioned by the first referee, the authors fail to give vital information on the turbulence data processing. Apart from the missing information on rotation methods and turbulence corrections, the authors also fail to motivate why they use a 10min averaging time, which in stable boundary layer is generally too long, and even for strong wind conditions the more appropriate averaging time would be 5 min, while for weak winds it is most likely 1 min or less. I suggest the authors calculate ogives or multi-resolution flux decomposition (e.g., Vecenaj et al, 2012) for their 40 episodes and estimate the most appropriate averaging time. If they need to have 10 min averages for comparison to the slow sensors, then the fluxes can be afterwards averaged to that value.

Referee#2 is right when pointing out that information about the corrections and data post-processing procedures was missing. This was also a query from Referee#1. As stated in the responses to Referee#1, this information has been included in the new manuscript (Lines 22-34 on Page 5 and Lines 1-6 on Page 6).
With regard to the appropriate averaging time, Multi-resolution flux decomposition (MRFD) of the friction velocity and kinematic heat flux for the three individual events have been calculated at both 4 and 8 m, to support the election of the 10-min window. They represent the distinct turbulent conditions that are found within the database of 40 events. We show MRFDs for the intense-downslope (27/07/2017), moderate-downslope (25/07/2017) and weak-downslope (13/08/2017) events only at 8 m, since the interpretation is very similar at 4 m.
The MRFD of both the friction velocity and kinematic heat flux for the intense event (Fig. I) show that the centre of the spectral gap is between 5 and 10 min. However, an averaging time of 10 min seems to be more appropriate than 5 min to capture all the turbulent scales. The MRFD of the friction velocity for the moderate event (Fig. IIa), shows the centre of the spectral gap also between 5 and 10 min. On the other hand, the spectral gap from the kinematic heat flux is unclear.
Finally for the weak downslope event, in which the uncertainty is greater, the centre of the spectral gap between 1600 and 1800 UTC is located between 5 and 10 min as for the two other events. If we choose 5 min as the averaging time we lose some scales, whereas when choosing 10 min we may include a few non-turbulent scales. After 1800 UTC turbulence is very weak and the spectral gap is hardly distinguished.
After exploring the MRFDs for the three events we can conclude that in general 10 min is the most appropriate averaging time in order to include all the turbulent scales for the distinct downslope times. Many studies have found that due to factors such as stability, mesoscale circulations and the synoptic forcing, the spectral gap can turn vague or highly variable (e.g. Hess and Clarke, 1973; Viana et al. 2010; Román-Cascón et al. 2015; Schalkwijk et al., 2015; Babic et al., 2017). In particular, when working with a large database, changing the

(a) (b)

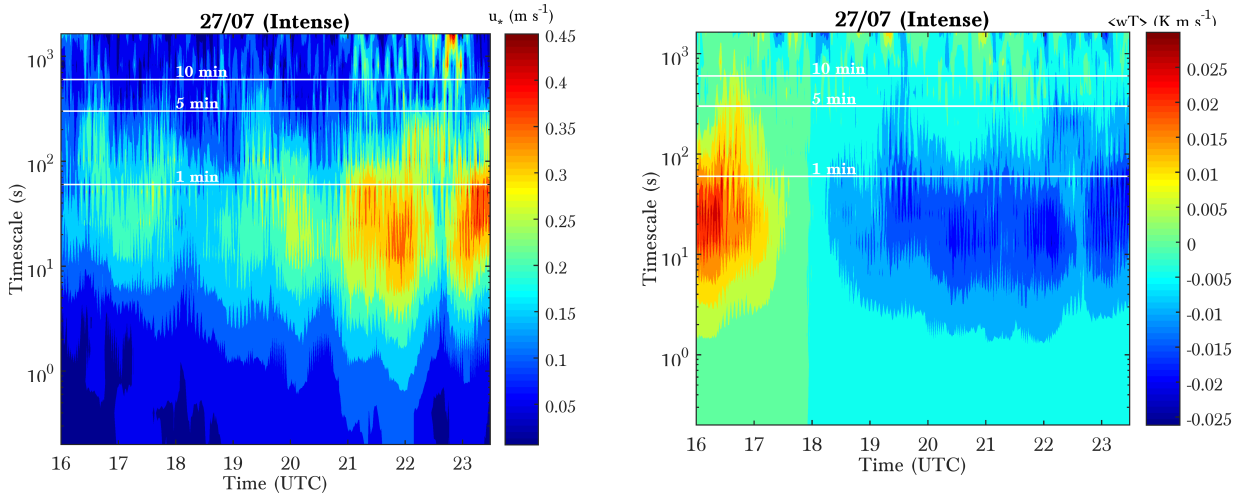

Figure I: *MRFD analysis of the friction velocity and (b) kinematic heat flux at 8 m for the intense downslope event (27/07/2017) between 1600 and 2330 UTC. Horizontal white lines indicate timescales of 1, 5 and 10 min.*

(a) (b)

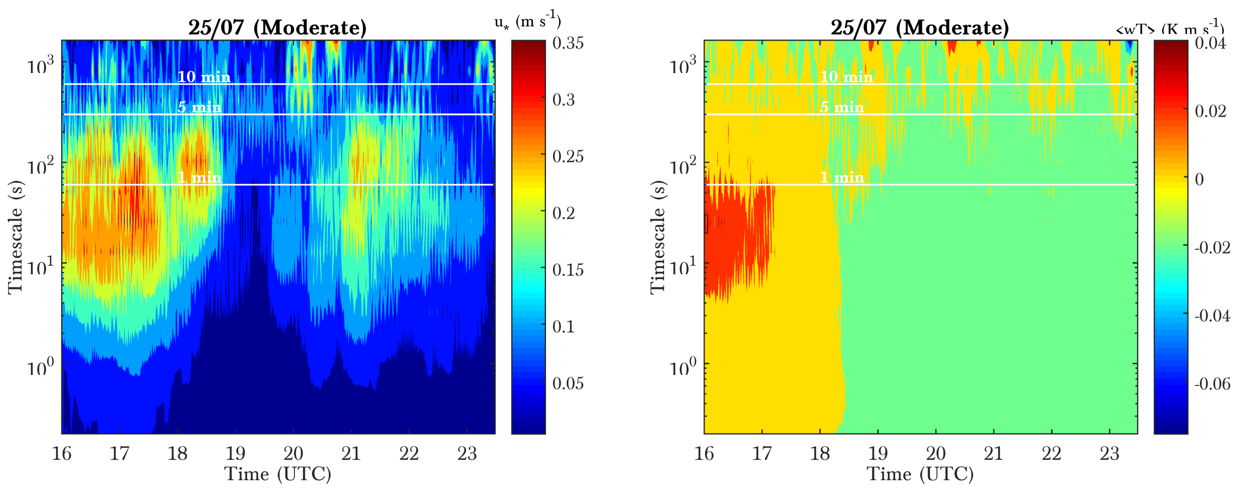

Figure II: *Same as Fig. I for the moderate downslope event (25/07/2017).*

averaging time by adapting it to different turbulent conditions is impractical and subjective, so it is preferable using a standard averaging time. 10 min is considered standard for micrometeorological datasets (Mauritsen et al., 2017).

References:

Babić, N., Večenaj, Z., and De Wekker, S. F. J. (2017). Spectral gap characteristics in a daytime valley boundary layer, Q. J. R. Meteorol. Soc., 143, 2509–2523. DOI: `https:`

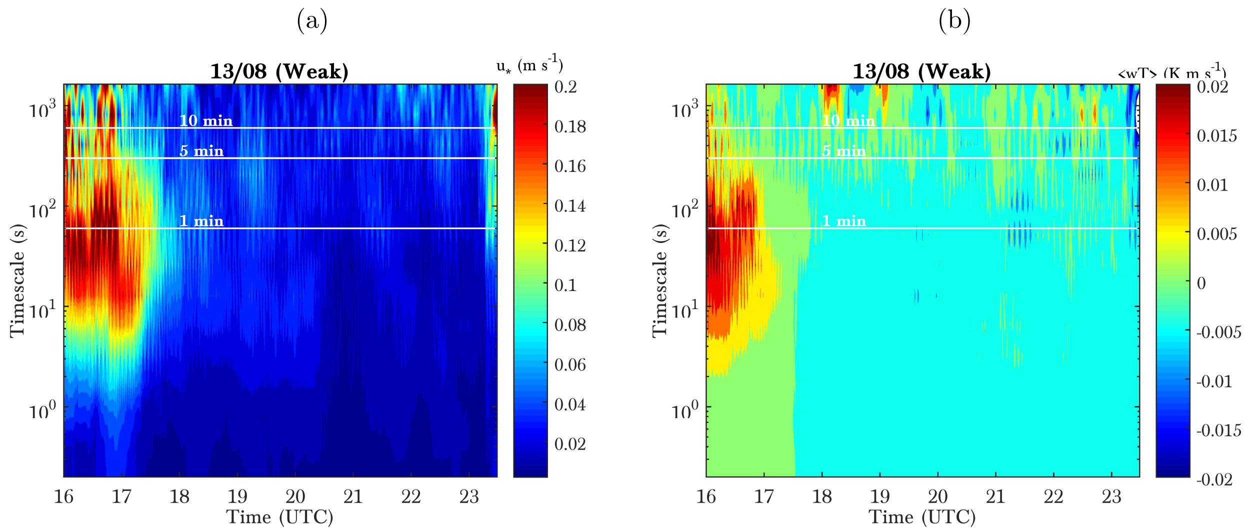

Figure III: *Same as Fig. I for the weak downslope event (13/08/2017).*

//doi.org/10.1002/qj.3103.

Hess, G. D. and Clarke, R. H. (1973). Time spectra and cross-spectra of kinetic energy in the planetary boundary layer, Q. J. R. Meteorol. Soc., 99, 130–153. DOI: https://doi.org/10.1002/qj.49709941912.

Mauritsen, T. and Svensson, G. (2007). Observations of Stably Stratified Shear-Driven Atmospheric Turbulence at Low and High Richardson Numbers, J. Atmos. Sci., 64, 645–655. DOI: https://doi.org/10.1175/JAS3856.1.

Román-Cascón, C., Yagüe, C., Mahrt, L., Sastre, M., Steeneveld, G.-J., Pardyjak, E., van de Boer, A., and Hartogensis, O. (2015). Interactions among drainage flows, gravity waves and turbulence: a BLLAST case study, Atmos. Chem. Phys., 15, 9031–9047. DOI: https://doi.org/10.5194/acp-15-9031-2015.

Schalkwijk, J., Jonker, H. J. J., Siebesma, A. P., and Bosveld, F. C. (2015). A Year-Long Large-Eddy Simulation of the Weather over Cabauw: An Overview, Mon. Wea. Rev., 143, 828–844. DOI: https://doi.org/10.1175/MWR-D-14-00293.1.

Viana, S., Terradellas, E., and Yagüe, C. (2010). Analysis of Gravity Waves Generated at the Top of a Drainage Flow, J. Atmos. Sci., 67, 3949-3966. DOI: https://doi.org/10.1175/MWR-D-14-00293.1.

2. Footprint analysis. The authors themselves talk about the footprints influencing the values of the fluxes (Pg 4, ln 33 or Pg. 14, ln 23-24), however, no footprint analysis is provided. I suggest the authors use the footprint model of Kljun et al. (2015) to examine the differences in the source area of the turbulent fluxes for the three different categories. But on another note, the sentence on

Pg. 4 is erroneous: the footprint does not induce "uncertainty in estimation of fluxes" if the fluxes are calculated from the eddy covariance, they might just represent turbulence originating from other locations.

As suggested by the referee, we have added the footprint analysis in the new manuscript. It has been added in Appendix A. To estimate the footprint we have employed the approximate analytical model from Hsieh et al. (2000), which is based on lagrangian stochastic dispersion models and dimensional analysis, in combination with the 2D extension from Detto et al. (2006), to include the contribution of lateral spread. This footprint model was chosen because it is developed for thermally stratified surface layers, it is practical and has been applied in many studies, giving satisfactory results when compared with other footprint models. In order to use the model from Kljun et al. (2015), however, we would have to estimate the boundary-layer height. But, as pointed out by Referee#2, when having a low-level jet the turbulence above the jet maximum might be disassociated with the surface, and therefore the estimation of the boundary-layer height has a great uncertainty. Therefore, we have chosen the models from Hsieh et al. (2000) and Detto et al. (2006) instead of the one from Kljun et al. (2015).
With respect to the sentence from the old manuscript brought by the referee, we do agree it is erroneous. Hence, it has been eliminated from the new manuscript, and the explanation associated to the footprint analysis has been revised.

3. Structure of the katabatic flow. I find myself wondering if not doubting if the flow the authors are studying should be classified as katabatic at all or not. Katabatic flows possess very specific characteristics: a low level jet, formation due to surface temperature deficit and retardation due to surface friction (turbulent momentum transport towards the surface), very specific turbulent structure associated with its jet profile: negative momentum and positive horizontal heat flux below the jet and the opposite above, minimum in TKE at the jet maximum (see Grachev et al. 2016). The profiles in Fig. 11, particularly for the strong cases do not resemble katabatic ones at all, and the weak cases have a low level maximum that could be also just due to the interpolation scheme, and then appears to have a secondary maximum above the height of the tower. On a side note: why are the sonic measurements not used in the wind speed profiles such as in Figure 11? Could it be that it actually is the basin flow (Pg 2, ln 15. How do you ascertain that your flow is not actually influenced by the Madrid basin and is purely katabatic). The authors should look at the profiles of the turbulence quantities to first identify if their flow qualifies as katabatic and second to actually show if their profiles in Fig. 11 are physical at all or the low level jet in the weak case is purely a construct of interpolation scheme, and what is happening with the secondary maximum. The profiles of turbulent quantities would also allow them to estimate the jet maximum height in each individual period. The jet maximum height is indeed the vital parameter when studying anything related to katabatic flows since at jet maximum wind speed will be maximal but the turbulence will be zero – and thus exactly the opposite of standard flat-terrain stable boundary layer structure that the authors so heav-

ily rely on in the HOST, MOST, shear capacity and other diagnostics. In that respect, if there is really a low level jet maximum below 3 m in the weak cases, then the turbulence above that height light be disassociated with the surface and therefore not exhibit standard boundary layer characteristics. Not taking this fact into account invalidates the conclusions.

Regarding referee's first wonder, and as previously explained, we have changed the denomination of all the events as a whole to "downslope flows". As explained in Sect. 4 of the new manuscript, weak downslope flows share the characteristics of katabatic flows, but moderate and particularly intense downslope flows show a distinct behaviour due to the dynamical input from the nearby slope. We have explored the physical mechanisms responsible for their formation by calculating the heat and momentum budgets for the three representative events in Sect. 4.1. In addition, we have included the profiles of the turbulent fluxes in Figs. 8–10, which support the existence of the katabatic jets on the weak downslope events (rejecting therefore the idea about being a construct of the interpolation scheme), and of the jet maxima above 10 m particularly on the intense events. A deep analysis about the physical mechanisms underlying, the thermal structure of the flow, as well as their interaction with turbulence for a representative weak, moderate and intense downslope event has been included in Sect. 4.
With respect to the wind-speed measurements from the sonic anemometer, they have not been included in the profiles because they introduce an extra instrumental bias on the wind profile, which is based on the cup-anemometer measurements at 3, 6 and 10 m. In some weak events, wind speed is very weak at all levels ($\simeq 1$ m s^{-1}), and therefore the instrumental bias could introduce an important deviation from the real profile. An example of this instrumental bias for the investigated weak event (13/08/2017) is shown in the following Fig. IV. It can be observed that the form of the peaks and minima is not always coincident between both instruments. Since from the cup anemometers we cover a larger vertical profile, we use those measurements to characterise the wind profile.
With regard to the downbasin flow, it is easily discriminated from the local downslope flow in our study site. Downslope flows are directed from the Guadarrama mountain range (i.e. from the NW), whereas downbasin winds approximately follow the direction of the main rivers of the area (i.e. from the NE during night-time). This distinction was also made in Plaza et al. (1997). Despite some of the events are affected by the irruption of downbasin winds, in the figures we just represent the profiles at times in which downslope flows are blowing, as required by the selection algorithm. Fig. 1a in the new manuscript has been changed, so that local slopes and the basin are better distinguished.
And regarding the last comment about the connection of the measured turbulence with the surface, the analysis of the regime transition from non-dimensional parameters (Sect. 4.2 from the old manuscript) has been eliminated, and therefore MOST does not need to be assumed anymore. With regard to the figure with the HOST transition (Fig. 7b), we believe that the transition of nocturnal regimes explained in Sun et al. (2012) is clearly identified from the represented turbulence data at 8 m. Furthermore, Sun et al. (2012) relate the occurrence of the distinct turbulent regimes with the existence of low-level jets during CASES-99.

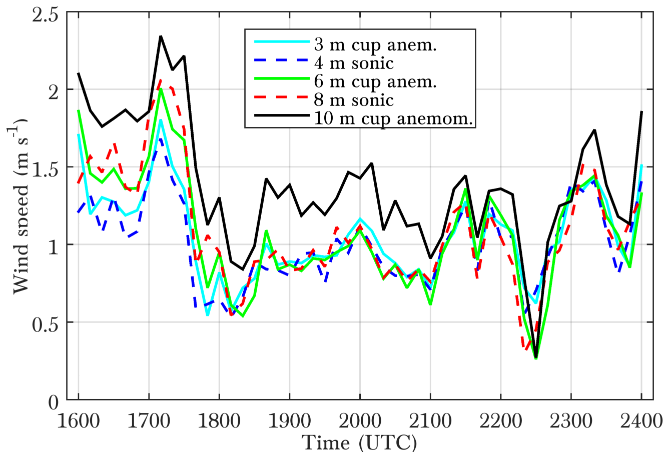

Figure IV: *Times series of the wind speed from 1600 to 2400 UTC on the 13/08/2017. Solid lines represent the measurements from cup anemometers, and dashed lines from sonic anemometers.*

4. Study of budgets The authors should present budget of the momentum and heat to substantiate their claims (such as the section 3 and 4 when talking about the development of the flow and its interaction with turbulence and transition to very or weakly stable boundary layer), and also to more fully understand the processes at hand. By examining the budgets of the katabatic flow one could isolate the importance of individual terms (local generation, dissipation, advection etc) on the weak, intermediate and strong katabatic flows and therefore show if the weak katabatic flow for example is locally driven and the strong katabatic flow is advected from the steep slopes 2km away, whereby the change in slope (from 25° to 2°) leads to the deepening of the flow as observed by Smith and Skyllingstaad (2005). The budgets will also show the importance of mesoscale and not just the large-scale pressure gradients on the flow, even if only as a residual term. The budgets could answer where the claims that stronger unstable turbulence facilitates intense katabatics. This indeed is counterintuitive as for the katabatic flow to develop one needs a large temperature deficit (i.e. cooling) and turbulence suppresses the katabatic flow while unstable stratification does not even allow the development of katabatic flow (Pg. 8, ln 7-13).

As requested by the referee, the analysis of the heat and momentum budgets has been included in the revised manuscript (Sect. 4.1). Indeed, we have been able to prove that weak downslope flows (which behave as pure katabatic flows) are driven by the buoyancy acceleration triggered by the local temperature deficit, whereas moderate and particularly intense downslope flows, have an important dynamical contribution from the nearby steep slope. Hence, the arrival of the downslope flow can take place before the thermal profile becomes stable at the measuring point, and the strengthening of turbulence is not constrained by negative buoyancy.

5. Stratification How was the virtual potential temperature calculated? Was the humidity needed to convert air temperature to virtual potential temperature used from Irgason and at which level? Also about the calculation of the potential temperature gradient: On Pg. 7, ln 20 and Equation 1, if you are using a 3th order polynomial why is the stratification calculated only from delta? The true temperature gradient dTheta/dz (if one takes the derivative of Eq 1) has contributions from beta, gamma and delta and depends on height.

As explained in Lines 22-23 on Page 8, virtual potential temperature was calculated from temperature measurements from aspirated thermometers at 3, 6 and 10 m, and humidity measurements in a T/RH probe at 2 m.
With regard to the logarithmic fit of the virtual potential temperature profile, even though θ_v also depends on β and γ, the static stability is best described from the value of δ. This information has actually been extended and included in Appendix B, by showing an example of the distinct static stabilities of the thermal profiles during a moderate event. We did not mean to say that the gradient is independent of β and γ, but that the static stability of the profile can easily be inferred from this parameter. The classification from Eq. B2 was designed after a thorough check.

6. Origins of the flow. Tied to the previous comments, the paper fails to determine the origin of the katabatic flows. For example, on Pg. 8, ln 5 the authors mention that the stratification is unstable and net radiation positive during the onset of the strong katabatic episodes. Given that the katabatic flow is caused by stable stratification (temperature deficit) and therefore cannot develop in unstable stratification, the authors should show evidence of why they think their flow is katabatic, and how and where it originates from (does it originate on the steep slope where the stratification has already turned stable due to shadowing? And is now merely advected to the study site?)

As explained in previous responses to queries, the investigation of the budgets has provided further proof about the origin of the distinct downslope flows: weak downslope being katabatic, and moderate and intense downslope being partly or mostly dynamically induced by the nearby slope. Considering that the axis of the mountain range is directed SW-NE, sunset takes place at the back of it, and therefore the cooling down of the surface starts earlier in the slope than at the foothill. If the low soil moisture favours the stronger cooling and the synoptic wind, despite being weak, is from the NW, the downslope advection of cold drainage fronts is possible, arriving at the foothill when still the thermal profile is unstable and net radiation positive. Such scenario was for instance observed in Papadopoulos and Helmis (1999).

7. Figure 7 and the correlation to soil moisture Putting the 4th order fit through the data presented in Figure 7 is stretching it beyond any justifiability. Indeed, the spread of the data is so large that a linear fit would be possible at maximum to show that for low soil moisture G is slightly positive, but for high it is mostly negative. The results for longwave-radiative loss show no correlation between the data, both linear or non-linear. I therefore protest against any conclusions

based on these fits and the identified two maxima.

We agree with the referee that the spread of the data is large and that the correlation is low. Therefore, we have removed the figure and the associated explanation from the manuscript. Instead, a short comment about this vague correlation has been included in the revised manuscript (Lines 21-24 on Page 9).

8. Energy balance closure and the ground heat flux. It is interesting to note that the level of energy balance closure is so high in the study site. How did the authors calculate the ground heat flux and the heat storage in the layer above the heat flux plate? Given the nature of the weak and the strong flows, one could also argue on the importance of advective processes, but the energy balance appears to suggest that advection is not important for strong katabatic flows.

Given the uncertainty in the calculation of the energy-balance closure, the figure in which we showed the different components has been eliminated. Instead, we have preferred to explore the nature of different downslope flows by analysing the heat and momentum budgets, as suggested by this referee. In fact, the analysis of the energy-balance closure is out of the scope of this study.

9. Interaction with turbulence The second motivation of the study talks about the interaction between turbulence in SBL and katabatics but actually, the relevant turbulence that is interacting was found to be unstable stratification before the onset of the wind itself.

The referee is right when stating that not just turbulence in the SBL is interacting with downslope flows. Indeed, the moderate and intense downslope flows that are taken as case studies, are established before the onset of the SBL. For that reason, the second motivating aspect of the paper has been changed from "The interaction of katabatic winds with local turbulence in the SBL and the implication in turbulent characteristics" to "The interaction of downslope winds with local turbulence and the implication in the characteristics of the SBL". Note that we still mention the SBL, since the characteristics of the SBL (once it is established) are strongly affected by the nature of the different downslope flows, and is one of the motivating aspects of the study. On the other hand, the term "stable boundary layer" has been replaced by "boundary layer".

10. Language I suggest a professional or native speaker to check the language as I didn't want to enumerate all the things that need to be changed (e.g. "avoids" should be "prevents", "striked" should be "stricken" or rather something more appropriate, "fogs" as plural does not exist, it is always "fog", "emplacement" sounds awkward etc.)

As suggested by Referee#2 and Referee#3, a native speaker has revised the manuscript and given some language corrections and improvements, apart from those provided by the referees.

Individual Major Corrections

2. Pg. 1, ln 1. What are the "dynamic and turbulent" features of SBL?

We have changed it to "the turbulent characteristics and thermal structure".

3. Pg. 1, ln 8: In Figure 6, the limits is 3.5 m/s not 6. What is the correct number?

The lower limit is 3.5 and the upper limit 6: it has been clarified in the new manuscript.

4. Pg. 3, ln 8-14: No, even over flat terrain with the existence of a low level jet or even in very stable stratification without a low level jet MOST is not valid

As commented in the response of Query 6 from Referee #1, Fig. 10 from the old manuscript was eliminated for various reasons. Therefore, the validity of MOST is not assumed anymore in this analysis.

5. Pg 4, ln 24: why would a strong surface thermal inversion necessarily be allowed to develop just because the slope angle is low, if there is enough wind to prevent its development?

This referee is right when stating that strong wind can prevent the development of the thermal inversion. However, what we mean is that over a shallow slope the buoyancy acceleration is smaller than over a steep slope, and therefore the thermal inversion can be stronger, just with the locally generated flow and without the erosion of drained downslope flows from the nearby steep slope. This has been clarified now.

6. Pg. 4, ln 35: you have not mentioned the CO2 fluxes at all until the moment when you mention the negligible effect of the urban area. Or do you mean the effect of urban area on all the fluxes?

We meant the effect on all the turbulent fluxes. In any case, the explanation associated with the footprint has been changed in the new manuscript (Lines 4-8 on Page 5 and Appendix A).

7. Figure 3. Why is there no data from the sonics? Also, the way the data are presented all lumped together does not show if there are wind maxima at different heights for the different episodes, periods. I suggest the authors calculate the jet maximum if possible, normalize the height with it and then plot the normalized profiles.

With respect to the wind data from the sonic anemometers, as explained in the Specific Major Comment 3, they have not been included in the profiles or Fig. 3 due to the instrumental bias they introduce. Apart from that bias, due to the closeness between the levels and to the fact that sonic levels are in between cup-anemometer measurements, they do not provide further information of interest about the wind profile, as can be seen from the following Fig. V.

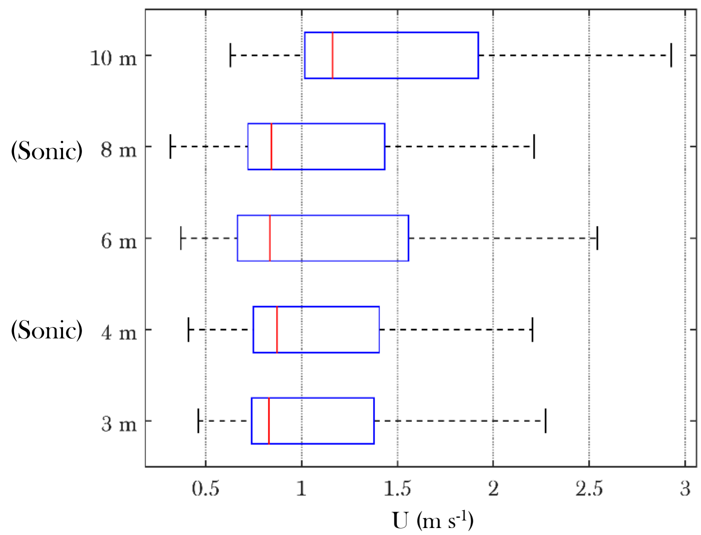

Figure V: *Same as Fig. 3a from the manuscript but including sonic measurements at 4 and 8 m.*

On the other hand, the referee is right that this plot does not show the location of wind maxima. In fact, as inferred from the sign of the turbulent fluxes in Figs. 8–10, the jet maximum in many cases is probably located above 10 m. This plot was included in order to show the wind-speed frequency distributions and range of values at different levels, and to introduce and motivate the classification of events. In addition, as shown for the three representative events in Sect. 4.2, the determination of the jet-maximum height is not always possible only with two sonic measurements. Therefore, even though the normalisation of the height with the jet-maximum location is an interesting exercise, it is not feasible in this study without carrying great uncertainty.

8. Pg. 6, ln 20-26: Nowhere in Figure 3 is it visible that there is a development of skin flow or where the jet maximum is. Indeed, the figures seem to suggest that the jet maximum is always above 10 m.

We agree that from Fig. 3 the development of a skin flow and the position of the jet maximum are not visible. We only state that the median at 3 m is similar to that at 6 m, and the first quartile is even smaller at 6 m than at 3 m, which does not occur for the third quartile. This occurs as a consequence of the skin flow on the weak downslope events, but not for all the downslope events, and therefore it is not observed for the whole distribution. The skin flow is shown in Fig. 10b (weak event), and is clearly absent in Fig. 12b (intense event), since the jet maximum is above 10 m.

9. Figure 3 should also include the information on the temperature profiles and turbulence.

We acknowledge this suggestion but we prefer just to include the box plots for the wind speed. At the point of the manuscript where this Fig. 3 is introduced, frequency distributions for the temperature and turbulence would not contribute to the motivation of the classification into the three downslope events, which is the main purpose of this figure. On the other hand, thermal and turbulence profiles are shown in Figs. 8–10, and we think they provide more interesting information on the thermal structure and interaction with turbulence than the frequency distribution of these variables itself.

10. Pg 7, ln 6-7: I find it very strange that the results at 3 and 10 m do not show conformation to the classification and only 6m is so good. The sonic data should be used to study this more in detail and give a physical explanation why this is so.

In those lines (Lines 10-11 on Page 8 of the new manuscript) we state the following: "At the levels of 3 and 10 m the events showing different features cannot be so clearly detached, and therefore the level of 6 m is employed for the classification". We did not mean that the levels of 3 and 10 m do not show conformation to the classification, but that the classification into the three downslope types with contrasting turbulence conditions is better produced using the level of 6 m. On the other hand, as commented above, due to the instrumental bias we prefer not to use measurements from sonic anemometers, but from cup anemometers.

11. Flocas et al. reference is missing from the list of references

Thank you for pointing out the missing reference. It has been included in the revised manuscript.

12. Pg. 7, ln 17: is it the soil or the skin temperature?

It is actually the skin temperature. It has been corrected.

13. Pg. 8, ln 1: is the low value of TKE due to the jet maximum being close to the measurement height or because one is above the jet?

In some cases it could be due to the closeness of the jet maximum, but in that group some moderate downslope flows are also included, and the skin flow is not always developed. With the available information, we cannot specify the position of the jet maximum for all the events within the group of low TKE. Note that Figs. 4 and 5 from the old manuscript have been merged into Fig. 4 of the new manuscript.

14. Pg 8, ln 6: katabatic flow develops turbulence through shear generation. What you mean to say by "relation between katabatic flow and turbulence" I

guess is, the turbulence before the onset of the flow

We think that the interaction is bidirectional. The turbulence at the onset influences the downslope flow, and at the same time, the downslope flow itself affects the turbulent characteristics of the boundary layer. This can be checked up for instance from Figs. 8–10.

15. Pg. 9, ln 3: why would large soil moisture after precipitation during nighttime lead to the enhanced cooling of the soil?

From the available data, we cannot draw conclusions about the mechanism explaining that fact without being speculative. Additionally, the figure associated with this explanation has been eliminated from the manuscript. Hence, investigating the mechanism that explains why after strong precipitation surface cooling can be enhanced is not within the scope of the paper.

16. Pg 9, 7-13: The study on the influence of stratification needs to be associated with momentum and heat budgets of the flow to show whether the conclusions drawn are substantiated in the text.

Now, the heat and momentum budgets have been calculated and analysed in Sect. 4.1.

17. Pg. 10, ln 8-19: the transition will depend on the location of the jet maximum and if it is below 6m or above or is moving between. The exact value that is lower than in Sun is indeed no wonder given the fact that there is a jet maximum present and not in Cases-99.

As explained in the Specific Major Comment 3, Sun et al. (2012) relate the occurrence of the distinct turbulent regimes with the existence of low-level jets during CASES-99. In our case, the transition occurs independently of whether the jet is located below or above the sonic measurements. Even if the skin flow is present (below 3 m) for many weak downslope events, we cannot assure that the jet maximum is close to the sonic measurements whenever $U < 1.5$ m s^{-1} (including some moderate events in black). We can only comment about this possibility (sentence included now on Page 11 Lines 3-4).

18. Pg. 11, ln 1-3. The two sentences on MOST cannot be applied to the current study without more understanding of the processes studied. MOST will only be applicable very close to the surface if the stratification is weakly stable and turbulence is well developed, and if the terrain is horizontally homogeneous. If there is a low level jet close to the tower height or even worse, within the tower height, MOST by definition is not valid as there is another height scale that is more important than z/L.

For the reasons presented in the response to Major Point 6 from Referee#1, Fig. 10 from the old manuscript has been eliminated. Therefore, the compliance of MOST is not assumed anymore in this work.

19. Pg. 11, ln 25: Isn't the fact that Fig 10b resembles Fig. 8b by construction since you change the definition of shear capacity to match the HOST?

Idem to the previous response, Fig. 10 has been eliminated.

20. Pg 12, ln 4-6: The calculation on Rb will again depend on the existence of the jet maximum if it is below, and therefore it doesn't make much sense as a measure. A better measure would be the gradient Richardson number Ri which the authors could calculate from the interpolated profiles and therefore obtain a profile of Ri.

Idem to the previous response, Fig. 10 has been eliminated.

21. Pg 12, ln 24: say that the value of the diurnal peak is not shown, or do you refer to the little part before the transition shown in Fig. 11?

We refered to the diurnal peak throughout the day, so we include "(not shown)" in the manuscript.

22. Pg. 12, ln 25: does the flow arrive or develop? Show the budgets

This is an important and interesting point that has been clarified in the new manuscript after showing the budgets. As it has been demonstrated, the weak downslope events are mainly locally generated katabatic flows, whereas some moderate and particularly intense downslope flows are dynamically induced and propagated from the nearby steep slope, so that we can say that the flow "arrives" for them.

23. Pg. 12, ln 1-2: how accurate is this wind maximum that does not exist in the measurements but only in the interpolation?

From the measurements, particularly at 2230 UTC, the existence of the jet maximum around or below 3 m can be guessed ($U_{3m} > U_{6m}, U_{10m}$; Fig. 10b). Moreover, the profiles of the momentum and horizontal-heat turbulent fluxes (Fig. 10d) support the existence of the jet below 4 m.

24. Pg. 12, 5-6: In Grachev et al. (2016) paper it says that the flow is stationary but only in the well-developed phase. You are focusing on the transition.

Thank you for pointing this out. That sentence has been eliminated from the manuscript.

25. Pg. 15, ln 23: "form when maximum wind speed is kept" should be "have maximum wind speeds below", because indeed you are talking about the katabatic wind speed of 1.5 and not the ambient wind speed into which the katabatic wind impinges.

Thank you for the suggestion, it has been accordingly changed.

26. Pg. 15, 26: Wind shear is not driving katabatic flow, the driver is the negative buoyancy and wind shear is the product of the katabatic flow itself.

We do agree with the referee. That sentence has been eliminated and the whole explanation has been revised.

27. Pg. 15, ln 29: "intense katabatics are found" should be "int. kat. have maximum wind speeds..". It is again a question of cause and effect.

Thank you for the suggestion, it has been accordingly changed.

28. Pg. 16, ln 10: the scaling regime expected to be valid for at least very stable conditions is local or most likely z-less scaling.

Idem from Specific Major Comments 19 and 20. Fig. 10 from the old manuscript and the associated conclusions have been withdrawn.

29. Pg. 16, ln 25: influence of submesoscale phenomena will be visible in the calculated ogives or multi-resolution flux decomposition.

The referee is right that the influence of submeso motions is visible from the calculated MRFD plots (Figs. I-III), particularly over a timescale of around 10^3 s. In any case, the analysis of submeso phenomena was not within the scope of the article, and therefore, MRFD analyses have not been included in the revised manuscript.

Responses to comments from Referee #3

MANUSCRIPT: acp-2018-944

TITLE: From weak to intense downslope winds: origin, interaction with boundary-layer turbulence and impact on CO2 variability

AUTHORS: Jon A. Arrillaga, Carlos Yagüe, Carlos Román-Cascón, Mariano Sastre, Maria Antonia Jiménez, Gregorio Maqueda and Jordi Vilà-Guerau de Arellano

---

MAIN CHANGES IN THE MANUSCRIPT:

o Title.

o Abstract and motivating aspects.

o Denomination: katabatic → downslope.

o Further information about data postprocessing in Sect. 2.2.

o New Sect. 4 in the revised manuscript: analysis of the heat and momentum budgets, profiles and the estimation of the jet-maximum height for three representative events.

o Summary and conclusions.

o Appendix A (footprint estimation) and B (assessment of the thermal profile).

o Removed figures (numbers from the old manuscript): Fig. 7, Fig. 10, Fig. 11 and Fig. 12.

o Merged figures (numbers from the old manuscript): Figs. 4 and 5, Figs. 8 and 9.

o New figures (numbers in the revised manuscript): Fig. 7, Fig. 8, Fig. 9, Fig. 10, Fig. A1 and Fig. B1.

o Slightly modified figures (numbers in the revised manuscript): Fig. 1 and Fig. 11.

o Wording and English revision.

General Comments:
The manuscript investigates katabatic flows on the basis of occurrences observed during one summer season at the foothills of the Guadarrama Mountain Range in Spain. The data set has been split up into weak, moderate and intense events, based on the observed maximum wind speed observed during each individual case and is then analyzed under various aspects. The study shows distinc differences between the different classes of katabatic flow, the number of intensive katabatic flow cases is, however, very low (3) and rises thus questions on the statistical significance of the reported results. The paper is in general well structured and includes a good literature overview on the subject. The figure layout is in general rather inhomogeneous over the paper and should be reworked. Several of the figures are in addition hard to read, mainly due to small labels and legends. Finally, the manuscript requires a thorough makeover by a native English speaker. Main points in this context the rather complicated sentence structures, unconventional wording obviously taken from the dictionary (e.g. emplacement instead of site/location), missing commas, the improper use of prepositions and articles, and grammatically incomplete sentences. I have marked a quite a few, but far from all, instances in my specific comments.

We thank Referee #3 for his/her comments about the article. We agree that the number of intense flows is small, but anyway, some of the most important conclusions about the nature and characteristics of the downslope flows (note that we have changed their denomination from katabatic to downslope), are drawn from the analysis of representative individual events and not from the statistical parameters of the distributions. In any case, this new database could be enlarged in time by including further measurements. Furthermore, we have revised the figures and modified them in order to be legible and clear enough. Finally, a native speaker has revised English along the manuscript, providing language corrections and improvements, apart from those given by the referees. It must be noted that Sect. 4.2 and 5.1 have been eliminated from the old manuscript and new sections have been added in the new manuscript (Sect. 4, Appendix A and B). Below, we provide point-by-point responses to the specific queries from the referee. The modifications undertaken in the manuscript can be checked up both from the revised manuscript and the tracked-changes version.

Specific comments:

1) P1, L1: “on the dynamics” instead of “”in the dynamics”

We thank Referee#3 for all the language corrections and improvements suggested. The manuscript has been accordingly corrected.

2) P1, L5: insert comma after “moderate and intense”

Inserted.

3) P1, L9: insert “flow” after “katabatic”

Inserted.

4) P2, L26: “at contrasting” instead of “in contrasting”

Changed.

5) P2, L28: insert comma after “model”

Inserted.

6) P2, L33: “In contrary” instead of “At contrary”

Changed.

7) P3, L8 and 11: “emplacement” is rather uncommon, better “site or location”?

It has been changed to both location and site.

8) P3, L15-16: “on the concentration” instead of “in the concentration”

Changed.

9) P3, L16: remove “the” before “CO2

Changed.

10) P3, L16: “in coastal areas” instead of “at local areas”

Changed.

11) P3, L27: sentence incomplete; “the role of: ......, in CO2 mixing ratios” ; should be “in controlling/affecting CO2 mixing ratios”

Completed.

12) P3, L34: insert “concentrations” after “CO2”

Inserted.

13) P4, L23: “a relatively” instead of “an relatively”

Changed.

14) P4, L23-24: "immediately besides" is quite strange; better "close to"?

It has been changed to "close to".

15) P4, L29-30: "needleleaved evergreen tree cover", sounds complicated; isn't it just "coniferous"?

This name was obtained from the database and maps of land-use types from Land Cover CCI from ESA. In any case, in order to clarify, we have added "coniferous" in brackets.

16) P4, L34: replace "inexistent" by "absence of"

As the native speaker suggested, it has been changed to "non-existent".

17) P5, L8: formatting error "CO2" subscript

Changed.

18) P6, L5: insert "concentrations" after "CO2"

Inserted.

19) P6, L7: "Forty were selected as days: : :: : :.." The sentence is grammatically poorly formulated and hard to read. Please rephrase

It has been changed to "Forty events with the formation of a thermally-induced downslope flow were selected from the analysed summer period with available data (94 days in total)".

20) P7, L2: insert "the criteria" after "meet"

It has been accordingly changed.

21) P7, L2 (and other instances): replace "minutal" by "minute"

Replaced.

22) P7, L4: replace "weak" by "low"

Replaced.

23) P7, L29: there is no Figure 5a)

The former Fig. 5 has been eliminated, so this sentence is not present anymore.

24) P8, L34: Why are you presenting a 4th-order polynomial fit; any physical reasoning for this? A simple trend could also be seen from a linear regression, and the two peaks resulting from your fit seem to be rather arbitrary; Thus I see a big danger of an over-interpretation of non-existing features in the corresponding paragraphs on page 9, L1-13 (see also my comment on Figure 7)

As commented in the response to the Specific Major Comment 7 from Referee#2, the reason for using the fourth-order fit was to justify the bimodal behaviour. However, due to the vague relationship between the variables presented, that figure and the associated explanation have been removed from the manuscript. A short comment about this vague correlation has been included in the revised manuscript (Lines 21-24 on Page 9).

25) P9, L17-18: "......, the shear associated with the katabatic flow increases, and the downslope flow strengthens progressively." I do not understand the direct link between this two statements; How can increase in shear strengthen the downslope flow? Might also be a misunderstanding from my side, but then the sentence should be rephrased.

That sentence has been changed to "If the downslope flow arrives when the stratification is still unstable and the surface thermal inversion (hereinafter measured from θ_v) is not formed yet, the downslope flow strengthens progressively" (Page 9 Lines 33-34).

26) P9, L20: insert "the" before "surface"

Inserted.

27) You should define the calculation of VTKE already here, and not two lines under.

As suggested by the referee, it is defined two lines above.

28) P10, L2: insert comma after the parenthesis with the wind speed.

Inserted.

29) P10, L10: "increases linearly"; I could also see a square root dependency here

Given the wonder from Referee#3, we have represented in green the linear fit (Fig. Ia) and the square-root fit (Fig. Ib) over the scatter plot of V_{TKE} vs U when $U > 1.5$ m s^{-1}, together with the value of r^2. The correlation is very similar for both plots (the rounded r^2 is equal), indicating that it is not clear whether the dependency is linear or square root. Therefore, we have changed the mentioned sentence to: "increases approximately at a linear rate with U" (Line 28 on Page 10).

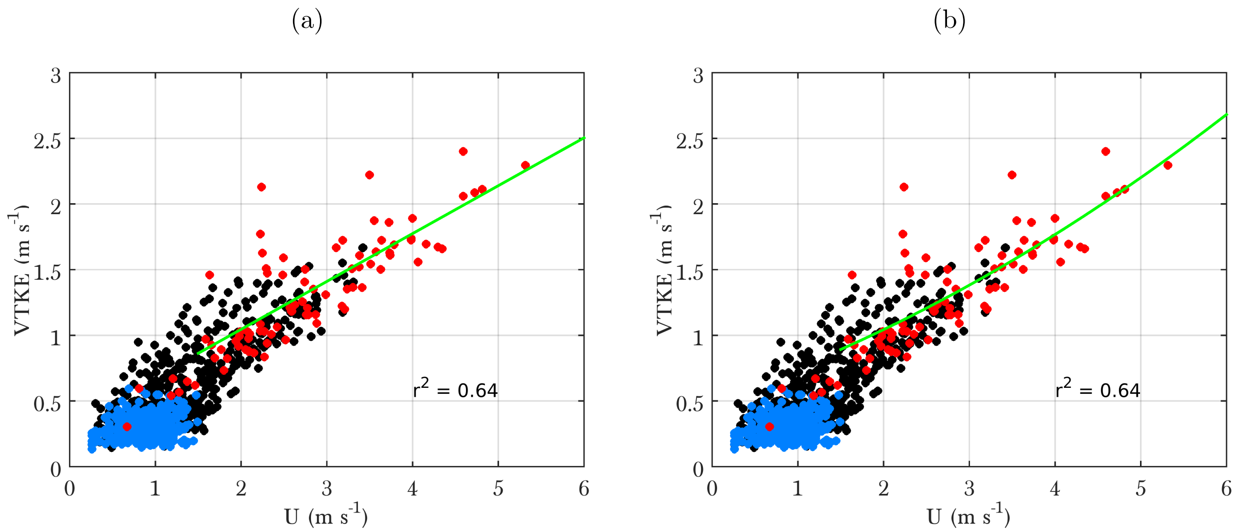

Figure I: *Same as Fig. 7b from the manuscript including in green (a) the linear fit, (b) the square-root fit, and the value of the square of the multiple correlation coefficient (r^2) for the fit .*

30) P10, L29: replace "on" by "for" or "during"

That sentence is eliminated from the revised manuscript.

31) P10, L32: insert comma after "night"

Inserted.

32) P11, L17: Sentence has to start with an upper case letter; "Van Hooijdonk: : :.."

Corrected.

33) P11, L25-26: "intense and weak katabatics cluster into two clearly distinct regimes"; at 8 m I still see a considerable amount of black and red data points for SC¡3 with distinct elevated VTKE levels; can you explain/comment on this.

We thank the referee for this comment but Fig. 10 has been eliminated from the manuscript, as well as the associated text.

34) P12, L4: put "by definition" between commas.

That sentence has been eliminated from the manuscript.

35) P12, L17: replace "related with" by "related to"

Replaced.

36) P13, L7-8: start the sentence with "In contrary, U remains: : :.."

Changed.

37) P13, L12: insert comma after "takes place"

Inserted.

38) P13, L25: replace "so doing" by "doing so"

Changed.

39) P14, L9: insert comma after "SBL"

Inserted.

40) P14, L20: insert comma after "nearly 0"

Inserted.

41) P14, L21: insert comma after "assumption"

Inserted.

42) P14, L22: insert comma after the reference

The comma has been inserted before "following the methodology", since we think it is better for the meaning we want to express.

43) P14, L25: insert comma after "equation"

Inserted.

44) P 15, L8-10: this sentence has to be rephrased, maybe even better split in to or three! In particular complicated is the part ": : :by the presence upwind of a land use component of forest: : :: : :: : :"

That sentence has been changed to: "This positive CO_2 advection is probably induced by the presence of a land use composed of forest, mosaic trees and shrubs upwind, towards the downslope direction. Given the increased plant respiration and soil flux, greater CO_2 concentrations are accumulated close to the surface during the night" (Lines 8-10 on Page 17).

45) Some small inconsistencies in the references a. Boundary Layer Meteorol. vs Boundary-Layer Meteorol.; I believe the latter one is the usual b. A few journal abbreviations are not terminated by a period; e.g. Borge et al. and Plaza et al. c. Presentation of doi or not for articles

We thank the referee for pointing out these inconsistencies. Journal abbreviations and citations along the manuscript have been revised and accordingly corrected. The DOI of all articles has additionally been included.

46) Page 22, Table 1; inaccurate caption, I suggest: "Specification of the values measured and the devices : : :: : :"; the specification of a value is not technical!

Changed.

47) Page 24, Table 3; add number of occurrences for each class in the table; maybe also an idea to place the measurement frequency directly in the table for each sensor instead of using the footnote solution.

As suggested by the referee, the number of occurrences of each type are included in Table 3, and the sampling rate is also included in Table 1.

48) Page 25, Figure 1a; the location names are difficult to read; use larger fonts and bold style; in addition have the degree symbols in the axes labels an underscore that should be removed.

The figure has been accordingly modified.

49) Page 27, Figure 3: I suggest to split this figure in 3 separate ones for the weak, moderate and intensive cases; as it is presented now you loose a lot of information by the averaging; I would also like to see the 40 individual profiles in this plots, e.g. as grey lines in the background.

We thank the referee for his/her suggestions about this figure. However, we prefer to keep it as it is for various reasons. First, one of the main purposes for including this figure is to represent the frequency distribution of the wind speed, show the differences between the levels at the onset and when the maximum intensity is achieved, and motivate the classification into the three types. Therefore, we think that at this point of the manuscript it is preferable to keep this figure as it is. Second, if we plot the 40 individual profiles in the background, the figure becomes fuzzy and unclear. Instead, we plotted the individual profiles for three representative events in Figs. 8–10. In this way, we compare in a clear way the structure of the downslope flows for the three types.

50) Page 31, Figure 7: I cannot see that the applied 4th-order fitting makes any sense; do you have any physical reasoning for your choice.

Please, see response to Comment 24 above.

51) Page 34, Figure 10: labels/legends too small.

This figure has been withdrawn from the manuscript.

52) Page 35, Figure 11: a) use different line styles for 4 and 8 m (in particular important for the intense event in red); why have you selected 21:00 as last time you present; from the time series it looks like that is more a transition phase, while e.g. 22:00 appears to be a more stationary situation; b), d), f): I suggest to use a common x-axis span at least for the wind speed

Thank you for these suggestions. This figure has been split into Figs. 8, 9 and 10 in the new manuscript. Different line styles are used for the different times represented. On the other hand, 2100 has been changed to 2230 UTC to represent a moment in which the SBL is already well developed. Besides, a common x-axis is used for all the panels in Figs. 8–10.

53) Page 36, Figure 12: axis labels too small!

This figure has also been eliminated from the manuscript: the evolution of the thermal stratification is shown in Figs. 8–10a; the time series of the wind shear is not needed either given that the friction velocity is also represented in Figs. 8–10a; and finally, the surface energy balance involves a great uncertainty, and hence, its interpretation is challenging.

54) Page 37, Figure 13: use different line styles for 4 m and 8 m

To better distinguish the two levels, instead of using different line styles, the level of 4 m is represented with the markers filled and the level of 8 m with the markers empty.

~~Weak and~~ From weak to intense ~~katabatic~~ downslope winds: ~~impacts on turbulent characteristics in the stable boundary layer~~ origin, interaction with boundary-layer turbulence and impact on CO_2 ~~transport~~variability

Jon Ander Arrillaga[1], Carlos Yagüe[1], Carlos Román-Cascón[1,2], Mariano Sastre[1], Maria Antonia Jiménez[3], Gregorio Maqueda[1], and Jordi Vilà-Guerau de Arellano[4]

[1]Departamento de Física de la Tierra y Astrofísica, Universidad Complutense de Madrid, Spain
[2]Laboratoire d'Aérologie, University of Toulouse, CNRS, France
[3]Departament de Física, Universitat de les Illes Balears, Palma, Illes Balears, Spain
[4]Meteorology and Air Quality Group, Wageningen University, Netherlands

Correspondence: Jon A. Arrillaga (jonanarr@ucm.es)

Abstract. The ~~role of thermally-driven local downslope or katabatic flows in the dynamics and turbulent features of the stable~~ interconnection of local downslope flows of different intensities with the turbulent characteristics and thermal structure of the atmospheric boundary layer (~~SBL~~ABL) is investigated ~~using~~ through observations. Measurements are carried out in a relatively flat area 2-km away from the steep slopes of the Guadarrama Mountain Range (~~Spain~~central Iberian Peninsula). Forty ~~katabatic~~ thermally-driven downslope events are selected from an observational database spanning the 2017-summer period, by using an objective and systematic algorithm that ~~is able to account for local and synoptic forcings~~accounts for a weak synoptic forcing and local downslope wind direction. We subsequently classify the ~~katabatic~~ downslope events into weak, moderate and intense~~according to the observed maximum~~, according to their maximum 6-m wind speed. This classification enables us to contrast ~~the main differences in dynamics~~ their main differences regarding the driving mechanisms, associated ABL turbulence and thermal structure, and the major dynamical characteristics. We find that the ~~stronger katabatic events are associated with an earlier onset time of these flows . We relate it to very low soil-moisture values~~ strongest downslope flows ($U > 3.5$ m s^{-1}) develop when soil moisture is low (< 0.07 m^3 m^{-3}~~, i.e. smaller than the median during the analysed period)and a weak synoptic wind ()~~, and the synoptic wind not so weak (3.5 m s^{-1} < V_{850} < 6 m s^{-1}) ~~having the same direction as the katabatic. The relative flatness of the area favours the formation of very stable boundary layers characterized by a longwave radiative cooling of around 60-70 W m^{-2} and very weak turbulence (friction velocity (u_*) < 0.1 m s^{-1}). They occur when katabatics are weak, and are occasionally associated with the formation of skin flows, that are manifested as weak jets (U < 1 m s^{-1}) at 3 m. Intense katabatics, instead, are characterised by a strong and increasing bulk shear (the maximum u_* is close to~~ and roughly parallel to the direction of the downslope flow. The latter adds an important dynamical input, which induces an early flow advection from the nearby steep slope, when the local thermal profile is not stable yet. Consequently, turbulence driven by the bulk shear increases up to friction velocity (u_*) $\simeq$ 1 m s^{-1}~~) that avoids~~, preventing the development of the surface-based thermal inversion, and giving rise to the so-called weakly stable boundary layer. ~~We identify the transition between the two regimes for a threshold katabatic wind~~

~~speed of around~~ On the contrary, when the dynamical input is absent, buoyancy acceleration drives the formation of a katabatic flow, which is weak ($U <$ 1.5 m s^{-1}~~, in agreement with the hockey-stick transition hypothesis. Our analysis is extended by calculating non-dimensional numbers to characterize the transition: the shear capacity,~~) and generally manifested in the ~~bulk Richardson number and z/L~~form of a shallow jet below 3 m. The relative flatness of the area favours the formation of very stable boundary layers marked by very weak turbulence ($u_* <$ 0.1 m s^{-1}). In between, moderate downslope flows show intermediate characteristics, depending on the strength of the dynamical input and the occasional interaction with downbasin winds. On the other hand, by inspecting individual weak and intense events, we further explore the ~~interaction between katabatic flows and turbulence, and the impact~~ impact of downslope flows on CO_2 ~~concentration~~variability. By relating the dynamics of the ~~two~~ distinct turbulent regimes with the CO_2 budget, we are able to estimate the contribution of the different terms. For the intense event, indeed, we infer a horizontal transport of 67 ppm in 3 h driven by the ~~katabatic~~ strong downslope advection.

1 Introduction

Thermally-driven slope winds develop in mountainous areas, when the large-scale flow is weak and skies are clear, allowing greater incoming solar radiation during daytime and larger outgoing longwave radiation during the night (Zardi and Whiteman, 2013). Under this situation, wind direction is reversed twice per day: thermally-driven winds flow upslope during the day and downslope during the night (Atkinson, 1981; Whiteman, 2000; Poulos and Zhong, 2008). The thermal disturbances that produce them have different scales and origin: from local hills and shallow slopes (Mahrt and Larsen, 1990) to large basins and valleys which extend horizontally up to hundreds of kilometers (Barry, 2008). The different scales, however, are not independent; for instance, local downslope flows converge at the bottom of the valleys generating larger-scale flows, which in turn influence the mountain-plain circulations.

Mountainous sites have ~~striked~~ struck the attention of many studies for plenty of reasons: in particular due to the influence on ~~the formation of fogs~~ fog formation (Hang et al., 2016), diffusion of pollutants (Li et al., 2018), and also due to the important role that slope flows play in the thermal and dynamical structure of the Atmospheric Boundary Layer (ABL) and its morning and evening transitions (Whiteman, 1982; Sun et al., 2006; Lothon et al., 2014; Lehner et al., 2015; Román-Cascón et al., 2015; Jensen et al., 2017).

In this work, we focus on the locally-generated thermally-driven ~~local~~ downslope winds (~~hereinafter *katabatic flows*) and on their role during the afternoon and evening transition of the ABL, affecting~~ i.e. not driven by the basin or valley) during nighttime, and the external factors and physical processes driving their formation and subsequent evolution. The latter is closely linked to the turbulent characteristics of the Stable Boundary Layer (SBL) and the ~~transport~~ variability of CO_2. ~~Despite the term *katabatic* is also used for refering to other non-thermally-driven winds (Zardi and Whiteman, 2013) , by following Barry (2008) we use it to refer to downslope winds driven by local thermal disturbances (i.e. not by the basin or valley).~~ Several external factors have been documented to affect ~~katabatic~~ these downslope winds: the steepness of the slope and the distance to the mountain range (Horst and Doran, 1986), the canopy layer (Sun et al., 2007), spatial variations in soil moisture (Banta and Gannon, 1995; Jensen et al., 2017), and the direction and intensity of the synoptic wind (Fitzjarrald, 1984; Doran, 1991). However, most of the investigations analysing the influence of those external factors are carried out using numerical simulations, and there is a lack of observational studies to validate them. ~~Hence, we firstly try to corroborate the findings from numerical experiments, particularly~~ Oldroyd et al. (2016) stressed the importance of adequately describing the conditions under which pure thermally-driven or katabatic flows form, versus downslope winds which have a partial dynamical contribution (further described in Chrust et al. (2013)). From our observational analysis of several events we particularly focus on how soil moisture and the large-scale wind affect the onset time~~and intensity of katabatic~~ , nature and different intensities of thermally-driven downslope winds, from an observational analysis of several ~~katabatic events. By way of example,~~ events.

Soil moisture acts enhancing or reducing the thermal component, whereas the large-scale flow introduces a dynamical input which can considerably intensify downslope winds and modify their onset time. Banta and Gannon (1995) carried out numerical simulations using a two-dimensional model and found that katabatic flows are weaker over a moist slope than over a dry one. They quantified a greater downward longwave radiation and soil conductivity under moister conditions, which gives rise to a reduced surface cooling. However, Jensen et al. (2017) found an opposite correlation, which they atributted to the sensitivity of the soil-moisture parametrisation in the numerical simulations. As a matter of fact, Sastre et al. (2015) showed with a numerical experiment ~~in~~ at contrasting sites that soil moisture differences do not affect the afternoon and evening transition values with the same intensity, but depending on the site. With respect to the background flow, by using a one-dimensional model, Fitzjarrald (1984) observed that the onset time of katabatic winds is affected by the retarding effect of the opposing synoptic flow and reduced cooling rates. ~~Our observational analysis aims at shedding light on the influence of those two external factors~~Jiménez et al. (2019) found that moderate background winds in the direction of the thermally-driven flow enhance the latter by adding a dynamical component.

On the other hand, knowing whether a certain night ~~katabatics~~ the downslope flows will be weak or intense enables us to predict how turbulence in the SBL will behave. It is well known that under weak large-scale wind, turbulence is weak and patchy (Van de Wiel et al., 2003, 2012a; Mahrt, 2014), giving rise to the so-called very stable boundary layer (VSBL). On the contrary, when the large-scale wind is strong, shear production increases substantially and turbulence is continuous, producing near-neutral conditions in the SBL (Mahrt, 1998; Sun et al., 2012; Van de Wiel et al., 2012b), and the so-called weakly stable boundary layer (WSBL). Being able to foresee the occurrence of these two regimes has been in the eye of many studies, and some attempts have been made to characterise the transition between the regimes using diverse criteria such as the geostrophic wind (Van der Linden et al., 2017), local (Mahrt, 1998) and non-local scaling parameters (Van Hooijdonk et al., 2015), and the wind speed (Sun et al., 2012). More or less directly continuous turbulence in the SBL has been linked with a stronger background wind (e.g. > 5–7 m s^{-1} in Van de Wiel et al. (2012b)) and low-level jets (Sun et al., 2012), or even with occasional irruption of sea-breeze fronts (Arrillaga et al., 2018).

~~Our aim is~~ Our second aim is therefore to explore the direct implication of ~~katabatic~~ thermally-driven downslope winds generated by the presence of steep topography, in the occurrence of the two SBL regimes.

A relevant aspect of our ~~emplacement~~ site is its location in a relatively small flat area ~~nearby~~ close to the mountain range. We therefore encounter a scenario different from other sites located at slopes where the SBL barely becomes very stable, since the shear production linked with the ~~katabatic~~ downslope wind is large and continuous, and buoyant turbulence production may occur even when the stable stratification is present (Oldroyd et al., 2016). In our ~~emplacement~~site, however, ~~very stable boundary layers~~ VSBLs associated with relatively strong surface-based thermal inversions take place ~~occassionally. Besides, over flat or almost flat terrain universal scaling according to Monin-Obukhov Similarity Theory (MOST) can be applicable and corrections due to measuring over a slope are not required (Stiperski and Rotach, 2016)~~ occasionally.

Connected also to the dynamics of the SBL, another relevant issue on this topic is the impact of ~~katabatic winds in~~ downslope winds of different nature on the concentration of scalars of high relevance such as the CO_2. Previous studies have documented its influence ~~at~~ in coastal areas (Cristofanelli et al., 2011; Legrand et al., 2016) and mountainous regions ~~(Sun et al., 2007) . Advection driven by katabatic winds can indeed dominate the total CO_2 transport; for instance,~~ (Sun et al., 2007; Román-Cascón et al., 2019) . Sun et al. (2007) found that downslope flows transported CO_2-rich air from the Rocky mountains, and Román-Cascón et al. (2019) observed that horizontal CO_2 advection can be relatively important over heterogeneous surfaces affected by different emission areas. Not only advection, but local turbulence fluxes can also be influenced: Sun et al. (2006) observed an anomalous positive CO_2 flux just after sunset, suggesting that it was due to the sudden transition from upslope to downslope flow. Being able to better quantify the influence of mesoscale flows on the CO_2 budget can help to reduce the large discrepancy from modelling studies in reproducing the land-atmosphere exchange for this gas (Rotach et al., 2014).

~~For the above-mentioned reasons, the main aspects that motivate research in this study, in short, are the following~~The aim of this work is to increase in the knowledge of:

[1] The external factors and physical processes that modulate the onset ~~of katabatic flowsand yield to different intensities~~time and nature of thermally-driven downslope flows.

[2] The interaction of ~~katabatic~~ these downslope winds with local turbulence ~~in the SBL~~ and the implication in ~~turbulent characteristics~~ the characteristics of the SBL.

[3] The role of ~~katabatic~~ advection and local turbulent fluxes, ~~associated~~ linked with the distinct downslope winds and the associated SBL regimes, in controlling CO_2 mixing ~~ratio~~ratios.

In order to shed light on those aspects, we perform an objective selection of ~~katabatic~~ downslope events and group them together according to their maximum wind speed, so that their intensity and the turbulent characteristics of the SBL are clearly associated. The article is structured as follows. We detail the observational data employed and the objective criteria for selecting ~~katabatic events in Section~~ downslope events in Sect. 2. Section 3 addresses the ~~principal~~ main characteristics of these events~~and~~ , explores the influencing factors ~~. We pursue~~ and the interaction with turbulence~~and the link with the different regimes in the SBL in Section~~. We pursue the analysis of representative events focusing on the underlying physical mechanisms and particular characteristics in Sect. 4. Section 5 deepens the analysis by inspecting in detail ~~two individual events, and estimates~~ the contribution of ~~the horizontal transport~~ downslope flows to the variability of ~~the CO_2~~ CO_2 concentrations. We finish with the relevant conclusions and two appendixes, which provide supplementary information about the footprint analysis and assessment of static stability in thermal profiles.

2 Data & Method

2.1 Site: La Herrería

The ~~emplacement for the observations used~~ observational site employed in this work (meteorological, soil and CO_2 mixing ratio) is located beside *La Herrería* Forest (40.582° N, 4.137° W, 920 m asl), from which the name is adopted. La Herrería is placed at the ~~foothills~~ foothill of the Guadarrama Mountain Range in central Spain, approximately 50 km NW of the city of Madrid (see Fig. 1a). ~~The emplacement chosen is a key aspect for the study carried out for various reasons explained below.~~

~~First, it~~ The site is placed at around 2 km from the steep slope of the Guadarrama mountain range (see Fig. 1b), which has an slope angle of around 25° in the main ~~katabatic~~ downslope direction (295°; approximately W-NW, from which the most intense ~~katabatic~~ downslope winds blow). The closest peak, Abantos, is 1763 m high, and the summit Peñalara is at 2420 m asl; both pointed in Fig. 1a. ~~Second, it~~

The site is close to a highly vegetated area to the W, being also close enough to the small urban areas of San Lorenzo de El Escorial to the NW and El Escorial to the E-SE. In addition, it is relatively close to the large metropolitan area of Madrid, where concern regarding high pollution levels has increased in the last years (Borge et al., 2016, 2018). The diffusivity of pollutants is highly affected by the presence of ~~down-basin~~ downbasin winds in the city and surrounding areas blowing from the NE (Plaza et al., 1997), which develop from converging ~~katabatic~~ nocturnal flows at the centre of the basin. Besides, the generation of ~~katabatic~~ downbasin drainages causes fog formation in the centre of the Iberian Peninsula, affecting visibility, amongst others, in Madrid-Barajas Adolfo Suárez airport (Terradellas and Cano, 2007). Understanding the ~~factors that modulate katabatic~~ mechanisms that modulate downslope winds in this region is therefore of high importance. ~~Third, the~~

The analysis is carried out during summer, a season that is characteristically very dry and warm and with nearly quiescent large-scale conditions in central Spain, even at the mountainous areas (Durán et al., 2013). The soil is particularly dessicated at the end of the season, which makes it different from other mountainous areas in Europe as the Pyrenees or the Alps. Summer 2017 was very warm and very humid (AEMET, 2017) in this region, following a very warm and very dry spring. In any case, it was not a particularly rainy season and in fact, precipitation during summer 2017 took place just over a few days, so that the dessicated soil experienced sharp moisture increases. This sets up a striking working frame to explore the role of soil moisture in the surface-energy balance and the ~~impact~~ associated consequences on the intensity ~~of katabatic~~ and nature of downslope flows. And finally, the area surrounding the station is located in ~~an~~ a relatively flat area (its slope angle is of around 2°) ~~immediately besides the~~ close to the Guadarrama mountain range (see Fig. 1b), which allows the formation of strong surface thermal inversions. These inversions are sporadically eroded by the ~~arriving katabatic~~ drained downslope flows, providing an interesting scenario for the investigation of the distinct SBL regimes.

Regarding the vegetation and land use, the observational site is placed in a pasture grassland with scattered ~~3–4~~ 3–5 m high shrubs and small trees, and the soil is composed of granite and gneiss. At around 2 km towards the SW, a broadleaved ~~decidious~~ deciduous forest is found, and at the same distance to the NW, approximately where the steep slope starts, a mixture of needleleaved evergreen (coniferous) tree cover and mosaic-tree and herbaceous cover. During ~~the katabatic stage~~nighttime, the footprint ~~can reach horizontally up to 200 m , lying~~ of the fluxes measured at 8 m lies broadly within the fetch of the ~~station~~

~~(Arrillaga et al., 2016)~~ surrounding area. Nevertheless, ~~under very stable conditions the footprint may increase substantially, which could induce uncertainty in the estimation of the turbulent fluxes and a possible impact of the urban area located to its NW. In any case, the direct implications of the urban area are negligible given the little traffic and the inexistent industrial activity~~the estimated footprint area can increase horizontally up to 150-200 m under very-stable conditions associated with the weakest downslope flows, inducing additional input from further inhomogeneities, although their contribution is generally small. An analysis of the calculated flux-footprint for three representative distinct downslope events is provided in Appendix A.

2.2 Data: Meteorological observations and post-processing

~~Eddy-covariance fluxes of energy, moisture and CO_2, and standard meteorological measurements are recorded over the warmest and driest season of the year, when thermally-driven slope winds are strongest and weak large-scale winds prevail.~~

Standard meteorological measurements and eddy-covariance (EC) fluxes are recorded in the 10-m high fixed tower in La Herrería. La Herrería tower is part of the Guadarrama Monitoring Network ~~(GuMNet, GuMNet (2018))~~(GuMNet, 2018) , which aims at providing observational meteorological and climatological records to deepen into scientific research in the mountainous area of *Sierra de Guadarrama* (Durán et al., 2018). ~~We record data~~ Data from aspirated thermometers, cup anemometers, radiometers, a wind vane and IRGASON devices among others ~~in a 10-m high fixed tower~~are recorded along the mast. From the IRGASON equipment the three components of the wind, temperature and $\mathrm{CO}^{\cancel{2}}_{2}$ measurements are obtained at high frequency (10 Hz), which allows the evaluation of different turbulent ~~fluxes~~parameters from the EC technique. Measurements of the ~~radiation components and the soil heat flux(G), as well as the calculated sensible-heat (H) and latent-heat (LH) fluxes, allow the analysis of the surface energy balance as well~~soil moisture are also taken.

~~Measurements~~ For this study, measurements were carried out over an intensive campaign in Summer 2017 (22/06–26/09)~~, with supplementary vertical levels~~. Supplementary instruments were deployed along the mast for additional measurements, including *inter alia* an extra IRGASON and radiometer. Table 1 gathers specifications about the devices and the variables employed in this study. ~~Depending on the instrumentation used and the variables measured, different sampling rates were employed . This information is also provided in Table 1~~All the variables are averaged over 10 min.

Main correction and processing procedures applied to raw high-frequency time series are based on the software from the EasyFlux DL program (Campbell-Scientific, 2017) , which provides fully corrected turbulent fluxes by applying some corrections frequently used in the related literature. The EasyFlux postprocessing software shows high correlation with the extensively used EddyPro software (Zhou et al., 2018) . Despiking of the high-frequency time series are carried out using diverse diagnostic codes and signal strengths. Turbulent parameters inferred from IRGASON measurements were discarded when the signal strength was below 0.9, associated mostly with high values of the relative humidity and/or precipitation. Nevertheless, that situation was rarely observed within the analysed database, since the algorithm employed and described in the following section ensures fair-weather conditions. Frequency corrections are applied by using transfer functions for block averaging (Kaimal et al., 1989) . An averaging time of 10 min was fixed for the calculation of turbulent parameters, which is considered standard for micrometeorological datasets (Mauritsen and Svensson, 2007) , and appropriate during the afternoon and evening transition of the ABL. The election of the averaging window was supported by multi-resolution flux decomposition analyses for few representative events (not shown). On the other hand, ~~all the variables employed in this analysis are averaged over 10 min.~~ the double-rotation method was applied to the sonic coordinate system (Kaimal and Finnigan, 1994) , so that errors in the measurement of the turbulent parameters associated with alignment issues were corrected. Other data-quality control checks include moisture corrections to the sonic temperature following Schotanus et al. (1983) to derive the air temperature and sensible heat flux, and air-density fluctuations were corrected by applying the WPL correction (Webb et al., 1980) to water-vapour and CO_2 turbulent fluxes. Additional minor corrections and quality-control checks are described in Campbell-Scientific (2017 Apart from those procedures, some other manual checks were considered. The results from the EasyFlux software were compared with the results obtained with our own programs, which also apply various postprocessing procedures. These, include quality-control checks and the rotation of the sonic-anemometer axes among others. The comparison showed high correlation and very good agreement.

2.3 ~~Method: Katabatic-detection criteria~~

~~The research strategy from Arrillaga et al. (2018) , in which they applied an objective and systematic algorithm to the observational data in order to select~~

2.3 Method: Downslope-detection criteria

The systematic and objective algorithm developed in Arrillaga et al. (2018) to detect sea-breeze events, ~~is followed. In this work, we~~ and adapted to select mountain-breeze occurrences in three different areas in Román-Cascón et al. (2019) , is used here. We adjust the algorithm for selecting events that fulfil predefined ~~katabatic criteria~~thermally-induced downslope criteria; i.e., when a shift of the wind direction is observed from the upslope to the downslope direction during the afternoon and evening transition, and always under a weak synoptic forcing. In this way, we evaluate the characteristics and impacts of the ~~katabatic~~ downslope flows in a more robust and objective way. Besides, the algorithm defines a benchmark which is the onset of the ~~katabatic~~ flow, enabling the clustering of different events and their analysis in a consistent way.

The algorithm consists of four different filters, which are shown in Table 2. The first three are coincident with the algorithm defined in Arrillaga et al. (2018), just modifying the precipitation-amount threshold for Filter 3: 0.5 instead of 0.1 mm/day, since weak and scattered showers (< 0.5 mm) do not alter the onset and development of ~~katabatic winds~~downslope flows. From detailed individual analysis we found that the large-scale conditions favourable for the formation of ~~katabatic~~ thermally-driven downslope flows are those that apply for sea breezes, i.e. quiescent synoptic forcing and not having the passage of synoptic fronts (Filters 1 and 2 respectively). This fact supports the strong value of this method. The last filter (Filter 4) is based on specific criteria for ~~katabatic~~ downslope flows in La Herrería, and was defined after a thorough inspection of the wind behaviour around sunset on days passing the first three filters. An event is selected as '~~katabatic~~downslope' when wind direction at 10 m is roughly perpendicular to the mountain-range axis (see Fig. 1a), i.e. within the range [250°–340°], for at least 2 ~~hours~~ h at a time between 1600 UTC and 2400 UTC (1800 and 0200 LT respectively). ~~The katabatic~~ With this filter, events mainly driven by downbasin flows (from the NE) are rejected. In any case, downslope events are occasionally, and during short periods, interrupted by downbasin winds.

The downslope flow usually lasts until sunrise, when a strong veering of the wind direction occurs. However, in this study we just focus on the first stage of these flows, since the main objective is to investigate their connection with the onset of the SBL (defined as when the sensible heat flux, H, turns negative), and the different regimes associated. During the summer months, the ~~katabatic onset usually takes place before sunset~~ onset of the downslope flow takes place usually before sunset, around 1800 UTC, but it can be considerably advanced or delayed depending on a number of factors, which are investigated in ~~See~~Sect. 3.2. A wide variability in the onset time of the katabatic flow was also reported in ~~the studies from Pardyjak et al. (2009) and Nadeau et al. (2013)~~ previous studies (Papadopoulos and Helmis, 1999; Pardyjak et al., 2009; Nadeau et al., 2013) .

We identify the onset of the ~~katabatic~~ downslope flow as the first value within the 2-h range of continuous ~~katabatic~~ downslope direction. Having that onset time as a reference, we explore the characteristics ~~of katabatic~~ and nature of downslope flows, their interaction with turbulence and the impact on CO_2 concentrations in the next sections.

3 Characteristics of the ~~katabatic~~ downslope flows

Forty ~~were selected as days with the formation of katabatic events~~ thermally-driven downslope wind events were selected from the analysed ~~summer period with available data~~ period (94 days in total). The algorithm is very rigorous to ensure that the selected events are ~~strictly thermally driven downslope flowsand not dynamically driven~~mainly thermally-driven downslope flows, since we just focus on the days with a weak large-scale wind in which there is a shift from the daytime upslope to the ~~night-time~~ nighttime downslope wind direction. The results presented hereinafter are related to these 40 ~~katabatic~~ downslope events.

3.1 Wind direction and intensity

~~Fig.~~ Figure 2 shows the direction and intensity of the ~~katabatic~~ selected events over the 2-h period subsequent to the onset of the downslope flow. The mean ~~katabatic~~ downslope direction is around ~~290–300~~295° and the variation around this direction is small; the largest oscillations in the direction are observed for weak intensities. Within the database of the 40 events we find diverse cases depending on the maximum intensity of the ~~katabatic~~ downslope flow. We represent in Fig. 3 the ~~wind vertical profile~~ vertical profile of the wind speed at the time of the ~~katabatic~~ downslope onset (a) and when the ~~katabatic intensity is maximum~~ intensity of the flow is maximum at 6 m (b) by using box plots, which contain information about the frequency distribution at each observational level (3, 6 and 10 m). At the time of the onset the ~~katabatic~~ downslope flow is weak at all levels (Fig. 3a); for instance the median at 10 m is slightly over 1 m s^{-1}. It can be noted that the median at 3 m is similar to that at 6 m, and the first quartile is even smaller at 6 m. This occurs because in some events prior to the identified onset at 10 m a very shallow katabatic or a skin flow is usually developed, and is only reflected at 3 m~~(as observed~~ . This skin flow (also denominated katabatic flow, as for instance in ~~Román-Cascón et al. (2015)) . This skin flow~~ Oldroyd et al. (2016)) can be observed when turbulence is very weak and thermal stratification is very stable ~~(Mahrt et al.~~

~~2001; Soler et al. 2002)~~(Mahrt et al., 2001; Soler et al., 2002; Román-Cascón et al., 2015) , and occasionally gives rise to a greater wind speed at 3 than at 6 m, and a few times even greater than at 10 m. However, when the ~~katabatic~~ downslope flow is more intense, wind speed increases with height within the 10-m layer from the surface (for instance note that the third quartile is greater at 6 than at 3 m). A maximum jet is probably found above 10 m, in accordance with the definition of *downslope flow* given in Oldroyd et al. (2016) , but we do not have the measurements to check it.

~~When the maximum katabatic intensity at 6 m is represented (Fig. 3b)~~ From Fig. 3b, the intensity distribution at all levels can also be observed, but in this case when the maximum 6-m wind speed is recorded. We find in this case that the distribution above the median is elongated at all levels. In fact, the level of 6 m is employed to classify ~~katabatic~~ downslope events according to ~~the~~ their maximum intensity and the associated erosion of the surface-based thermal inversion. The reasons for employing the level of 6 m are outlined below. Firstly, red crosses pinpoint an event identified as an outlier due to its high intensity at all levels (e.g. $U > 6$ m s^{-1} at 10 m). Together with the wind maximum, the surface thermal inversion is very weak or ~~inexistent~~non-existent, and the maximum of turbulence measured from the turbulent kinetic energy ($TKE = [(1/2)(\overline{u'^2}+\overline{v'^2}+\overline{w'^2})]^{(1/2)}$) and friction velocity ($u_* = [(\overline{u'w'})^2+(\overline{v'w'})^2]^{1/4}$) is even greater than the daytime maximum of the typical diurnal cycle (generally $u_{\cancel{*}}$$_{*,max}$ $\simeq$ 0.5–0.7 m s^{-1}). We find in addition two other events with the above-mentioned features which are included within the right whisker. These three events are classified hereinafter as intense ~~katabatics~~downslope events, and they all meet the criteria that the maximum ~~10-minutal~~ 10-min wind speed at 6 m is greater than 3.5 m s^{-1}. It must be noted that this threshold is not very high, but in the context of a weak synoptic forcing and comparing to the rest of the events, we can consider them to be relatively intense. Secondly, in some events turbulence is very ~~low~~ weak and the surface-based thermal inversion is not eroded ($u_* < 0.1$ m s^{-1} mostly). They all occur when wind speed is very weak, and hence we classify as weak events (14 in total) those in which the maximum wind speed at 6 m is below 1.5 m s^{-1}. The characteristics of these weak downslope flows conform with the definition of pure thermally-driven downslope or katabatic flows, as defined in Oldroyd et al. (2016) or Grachev et al. (2016) . Finally, the cases in which the maximum wind speed at 6 m is between 1.5 and 3.5 m s^{-1} are classified as moderate ~~katabatics~~ downslope flows (23 in total). A summary of the classification is shown in Table 3. ~~We employ the level of 6 m for the classification, since at~~ At the levels of 3 and 10 m the events showing different features cannot be so clearly detached, and therefore the level of 6 m is employed for the classification. Flocas et al. (1998) for instance studied katabatic flows at a similar height (7 m), since the influence of the large-scale wind was minimised at this level.

This classification is employed in the following sections to better illustrate the differences between the ~~katabatic events,~~ downslope events, their formation and development mechanisms, and the very distinct way in which they interact with local turbulence (in particular this is addressed in ~~Secs~~Sects. 4 and 5).

3.2 Factors influencing intensity

Once the ~~katabatic~~ downslope events are classified according to their maximum intensity, we first explore the factors that induce different intensities. ~~Fig.~~ Figure 4 shows a histogram with the difference between the onset time of the ~~katabatic~~ downslope flow and sunset time (it ranges from 1810 UTC in September to 1940 UTC in June), for different intensities in colours, and in lines for ~~different thermal stratification~~ a different static stability of the thermal profile at the moment of the onset. ~~To calculate the~~

~~thermal stratification we fitted~~ Values of the net radiation (R_n) and TKE are also indicated. The static stability was estimated by fitting the virtual potential temperature at the different vertical levels (~~soil~~surface, 3, 6 and 10 m) to a logarithmic profile~~. The soil~~, as explained in detail in Appendix B. Virtual potential temperature was calculated ~~from the upward longwave radiation. The fitting was carried out as follows:~~

$$\theta_v(z,t) = \alpha(t) + \beta(t)ln(z) + \gamma(t)ln^2(z) + \delta(t)ln^3(z).$$

~~The type of thermal stratification is inferred from the value of δ at the moment of the onset, and subsequently classified into the subsequent three groups:~~

$$Unstable: \quad \delta(t=onset) < -0.3\ Km^{-3},$$

$$Neutral: \quad -0.3\ Km^{-3} \leq \delta(t=onset) \leq 0\ Km^{-3},$$

$$Stable: \quad \delta(t=onset) > 0\ Km^{-3}.$$

~~From this classification~~ using measurements from aspirated thermometers and a T/RH probe (see Table 1). The skin temperature was calculated from the upward longwave radiation by employing the Stefan-Boltzmann law.

From the classification introduced in Appendix B we infer the relationship between the earlier or later onset of the ~~katabatic wind,~~ downslope wind, turbulence and the associated thermal stratification at the moment of its onset, and the intensity of the flow. On the one hand, intense ~~katabatics~~ downslope flows develop when the onset takes place prior to ~~2~~ 1.5 h before sunset~~and the stratification in~~, the stratification within the first 10 m is still unstable, and R_n and TKE are always greater than 80 W m^{-2} and 0.8 m^2 s^{-2} respectively. On the other, weak ~~katabatics~~ downslope or katabatic flows occur when the onset takes place later than ~~2 hours~~ 1.5 h before sunset and with neutral or stable stratification. ~~Moderate katabatics, however, can occur either earlier or later independently of the stratification.~~

~~Linked with the three different thermal-stratification regimes defined in Eq. ??, we explore the influence of the TKE at the onset of katabatic flows from Fig. ??a. By representing the maximum katabatic intensity at 6 m with respect to the TKE at the onset, two main groups result. In one of them TKE is very low at the onset~~ In this case TKE is almost an order of magnitude smaller (in the order of or smaller than 0.1 m^2 s^{-2}), ~~which includes all the weak katabatics. This group is associated with a later onset of the katabatic flow (Fig. 4), when the thermal stratification is already neutral or stable and~~ and R_{net} R_n < 40 W m^{-2} always; it is in fact negative in more than 80 % of the cases. ~~On the other group, TKE is about one order of magnitude greater and includes all the intense events, which are related with an earlier katabatic onset, when the thermal stratification is already unstable. R_{net} is in fact always > 80 W m^{-2} at the onset~~ Moderate downslope flows, however, occur either when the onset takes place earlier or later, and hence independently of turbulence and the associated thermal stratification.

~~This result implies that there is a strong relation between katabatic flows and turbulence, which is essential to fully understand their nature and development. This aspect is further addressed in Sect. 4. Regarding the moderate katabatics, we separate them into two subgroups: $U_{max} \leq 2.5$ m s^{-1} (triangles pointing downward) and $U_{max} > 2.5$ m s^{-1} (triangles pointing upward). Even though the weaker moderate katabatics are mostly related with the stable and neutral stratification and the more intense~~

~~moderate with the unstable stratification, the opposite occurs also in few of the cases.~~ This result suggests the existence of external factors affecting the earlier or later onset of ~~katabatic winds. For the reasons outlined in the introduction, we investigate two factors:~~ downslope winds. Particularly we focus on the soil moisture and the large-scale wind.

To explore the influence of soil moisture, we define an index that provides a measure of the relative dessication of the soil over the summer. This soil-moisture index is defined as the ratio between the observed liquid water volume and the maximum value throughout the analysed period (0.14 m^3 m^{-3}): $SM_i = SM/SM_{max}$. We separate the events into drier ($SM_{\rm i} \leq 0.5$) and moister ($SM_i > 0.5$) cases. On the other hand, to explore the influence of the large-scale wind ($V_{850,18}$: at 850 hPa at 18 UTC) ~~despite its low intensity required by the selection algorithm,~~ we separate the ~~katabatic~~ downslope events into very weak ($V_{850,18}$ $\leq$ 3.5 m s^{-1}) and weak ($V_{850,18}$ > 3.5 m s^{-1}) synoptic forcing.

The influence of the large-scale wind speed and direction, and soil moisture, are investigated in Fig. 5. The maximum ~~katabatic~~ downslope intensity at 6 m together with the direction of the synoptic wind are represented in wind-rose form for the ~~abovementioned~~ above-mentioned drier (a,b) and moister (c,d) cases, and for a very weak (a,c) and weak (b,d) synoptic forcing. The synoptic wind is estimated from the NCEP reanalysis wind speed employed in the selection algorithm, by choosing the grid point at 850 hPa closest to La Herrería (40.5° N, 4° W) at 18 UTC. At that point, the 850-hPa level is approximately at 800 m ~~agl~~above ground level (agl), sufficiently close to the surface as to be representative of the synoptic wind at the surface level, and far enough as to be out of the influence of ~~katabatic flows.~~ downslope winds.

We find that intense ~~katabatics~~ downslope flows (orange-reddish) develop when the soil is drier, the large-scale wind is weak and blowing from the N-NW (Fig. ~~2~~5b). This direction is perpendicular to the mountain range axis (Fig. 1a), and approximately coincident with the ~~katabatic~~ downslope direction (Fig. ~~2~~5). However, under those conditions we find weak ~~katabatics~~ downslope or katabatic flows (dark blue) when the large-scale wind blows from parallel or opposite directions (S or E-NE for instance), although most of the ~~weak~~ katabatics occur mainly when the soil is moister and the synoptic forcing is very weak (Fig. ~~2~~5c). ~~Weak katabatics~~ Katabatic flows establish primarily for W-SW and S-SE large-scale winds, but they can also occur for N-NW winds when their intensity is very weak (Fig. ~~2~~5a). Overall, the intensity of ~~katabatics~~ downslope winds increases with decreasing soil moisture, and increasing synoptic forcing with a N-NW direction.

~~To study the~~ The role of the soil moisture ~~and the relative dessication of the soil~~ in the surface energy balance, ~~we represent the observed average G and~~ is in general, complex. The longwave-radiative ~~loss (LWU–LWD) during the katabatic stage with respect to the SM_i in Figure **??**. To better show the trends of the scatter plots, a 4-th order polynomial fitting has been added. Both G and LWU–LWD show two maxima for high and low SM_i, at around 0.9 and 0.2–0.3 respectively. The peak for low SM_i is more pronounced, and implies that the cooling of the soil is stronger~~ loss and soil-heat flux show a peak when the relative dessication ~~is higher, since the average G is positive (opposing to $G < 0$ for the secondary peak)and the longwave-radiative loss is greater~~of the soil is large (not shown). However, ~~when the soil moisture increases considerably~~ after precipitation has occurred ~~($SM_{\rm i} \simeq 0.9$),~~ soil moisture increases considerably and the cooling of the soil can also be enhanced~~, inducing an enlarged thermal contrast between the slope and the overlying air layer, and therefore contributing to the intensification of the katabatic flow. The contrasting findings from Banta and Gannon (1995) and Jensen et al. (2017) for the impact of the soil~~

~~moisture in the katabatic intensity could be explained by this bimodal behaviour~~. This bimodal behaviour is in any case vague and ambiguous, and it must be supported by more conclusive observational results.

Overall, we ~~can conclude~~ find that the combination of low soil moisture~~and~~ , which enhances the thermal forcing, and the synoptic wind direction coincident with the downslope direction (N-NW), adding an important dynamical contribution, induces an earlier onset of ~~katabatic flows,~~ downslope flows. The onset occurs when stratification is still unstable and convective turbulence relatively strong, which ~~facilitates~~ enables the development of intense ~~katabatic~~ downslope flows. If those conditions are not met, the onset occurs later when stratification is already neutral or stable, which limits the intensification of ~~katabatic flows. Nevertheless, sharp enhancements in the soil moisture due to precipitation can give rise to a stronger cooling of the soil and an earlier onset of the katabatic flow.~~ downslope flows. To understand the evolution of ~~katabatic~~ downslope flows after their onset we explore their interaction with turbulence in the next ~~section~~subsection.

4 ~~Interaction between katabatics and turbulence~~

3.1 Interconnection between downslope flows and turbulence

Thermal stratification and the associated turbulence at the moment of the onset modulate the intensity ~~of the katabatic~~ and subsequent development of the downslope flow. If the ~~katabatic~~ downslope flow arrives when the stratification is still unstable and the surface thermal inversion (hereinafter measured from $\Delta\theta_v$) is not formed yet, the ~~shear associated with the katabatic flow increases, and the~~ downslope flow strengthens progressively. Later, due to the radiative energy loss ($R_{\cancel{net}n} < 0$) the stable stratification is already established ($\Delta\theta_v > 0$), and the katabatic (thermal) contribution of the downslope flow is enhanced. Given that ~~turbulence associated with wind shear~~ the wind shear associated with the downslope flow is already high, the negative H strengthens ($H < 0$) and after a while compensates the energy loss at the surface, impeding the development of the surface-based thermal inversion and inducing near-neutral stability conditions (Van de Wiel et al., 2012a) . In that way, intense ~~katabatics~~ downslope flows give rise to a ~~weakly stable boundary layer~~WSBL. On the other hand, ~~if the katabatic wind arrives laterand thermal stratification is already neutral or stable~~without a clear dynamical contribution of the large-scale flow, the downslope flow is established later, when negative buoyancy of the air adjacent to the surface enhances the katabatic input. However, this katabatic flow is not intense enough as to increase turbulent mixing substantially. Besides, the increase of ~~shear is~~ the downslope intensity and the associated wind shear are limited by the stable stratification itself. Thus, even the maximum sustainable heat flux does not compensate the radiative energy loss. Consequently, the bottom of the SBL cools down, which contributes to enhance the stable stratification. This positive feedback occurring under weak ~~katabatics~~ downslope flows suppresses turbulence and gives rise to a ~~very stable boundary layer~~VSBL (Van de Wiel et al., 2012b) . For moderate ~~katabatics~~downslope flows, any of the two regimes can occur depending on the onset time and the ~~surface-energy balance~~dynamical contribution of the large-scale flow. These mechanisms are explored ~~below by means of measured variables and calculated nondimensional relevant parameters~~in the following sections.

3.2 ~~Turbulence regimes in the SBL~~

Figure 6 shows the temperature stratification ~~$\Delta\theta_v$ and~~ $\Delta\theta_v = \theta_v$ (10 m) - θ_v (3 m), the turbulence velocity scale V_{TKE} and ~~*vs*~~H with respect to U at 6 m. ~~In this and subsequent figures we~~ V_{TKE} is calculated as the square root of the TKE. We just represent the 10-min average values ~~(just until 24 UTC)~~ in which the wind direction is ~~katabatic~~ downslope (until 2400 UTC) and H is negative, so that the ~~katabatic~~ downslope flow is present (not for instance the downbasin wind) and the SBL is already established. ~~V_{TKE} is calculated as the root square of the TKE.~~ By representing $\Delta\theta_v$ *vs* U we find a contrasting relationship for weak and intense ~~katabatics~~ downslope flows (Fig. 6a). ~~Weak katabatics~~ Katabatic flows give rise to a strongly stratified SBL ($\Delta\theta_v$ up to 2 K), whereas intense ~~katabatics~~ downslope flows are linked with very weak or almost ~~inexistent~~ non-existent surface-based thermal inversions. Interestingly, for ~~few 10-minutal~~ a few 10-min values with similar wind speed ($U \simeq$ 1–1.5 m s^{-1}), the thermal stratification is very different between weak and intense ~~katabatics~~downslope flows, which suggests the existence of distinct regimes in the SBL. On the other hand, we find for very weak wind speed (U < 1 m s^{-1}) a large variability of thermal stratification, that occurs because around the onset of ~~katabatics~~ the downslope flow the thermal inversion is still absent or very weak in most of the cases. At the upper limit, however, $\Delta\theta_v$ tends to zero when wind speed increases its value. Moderate ~~katabatics~~ downslope flows show both types of behaviour, with the transition taking place for $U \simeq$ 1.5 m s^{-1}.

By representing the turbulence strength V_{TKE} *vs* U at 6 m we confirm the sharp transition for U = 1.5 m s^{-1} (Fig. 6b). ~~Weak katabatics~~ Katabatic flows are associated with very weak turbulence (V_{TKE} < 0.5 m s^{-1}) that hardly increases with wind speed, while turbulence for intense ~~katabatics~~ downslope flows is considerably greater and increases ~~linearly~~ approximately at a linear rate with U. This behaviour was first observed in Sun et al. (2012), and defined as the HOckey-Stick Transition (HOST) in Sun et al. (2015). They identified three turbulence regimes in the SBL depending on the relationship between turbulence and wind speed. In ~~regime~~ Regime 1 turbulence is very weak and generated by local shear; in ~~regime~~ Regime 2 turbulence is strong and generated by the bulk shear U/z (hence the linear relationship with wind speed); and finally, in ~~regime~~ Regime 3 turbulence is moderate and mainly generated by top-down turbulent events. The three regimes are pinpointed in Fig. 6b. The threshold value for the wind speed depends on height, and sets the value above which the abrupt transition from ~~regime~~ Regime 1 to ~~regime~~ Regime 2 occurs. Since in our case z = 6 m, it is indicated as V_6 in the figure. ~~Weak katabatics~~ Katabatics are clearly associated with ~~regime~~ Regime 1 and intense ~~katabatics~~downslope flows, instead, with ~~regime~~ Regime 2. Moderate ~~katabatics~~ downslope flows can give rise to either the three of the regimes. We just show the relationship for z = 6 m, and HOST in our case occurs for V_6 = 1.5 m s^{-1}, which is significantly lower than the value at that height from Sun et al. (2012) ($\simeq$ 3 m s^{-1}) over relatively flat and homogeneous terrain (Poulos et al., 2002). This lower threshold could be partly induced by the proximity of the jet maximum, as for instance is shown in Fig. 8). Besides, V_6 coincides with the threshold value we anticipated for defining ~~weak katabatics~~ katabatic flows (Table 3). We measure a slope of $\sim$0.5 for *VTKE* vs U for regime 2, while is of $\sim$0.25 in the results from Sun et al. (2012).

In Fig. ~~??~~ 6c we explore how ~~katabatic~~ downslope intensities and turbulence strength are manifested in terms of heat flux. The downward H~~(~~, i.e. when the SBL is already established ~~:~~ (H < 0)~~is represented with respect to U at 6 m in Fig. ??~~, is represented in absolute values. The smallest H values are observed for ~~weak katabatics~~katabatic flows, when U < 1 m s^{-1}. The highest values take place for moderate ~~katabatics~~ downslope flows when U lies between 1.5–2.5 m s^{-1}. We find a few data from some intense ~~katabatics~~ downslope flows in which H is nearly ~~0~~ zero for that wind-speed range, when the thermal inversion ~~is still very weak~~has just been formed. For intense ~~katabatics~~ downslope winds the peak is reached at $U \simeq 3$ m s^{-1}, and above that intensity H decreases, since it is limited by the neutral stratification. ~~One of the key questions is whether this heat flux is able to compensate the surface radiative loss. This matter is addressed later in Sect. 4.1 by analysing the time evolution of the surface-energy balance on individual events .~~

3.2 ~~Regime transition from non-dimensional parameters~~

So far we have explored all the selected downslope events together, and learnt about their main characteristics, influencing factors and connection with the SBL regimes. We have observed ~~in Sect. **??** that~~ how the turbulent characteristics of the ABL and the nocturnal regime can be predicted from the ~~katabatic intensity~~ intensity of the downslope flow at 6 m. ~~In fact, by knowing in advance its maximum value during the night we can foresee whether the katabatic wind will give rise to a very stable regime or a near-neutral regime within the SBL. In Fig. **??** we characterise the regime transition from relevant non-dimensional numbers by representing V_{TKE} at 4 and 8 m as a measure of turbulence intensity with respect to three nondimensional parameters, both local and non-local. As stated in Sun et al. (2016) , Monin-Obukhov Similarity Theory (MOST) is only applicable in a thin layer above the surface (up to approximately z = 10 m) during SBLconditions. Since our measurements do not exceed that height, we can assume that MOST is complied in the subsequent calculations~~However, in order to better understand the mechanisms underlying their formation, development and their complex interaction with turbulence in the SBL, we target the analysis of individual representative events.

~~First, we investigate the use of a non-local parameter: the shear capacity (SC). It is derived from the TKE-budget equation by ignoring the transport and pressure-covariance terms. This dimensionless quantity was first introduced by Van Hooijdonk et al. (2015) , and it compares the measured shear with the minimum shear required to maintain a continuously turbulent state, which is given by the heat-flux demand (HFD) at the surface. The HFD is calculated from the surface-energy balance as $HFD = R_{net} - G - LH$. SC is therefore used to predict the regime transition from the weakly stable boundary layer to~~

4 Analysis of representative downslope events

We choose representative weak, moderate and intense downslope events, so that their contrasting features and distinct influencing mechanisms are revealed. The weak downslope event is August 13 and is characterised by the presence of a katabatic flow and a VSBL. In short, the synoptic situation was marked by the ~~very stable boundary layer, or viceversa. Since turbulence responds to~~ Azores high and a thermal low over the Iberian Peninsula inducing a weak S flow, which was related to a weaker downslope intensity in Fig. 5. The SM_i was high for this case. The moderate event is July 25, and this day the synoptic situation was also characterised by the Azores high, but in this case with a weak NE forcing, coinciding with the direction of the downbasin winds in the basin in which La Herrería is located. Besides, the soil moisture was low. This event was marked by the interaction between local downslope and downbasin winds. Finally, the intense event is July 27, again marked by the Azores high, but with a weak NW forcing coinciding with the direction of downslope flows, adding a dynamical input to the local flow. Soil moisture was also low for this case. In addition to the ~~bulk shear instead of the local shear for a wind speed $U > V_6 = 1.5$ m s^{-1}, we define the SC in this work as:~~

$$SC(U < 1.5\ m\ s^{-1}) = \left\{ \frac{\rho C_p (\kappa z)^2 \left(\frac{\partial U}{\partial z}\right)^3}{g/\theta_v(z)\ |HFD|} \right\}^{1/3},$$

$$SC(U > 1.5\ m\ s^{-1}) = \left\{ \frac{\rho C_p (\kappa z)^2 \left(\frac{U}{z}\right)^3}{g/\theta_v(z)\ |HFD|} \right\}^{1/3}.$$

strong turbulence associated with the intense downslope flow, this event is chosen due to its particular influence on the CO_2 transport, which is addressed in Sect. 5.

4.1 Origin and underlying physical mechanisms

In previous sections we have shown that external factors such as soil moisture and the synoptic wind modulate the intensity of downslope winds, which is at the same time linked with an earlier or later onset time. In order to understand the physical processes underlying the formation and subsequent evolution of the downslope flows, the momentum and heat budgets for the three individual events are explored following the two-dimensional simplified equations from Manins and Sawford (1979) , which were employed in the recent studies from Nadeau et al. (2013) and Jensen et al. (2017) . The slope-parallel momentum and heat budgets are respectively given by:

$$\frac{\partial \overline{u}}{\partial t} + \overline{u}\frac{\partial \overline{u}}{\partial s} + \overline{w}\frac{\partial \overline{u}}{\partial n} - \frac{g\overline{d}sin\alpha}{\overline{\theta_{va}}} + \frac{\partial \overline{u'w'}}{\partial n} + \frac{1}{\overline{\rho}}\frac{\partial(\overline{p} - \overline{p_a})}{\partial s} = 0,$$

$$(I) \quad (II) \quad (III) \quad (IV) \quad (V) \quad (VI) \tag{1}$$

$$\frac{\partial \overline{\theta_v}}{\partial t} + \overline{u}\frac{\partial \overline{\theta_v}}{\partial s} + \overline{w}\frac{\partial \overline{\theta_v}}{\partial n} + \frac{\partial \overline{w'\theta_v'}}{\partial n} + \frac{1}{\overline{\rho} c_p}\frac{\partial \overline{R_n}}{\partial n} = 0,$$

$$(I) \quad (II) \quad (III) \quad (IV) \quad (V) \tag{2}$$

~~θ_v is the virtual potential temperature, κ is the von Kármán constant (=0.4), zis the height agl, $\partial U/\partial z$ is the local shear, U/z the bulk shear,~~ where s and n are the slope-parallel and slope-normal coordinates in accordance with the double-rotation of the axes, t is time. u is the streamwise wind, ~~g~~w the ~~gravitational acceleration~~ slope-normal wind, $d = \theta_v - \theta_{va}$ is the temperature deficit defined as the difference between the perturbed vitual potential temperature and the unperturbed potential temperature, α ($\simeq 2°$) is the slope angle, g = (9.81 ~~), ρ is~~ m^2 s^{-2}) gravity acceleration, ρ the air density, ~~Cp~~ p is the measured local pressure, p_a the ambient pressure field and c_p ~~the specific heat at constant pressure~~(= 1005 J kg^{-1} K^{-1}) ~~and |HFD| is the absolute value of~~

~~the HFD at surface, since SC is defined only when $\overline{w'\theta_v'} < 0$. $\partial U/\partial z$ was computed by fitting the wind measurements at 3, 6 and 10 m to a log-linear profile as in (??).~~ the specific heat of the air at constant pressure. The bar is used for indicating 10-min time averaging, and the primes indicate a perturbation from the temporal mean.

~~Van Hooijdonk et al. (2015) observed over flat and homogeneous terrain thatindependently of the measurement height they could define a SC value ($\simeq 3$) for which the transition from very-stable (low SC values) to weakly-stable conditions (higher SC values)occurred. In this work we calculate the SC at~~ Term I in Eq. 1 represents momentum storage, terms II and III represent horizontal and vertical advection respectively, term IV is buoyancy acceleration, term V the momentum turbulent flux divergence and term VI represents the along-slope pressure gradient. Regarding the heat-budget equation (Eq. 2), term I is the heat storage, terms II and III horizontal and vertical advection respectively, term IV the kinematic heat flux divergence and the last term represents R_n divergence. For the calculation of $\overline{d}$, the difference between the levels of 2 and 20 m is calculated (as in Jensen et al. (2017)). For that, the values are obtained from the vertical extrapolation from the fit to the logarithmic profile (see Eq. B1). All derivatives are evaluated using forward finite differences, between the levels of 4 and 8 m ~~(Fig. ??a and b respectively), and we find two transitions (indicated with dashed vertical lines) : the first at $SC = 3$ above which both SBL regimes are almost equally found,~~ in term V in Eq. 1 and term IV in Eq. 2, and between the levels of 1 and 2 m in term V in Eq. 2. On the other hand, the terms with slope-parallel gradients are considered residuals of the equations due to the lack of additional spatial measurements, and vertical advection in both equations (term III) is null ($\overline{w} = 0$) due to the imposition from the double-rotation method. 10-min averages are used.

The times series of these terms are represented and compared in Fig. **??** for the representative weak, moderate and intense downslope events, from 1600 UTC until 2400 UTC. Due to the lack of spatial gradients, the ~~second at $SC = 4.5$, over which the SBL is always weakly stable. The observed transition is independent of height, but we are unable to select a single value for separating the weakly stable and very stable regimes. Instead, the shift between the regimes seems to occur along a transition regime, within which both intense a weak katabatics are observed. The transition is directly related with the HOST hypothesis, given that the SC is predominantly dominated by wind shear. As a matter of fact the hockey-stick shaped plot of Fig. ??b resembles Fig. 6b, except that the regime transition is sharper for the SC: intense and weak katabatics cluster into two clearly distinct regimes according to the dependence on local or bulk shear. The transition is less sharp at 4 m, since at this levellocal and bulk shear are closer than at 8 m.~~ estimation of the residual has some uncertainty in particular for the momentum budget, since there are two terms within the residual of Eq.1 and only one in Eq. 2. In any case, the comparison between the three events explains the differences in the physical mechanisms underlying the formation and development of the distinct downslope flows. While the vertical axis for the heat budget is kept constant and is limited to 0.02 K s^{-1} for better showing the differences, it is variable for the momentum budget due to the highly distinct relative weight of the different terms.

~~Two other local non-dimensional numbers are investigated: z/L and R_B, being the L the Obukhov length and R_B the bulk Richardson number (Stull, 1988) . They are frequently employed in the literature as stability parameters and turbulence-production indicators, with local significance. As occurs for the SC, when representing V_{TKE} versus z/L and R_B at 4 and 8 m the transition occurs over a range of values. This transition region was also observed by Mahrt (1998) . He found~~ Prior to the onset of the weak downslope flow (Figs. **??**a and **??**b), the bottom of the surface layer cools down driven mainly by the kinematic heat flux divergence, as observed in the analysis from Jensen et al. (2017) , whereas momentum is produced by the turbulent-flux divergence. This suggests the formation of a very shallow flow below the lowest observational level before the recorded onset. After the onset, the main source of momentum is buoyancy acceleration driven by the local surface cooling, in principle balanced by large-scale pressure and advective terms. This mechanism conforms also with the findings from Nadeau et al. (2013) , confirming that weak downslope winds share the characteristics of katabatic flows. The cooling after the onset is primarily ruled by the heat-flux divergence, compensated by the heating produced by the radiative divergence. Despite the radiometers had previously been calibrated by being compared at the same level, the calculation of the divergence can be subject to errors due to the closeness (= 1 m) between the devices. Furthermore, Steeneveld et al. (2010) eliminated the radiative measurements coinciding with wind speed at 10 m ~~that $z/L = 0.065$ is the limit for the weakly stable boundary layer and $z/L = 1$ for the very stable boundary layer. We set respectively these values at 0.05 and 0.25 at 4 m (Fig. **??**c), and 0.1 and 0.5 at 8 m (Fig~~below 1.5 m s^{-1}, to assure that radiometers were sufficiently ventilated. Hence, there might be certain uncertainty in the estimation of the radiative divergence, and the advective term could be responsible for balancing the cooling otherwise. In addition, this event shows a sudden turbulent burst at around 2400 UTC (which can be observed in Fig. 8a). ~~**??**d), the latter coinciding with the value found by Högström (1996) . This threshold appears to be very strong, since above it no intense katabatics are found. The regime transition is fuzzier for R_B, in particular the threshold for the weakly stable regime is difficultly identified~~ It produces an upward momentum transport from the skin flow and a sudden warming due to turbulent mixing, demonstrating that the very stable regime may be occasionally interrupted.

The onset of the moderate downslope event (Figs. ~~**??**e and f) . However, it should be taken into account that by definition this nondimensional parameter estimates wind shear from finite differences in height. It does not consider whether wind shear is produced by bulk or local shear, and it will be closer from one or~~ **??**c and **??**d) takes place rather earlier. According to the momentum budget, either advection or the ~~other depending on the vertical-level separation. In any case, we find that at $\sim R_B$ = 0.3–0.35 turbulence production has decayed so that the very stable regime is established, between~~ along-slope pressure gradient, or both, are responsible for the intensification of the downslope flow when the buoyancy acceleration is still negative. When R_n turns negative the downbasin wind arrives, and due to the collision between both, turbulence decreases and the further intensification of the downslope flow is prevented. Due to the interaction between the downbasin wind (NE) and the downslope flow (NW), turbulence is intermittent and of variable intensity, and the momentum balance is marked by the oscillating equilibrium between the momentum-flux divergence and the advective and pressure-gradient terms. Regarding the heat budget, the ~~measured critical values for the gradient Richardson number $Ri_c = 0.25$ and bulk Richardson number $R_B = 0.5$ (Stull, 1988) . Among the three nondimensional parameters, *SC* seems to be the sharpest and most adequate in foreseeing the regime transition~~main source of cooling is advection, even after R_n turns negative. After 2000 UTC, however, the advection produces warming and compensates the cooling from the heat-flux divergence.

5 ~~Analysis of representative katabatic events~~

~~So far we have explored all the selected katabatic events together, and learnt about their main characteristics and connection with the SBL regimes. However, in order to better understand the mechanism behind the complex interaction between the katabatic flow and turbulence in~~ During the intense event (Figs. **??**e and **??**f), the governing forcing in driving the intensification of the downslope flow is dynamical: either or both advective and large-scale pressure terms dominate over the local buoyancy acceleration, and are balanced by the turbulent-flux divergence. Given that the slope of the nearby mountain towards the NW is steep ($\simeq 25°$), and with an enhanced temperature deficit due to the ~~SBL, we target the analysis of individual events.~~ greater dessication of the soil, the buoyancy-acceleration term is considerably greater over the slope than in La Herrería. Furthermore, the mountain-range axis is directed SW-NE, so that sunset takes place at the back of it. Therefore, the cooling starts before along the slope than in La Herrería. The heat budget shows that before R_n turns negative, the source of cooling is advection from the slope, compensating the radiative heating. These findings confirm that the origin of the early flow is the advected cold drainage front from the nearby steep slope. Later, the main sources of cooling are the heat-flux divergence and the radiative divergence from 2100 UTC on, which are compensated by the warm advection. In any case, the cooling from the heat-flux divergence is smaller than in the moderate event, due to the constrain from the weak thermal stratification. A similar situation was reported in Papadopoulos and Helmis (1999) , where the flow reached the foot of the slope as a drainage front from more elevated cold-air sources, before the establishment of the thermal inversion. This earlier onset at the foot was observed when relative humidity was lower at the slope site, when the local thermal structure did not sustain katabatic motion, as occurs in our intense downslope event. They showed how advective effects dominated in this case and the arrival of the drainage front produced a temperature fall. Additionally, going along with our findings, they observed that the growth rate of this downslope flow was more intense due to weaker ambient stability, whereas the existence of a surface-based thermal inversion opposed the flow progression.

4.1 ~~Inspecting individual events~~

4.1 Nature and interaction with turbulence

~~We choose a weak and an intense event, so that their contrasting features are revealed. The weak event is August 13 and shows~~ After inspecting the physical mechanisms underlying the different evolution of the ~~presence of a skin flow and a very stable SBL regime. In short, the synoptic situation was marked by the Azores high and a thermal low over the Iberian Peninsula inducing a weak S flow, which was related with a weaker katabatic intensity (Fig. 5). The intense event is July 27, and this day the synoptic situation was also characterised by the Azores high, but in this case with a weak NW forcing, associated with greater katabatic intensity. In addition to the strong turbulence associated with the intense katabatic flow, it is chosen due to its particular influence on the CO_2 transport, which is addressed in Sect. **??**.~~

~~To determine how turbulence in the surface layer responds to both katabatic events, we start our analysis showing u_* in Fig. **??**a. The onset of the intense katabatic takes place around 1640 UTC during the afternoon transition of the ABL. After this time, u_* continues increasing slowly up to 0.5–0.6 m s^{-1} at 8 m when the SBL is already developed at around 2000–2100 UTC, and even up to 0.9 m s^{-1} later, exceeding the value associated with the diurnal peak. For the weak event the values of u_* at around~~

~~1600–1700 UTC are similar to the intense event, but by the time the katabatic flows arrives (at 1830 UTC, coinciding with the moment at which R_{net} turns negative), u_* has already decreased down to 0.1–0.15 m s^{-1}. Except for some sporadic bursts at~~ three representative downslope events, we characterise the associated wind and thermal profiles, as well as the interconnection of the flow with local turbulence, in Figs. 8, 9 and 10, for the weak, moderate and intense downslope events respectively. We show the time series of thermal stratification and friction velocity at 8 ~~m, probably induced by isolated top-down turbulence turbulent events, u_* is maintained below 0.1 m s^{-1}, revealing the presence of the very stable regime.~~

m in (a). Vertical profiles of ~~U and θ_v are shown below (Figs. **??** (b-g)) at three relevant stages~~the wind speed (b), θ_v (c) and heat and momentum horizontal turbulent fluxes (d) are shown below at three times of interest: at the moment of the ~~katabatic~~ onset, when ~~R_{net}~~R_n turns negative and finally at ~~2100~~ 2230 UTC when the SBL is already well formed. The logarithmic fitting of the discrete observed ~~profiles for both variables and~~ measurements for both wind speed and θ_v is also depicted in (b) and (c). With respect to the turbulent fluxes, we can infer from their sign whether the jet associated with the downslope flow is located below or above the measurements (Grachev et al., 2016; Oldroyd et al., 2016) . At the height of the wind-speed maximum both turbulent fluxes become zero, and above the jet $\overline{u'\theta_v'} < 0$ and $\overline{u'w'} > 0$, whereas below the jet $\overline{u'\theta_v'} > 0$ and $\overline{u'w'} < 0$.

Prior to the onset of the weak downslope or katabatic flow, the ~~measurements are shown. As stated in previous sections, intense katabatics arrive earlier in La Herrería when the stratification is still unstable, which is clearly inferred from Fig. **??**c. In contrast, the weak katabatic arrives when R_{net} turns negative and the stratification is already stable~~thermal stratification turns positive (Fig. 8), which induces the increase of the buoyancy-acceleration term as shown in Fig. **??**. However, the local slope is shallow, and in the absence of a dynamical contribution from the nearby steep slope, the katabatic flow and the associated turbulence are very weak. u_* is maintained below 0.1 m s^{-1} throughout most of the event, revealing the presence of the VSBL. In fact, the thermal inversion strengthens up to 1.5–2 K until around 2100 UTC. As commented before, there is just a turbulent burst at around 2400 UTC, identified by an increase in u_* of up to 0.3 m s^{-1}. The wind profile ~~for the weak event~~ at the moment of the onset shows a ~~low-level~~ jet below 3 m associated with a skin flow ($U < 1$ m s^{-1}), ~~while U is stronger and increases linearly with height between 3 and 10 m for the intense event. U continues increasing in the intense event, exceeding 2 m s^{-1} at 6 m when R_{net} turns negative and 3 m s^{-1} at 2100 UTC. This intensification of the katabatic flow shows a different pattern from for instance Grachev et al. (2016) . Based on observations from the MATERHORN field campaign, they reported that the wind profile is stationary in time during the katabatic flow. By the time $R_{net} < 0$, as a consequence of the flow intensification, the layer between 3 and~~ which is even sharper at 2230 UTC. The stronger stability is also reflected in the thermal profile at that time. At 2230 UTC, $\overline{u'w'}$ and $\overline{u'\theta_v'}$ become zero below 4 m (in particular the second), corroborating the presence of the katabatic jet or skin flow. At the moment of the onset, however, $\overline{u'w'}$ is slightly negative, suggesting the potential existence of an additional jet above 10 m~~is well mixed ($\Delta\theta_v \simeq 0$) despite the surface is already cooling down ($\theta_s < \theta_3$). On the contrary,~~ , probably associated with the downbasin flow.

The moderate downslope wind is established when the thermal profile is still unstable (Fig. 9). When R_n turns negative and the thermal inversion starts to develop, turbulence is still strong (~~U~~u_* ~~keeps below 1~~ = 0.5 m s^{-1}~~throughout the entire weak katabatic event, and the stable stratification sharpens progressively (for instance $\Delta\theta_v(10-3) \simeq 2$ K at 2100 UTC).~~

~~In order to shed more light on the possible factors inducing such a behaviour of the lower SBL in both cases, we explore the time-evolution of the measured shear at 4 and 8 m, $\Delta\theta_v$ and the surface energy balance for the weak and intense katabatic event in Fig. ??. When the onset of~~). Subsequently, however, the ~~weak katabatic flow takes place wind shear is weak (< 0.1 s~~arrival of the downbasin wind and the produced collision, reduces turbulence. Throughout the night, turbulence and the thermal inversion have an intermittent behaviour due to the alternation between the downslope and downbasin flows. Note that for this event 2300 UTC is chosen as the reference time instead of 2230 UTC, since at the latter time the downbasin wind is blowing. The form of the wind profile is rather homogeneous during the event (all the times shown are during the downslope stage), even under contrasting thermal profiles. It shows the presence of a possible jet below 3 m, although the profile is rather homogenised. $\overline{u'\theta_v'}$ is maintained negative at all times but the tendency with height is variable, as well as in the case of $\overline{u'w'}$, which turns positive throughout the night. This complex behaviour could be explained by the alternation between the downslope and downbasin flows, and the presence of a subtle jet below 3 m, and another jet above 10 m.

The onset of the intense downslope wind takes place around 1640 UTC (Fig. 10), during the afternoon transition of the ABL. After this time, u_* continues increasing slowly up to 0.5–0.6 m s^{-1}~~), $\Delta\theta_v > 0$ and the heat fluxes ($H+LH+G$) are unable to balance the radiative loss. As a consequence of the negative imbalance,~~ , and even up to 0.9 m s^{-1} a few hours later, exceeding the value associated with the diurnal peak (not shown). As occurs with the moderate downslope wind, due to the dynamical input from the steep slope towards the NW, the intense downslope wind arrives when the ~~surface-based thermal inversion intensifies (up to 2 K) limiting the increase of wind shear: it is mostly below 0.05 s^{-1} after the onset at 4 m. The limitation of wind shear confines H (see the low values in Fig. ??), intensifying the thermal inversion in turn and producing a positive feedback in which the very stable regime is set up. For the intense katabatic, however, the onset takes place when $\Delta\theta_v < 0$ and $R_{net} \simeq 200$ W m^{-2}. Wind shear increases particularly at 8 m, without being limited by the stable stratification . By the time~~ stratification is still unstable. After $R_{\cancel{net}n}$ turns negative slightly before 1900 UTC, ~~wind shear is already very high ($\simeq 0.5$ s^{-1}) and due to the turbulent mixing,~~ $\Delta\theta_v$ is ~~maintained always~~ always maintained below 0.2–0.3 K ~~. In fact, 2–3 hours after the onset the heat fluxes balance the radiative loss and the thermal gradient is almost completely destroyed~~ due to the strong turbulent mixing. The wind profile is different from both the moderate and weak events: wind speed increases linearly with height between 3 and 10 m and intensifies throughout the night, exceeding 2 m s^{-1} at 6 m when R_n turns negative, and 3 m s^{-1} at 2230 UTC. After stable conditions are established, the layer between 3 and 10 m ~~, limiting the thermal inversion~~ is well mixed ($\Delta\theta_v \simeq 0$) despite the fact that the surface is already cooling down ($\theta_s < \theta_3$). The thermal inversion is limited to a thin layer close to the surface (below 3 m). This indicates the presence of near-neutral conditions and the set up of the ~~weakly stable regime~~WSBL. At the moment of the onset, the heat and momentum turbulent fluxes become near zero close to 4 m, indicating the possible presence of a low-level jet. Nevertheless, $\overline{u'w'}$ becomes more negative and $\overline{u'\theta_v'}$ more positive throughout the night, confirming the presence of the jet above 10 m.

4.2 ~~Impact of katabatic flows and turbulence on CO_2~~

5 Impact on CO_2 variability

We finally explore the ~~role of the transport produced by the katabatic flow~~ impact of downslope flows of different intensities and the associated different turbulent ~~patterns within the SBL in~~ characteristics on a relevant scalar: ~~the~~ CO_2. For this analysis, the weak and intense downslope events are solely compared, since the budget for the moderate event is more complex due to the alternation of the downslope and downbasin winds.

The mixing ratio of CO_2 and the vertical turbulent fluxes are represented in Fig. 11 for the weak and intense ~~katabatic~~ downslope events. The CO_2 mixing ratio is normalised with respect to the daily mean. By ~~so doing~~ doing so, we aim to reduce the uncertainty due to possible biases. In Fig. 11b the measured turbulent fluxes at 4 and 8 m, and the estimated soil respiration flux (R_s) are represented. Since the soil respiration is an important CO_2 source term near the surface, we decided to include it in the analysis. It has been calculated following Lloyd and Taylor (1994) and Jacobs et al. (2007a):

$$R_s = R_{10}\Big(1 - f(SM)\Big)\left(exp\left(\frac{E_0}{283.15R^*}\right)\left(1 - \frac{283.15}{T_s + 273.15}\right)\right), \tag{3}$$

where $R^* = 8.31 \cdot 10^{-3}$ kJ K^{-1} mol^{-1} is the universal gas constant, E_0 is the activation energy (we employ a value of 53.30 kJ mol^{-1}) and T_s is the soil temperature, which has been estimated from the upward longwave radiation. R_{10} is the reference soil-respiration value at 10° C under no water-stress condition, and it can vary significantly from site to site (Jacobs et al., 2007b)~~;~~ ~~in~~. In this case, given the dry-soil conditions, we consider a value of $R_{10} = 0.10 \pm 0.02$ mg m^{-2} s^{-1} ~~given the dry-soil conditions~~. Finally, (1 - *f(SM)*) is a water-stress correction (Jacobs et al., 2007a) where:

$$f(SM) = C\frac{SM_{max}}{SM + SM_{min}}, \tag{4}$$

with C(=0.0016) being a constant, and *SM* the observed soil moisture at 4-cm depth. SM_{max} and SM_{min} are the respective recorded maximum (= 0.14 m^3 m^{-3}) and minimum (= 0.01 m^3 m^{-3}) soil-moisture values throughout the summer.

The normalised CO_2 mixing ratio at 4 and 8 m for the weak and intense events has the same values at 1600 UTC before the surface thermal inversion is set up (Fig. 11). It is therefore of great interest comparing these particular weak and intense events having the same initial mixing ratios but contrasting subsequent dynamical and stability conditions. ~~On~~ During the weak event, the CO_2 starts increasing at around 1730 UTC when the turbulent fluxes at 4 ~~an~~ and 8 m become positive. Slightly after the onset, which coincides with the set up of the SBL as reported in Sect. 4.1, the CO_2 starts to accumulate close to the surface until 2000 UTC approximately, due to the dominance of the soil flux over photosynthesis and dynamic transport. Later on, the balance between the divergence of the turbulent fluxes and the horizontal and transport explains the variability of the scalar.

The CO_2 for the intense ~~katabatic~~ downslope event shows a contrasting evolution. The onset occurs almost 2 ~~hours before~~ h before the weak event, and the diurnal positive vertical CO_2 gradient is reduced beforehand. Due to strong turbulence, the vertical CO_2 fluxes reach values of up to 0.2–0.3 mg m^{-2} s^{-1} slightly after the establishment of the SBL at around 1900 UTC (see Fig. ~~??)at around 1900 UTC~~10), following closely the estimated values of the soil respiration. From that moment and until 2200 UTC, the vertical gradient of the CO_2 is almost null, but the concentration increases around 6 ppm at both levels (note that it cannot be inferred from the normalised concentration in Fig. 11a). Considering in addition that the divergence of the vertical fluxes is mostly positive in that time range $((\overline{w'CO_2'})_{8m} > (\overline{w'CO_2'})_{4m})$, the increase of the CO_2 concentration is explained by the non-local horizontal transport associated with the intense ~~katabatic~~ downslope flow. From the null vertical gradient of CO_2 between 4 and 8 m, and of θ_v between 3 and 10 m (see Fig. ~~??g~~10c), we can assume that the layer between 4 and 8 is well mixed~~, and~~. Furthermore, since *w* close to the ground is nearly ~~0~~ zero, vertical advection can be neglected. ~~From this assumption we can additionally~~ After those assumptions, we can infer the horizontal transport in that 4-m layer between 1900 UTC and 2200 UTC, following the methodology from Casso-Torralba et al. (2008) based on well-mixed layers.

We based our analysis on the one-dimensional governing equation for CO_2 in between 4 and 8 m. We therefore neglected the effects of soil CO_2. In short, after applying the Reynolds decomposition and averaging of the velocity fluctuations, and by considering the continuity equation, we get Eq. 5 for the average CO_2 in the layer between 4 and 8 m. The wind has been aligned in the main component. We additionally neglect the horizontal turbulent flux divergence, since ~~under near-neutral conditions~~ for this event the flux-fetch condition in the ~~katabatic~~ downslope direction is met ~~in our emplacement~~at 8 m (see Fig. A1).

$$\frac{\partial \overline{CO_2}}{\partial t} + \overline{u}\cancel{\frac{\partial \overline{CO_2}}{\partial x}}\frac{\partial \overline{CO_2}}{\partial s} + \cancel{\frac{\partial \overline{w'CO_2'}}{\partial z}}\frac{\partial \overline{w'CO_2'}}{\partial n} = 0. \qquad (5)$$

The first term represents the storage, the second term horizontal advection and the third term, the divergence of the turbulent fluxes in the layer between 4 and 8 m. Since the layer is well mixed, we assume linearity of the turbulent fluxes with height ~~(Casso-Torralba et al. 2008). For the sake of simplicity we consider that the advective term is maintained constant from 1900 to 2200.~~ (Casso-Torralba et al., 2008) . Integrating Eq. 5 in time we get to the following equivalence for the horizontal-transport term:

$$\int_{1900}^{2200} \overline{u}\cancel{\frac{\partial[\overline{CO_2}]}{\partial x}}\frac{\partial[\overline{CO_2}]}{\partial s}dt = -\int_{1900}^{2200}\frac{\partial[\overline{CO_2}]}{\partial t}dt - \int_{1900}^{2200}\cancel{\frac{\Delta\overline{w'CO_2'}}{\Delta z}}\frac{\Delta\overline{w'CO_2'}}{\Delta n}dt \qquad (6)$$

The time evolution of the three terms ~~in~~ is shown in Fig. 12, together with the ~~katabatic speed~~ wind-speed evolution. Since the horizontal gradient of the CO_2 concentration increases upwind of the ~~katabatic~~ downslope flow, the sign of the advective term is negative (note that it is represented in absolute values). After the corresponding calculations in Eq. 6, we obtain that a horizontal transport of 67 ppm over 3 h induced by the intense ~~katabatic flow compensates~~ downslope flow compensates for the loss due to the vertical divergence (around 61 ppm in 3 h), resulting in an increase of the CO_2 storage of 6 ppm. This positive CO_2 advection is probably induced by the presence ~~upwind~~ of a land use composed of forest, mosaic trees and shrubs ~~towards the katabatic direction, which accumulates~~ upwind, towards the downslope direction. Given the increased plant respiration and soil flux, greater CO_2 concentrations are accumulated close to the surface during the night~~due to increased plant respiration and soil flux. Intense katabatics~~. Intense downslope flows, as demonstrated in previous sections, induce strong wind shear and considerable mixing of the lower SBL, which together with the strong flow, contribute to cause important transport of scalars such as the CO_2.

6 Summary and conclusions

Forty ~~katabatic~~ downslope events of different intensities, and with contrasting impacts on the turbulent characteristics of the SBL and ~~on the CO_2 transport and mixing~~ CO_2 variability, were investigated. Measurements were carried out in ~~a relatively flat area with a relatively dessicated soil~~ an approximately flat area at the foothill of a high mountain range in central ~~Spain during one summer~~ Iberian Peninsula during summer 2017. During that period, the soil underwent relatively strong dessication alterations. Observations of ~~energy fluxes(heat and momentum)~~turbulent fluxes, CO_2 mixing ratios and other meteorological variables were recorded ~~in a tower~~ at various vertical levels ~~up to 10 m~~along a 10-m tower. A systematic algorithm was employed in order to select unambiguously thermally-driven downslope winds, by using objective filters to account for large-scale and local forcings.

The selected ~~katabatic~~ downslope events were classified into three groups according to the observed maximum ~~katabatic intensity~~ 6-m wind speed until midnight: weak, moderate and intense. By clustering them into these three groups, we were able to ~~analyse~~ explore the factors that produce different intensities ~~,~~ and their relationship with the different turbulent patterns in the SBL. Moreover, by exploring individual representative events, we investigated the mechanisms underlying their formation and development, and their specific thermal and dynamical features.

Weak ~~katabatics form when the maximum wind speed is kept~~ downslope flows have maximum 6-m wind speeds below 1.5 m s^{-1}. They particularly take place when the large-scale wind opposes the ~~katabatic~~ downslope flow and soil moisture is greater than the summer median, which in general induces a smaller radiative cooling. These factors give rise to ~~a delayed arrival of the~~ the formation of a prototypical katabatic flow, ~~when the stratification is already neutral or stable, which limits the increase of the wind shear~~driven mainly by the buoyancy acceleration. Since the local slope is gentle, and in the absence of a clear dynamical input, their intensity is very weak. The katabatic jet is located below 3 m, and the associated turbulence is very weak. A positive feedback between the weak turbulence and the progressive cooling of the surface, which induces a more stable stratification, explains the formation of the very stable regime. ~~A skin flow below 3 m and intermittent~~ Intermittent but weak turbulence ~~are sporadically~~ can sporadically be observed.

Intense ~~katabatics are found when the maximum wind speed~~ downslope flows have a maximum 6-m wind speed that exceeds 3.5 m s^{-1}~~at 6 m agl~~. They mostly ~~occur~~ take place when soil moisture is lower than the summer median, the large-scale wind blows ~~in the katabatic~~ approximately in the downslope direction and its speed is greater than 3.5 m s^{-1} at 850 hPa. These factors ~~induce an earlier katabatic~~ add an important dynamical input in the form of an advection from the nearby steep slope. It induces an early onset, when the ~~stratification is still unstable. Wind shear can therefore increase~~ thermal stratification is not stable yet, and an approximately linear wind profile above 3 m. The jet in this case is located above 10 m. Therefore, wind shear associated with the flow increases without being damped by the stable stratification itself. By the time the SBL is formed, ~~wind shear is considerably high (up to 0.5 s $^{-1}$), and~~ the layer between 3 and 10 m is maintained well mixed ~~. Given the strong turbulence, the downward heat flux is finally able to compensate the radiative cooling at the surface, and therefore~~ and the thermal inversion is limited to a very thin layer close to the surface, reducing the thermal contribution of the katabatic flow. In this way, near-neutral conditions are reached and the ~~weakly stable boundary layer~~ WSBL is established.

Moderate ~~katabatics~~ downslope flows lie between weak and intense ~~katabatics, and their impact on the SBL regime and the associated turbulence is not so clearly assessed. Among all the moderate ones, the weakest events mostly approach the weak katabatics and the strongest events the intense katabatics, although the boundary for the transition between the regimes in this case in unclear.~~

~~Our findings show that the regime transition in the SBL is defined by using various values of dimensionless parameters. Instead, it occurs over a certain transitional range which~~ downslope flows, and show intermediate characteristics. Depending on the relative weight of the dynamical contribution to the flow and the interaction between local downslope and downbasin flows, their characteristics may be closer to either weak or intense downslope winds. Their impact on the turbulent characteristics of the SBL strongly depends on the ~~observational height for z/L and R_B, and is independent of that height in the case of the shear capacity. The latter is the best in predicting the regime transition, as long as the HOST transition is taken into consideration for the corresponding wind-speed threshold~~maximum flow intensity that is reached. We found, indeed, that the wind speed is the most precise variable for representing the nocturnal regime transition: above a 6-m wind speed of 1.5 m s^{-1} ~~at 6 m~~, it is the bulk shear which dominates the turbulence production, and the thermal inversion is eroded significantly, giving rise to a regime transition.

Finally we inspected ~~individual intense and a weak katabatic events, and their contribution to~~ the impact of contrasting weak and intense downslope events on the CO_2 budget. ~~On~~ For the weak event, ~~the slight turbulence contributes~~ minimal turbulence levels contribute to the accumulation of CO_2 close to the surface, and its concentration is sensitive to slight changes in the turbulent fluxes. For the intense event, instead, turbulence is considerably greater and consequently the layer between 4 and 8 m is well mixed. Under these conditions, we estimated the contribution of the horizontal transport in the ~~katabatic~~ downslope direction, which is of around 67 ppm in 3 h, contributing to the increase in storage of this scalar.

To sum up, we have ~~been able to characterise the evening transition and foresee the turbulent characteristics of the SBL during the night by~~ assessed the main external factors and physical mechanisms underlying the formation and development of thermally-driven downslope winds of different intensities. By measuring the maximum intensity of ~~the katabatic flow, which depends on external factors such as the large-scale wind and soil moisture. In particular, the influence of the latter in the surface-energy balance needs further investigation~~downslope flows we are able to diagnose the turbulent characteristics of the SBL during the night. Being able to predict ~~these~~ the influencing external factors more precisely is therefore of high interest to better forecast the ~~night-time~~ nighttime turbulence and regime transition. ~~However~~Further observational investigations of the influence of soil moisture in the surface energy balance are needed. On the other hand, sudden turbulent bursts and collapses, and the interaction with gravity waves have not been explored in this work, which can also be relevant in producing perturbations in the SBL and regime transitions. Future studies should tackle with those features and a better performance of numerical models in reproducing them over complex terrain.

Data availability. Original data are freely available upon request through the GuMNet web: https://www.ucm.es/gumnet/.

Appendix A: Footprint estimation

The footprint of the turbulent fluxes is estimated by using the approximate analytical model from Hsieh et al. (2000) , which is based on a combination of results from lagrangian stochastic dispersion models and dimensional analysis. This footprint model was chosen in this work because it is developed for thermally stratified surface layers, it is practical and has been applied in many studies, giving satisfactory results when compared with other footprint models.

The cross-wind integrated footprint has the following form:

$$F^y(x,z_m) = \frac{1}{k^2x^2} D z_u^P |L|^{1-P} e^{-\frac{D z_u^P |L|^{1-P}}{k^2 x}}, \tag{A1}$$

where z_u is a length scale, z_m the effective height of the sensors, D and P similarity constants which depend on the thermal stratification, L the Obukhov length and k the Von Kármán constant. The footprint estimation is extended to 2D by adding the contribution of lateral spread assuming that is Gaussian, based on the formulation from Detto et al. (2006) :

$$f(x,y,z_m) = \frac{1}{\sqrt{2\pi}\sigma_y} e^{-\frac{1}{2}\left(\frac{y}{\sigma_y}\right)^2} F^y(x,z_m), \tag{A2}$$

with σ_y being the standard deviation of the lateral wind fluctuations.

By considering an approximate average height of the surrounding trees of h = 5 m, the footprint function is calculated and represented for the three representative events of the weak, moderate and intense downslope types in Fig. A1. It is depicted in the main downslope direction when the downslope wind is already developed (at 2100 UTC), superimposed on the map of the surrounding area from La Herrería. It is just shown for the sensor height of 8 m, since for 4 m the footprint area is smaller and hence the flux-fetch condition more easily fulfilled.

Most of the footprint area, delimited by the large black curve which corresponds to 90% of the total measured flux, is only affected by sparse bushes and short-medium trees of up to 5 m (the tallest ones located at 30-40 m towards the W-SW), so that the flux-fetch requirement is fulfilled. For the intense downslope event, the footprint is even unaffected by those inhomogeneities. Just in the weak downslope flow the footprint might be slightly affected by the tall poplars located towards the N, even though its input is anyway small.

Appendix B: Assessment of the thermal profile

The thermal profile within the first 10 m over the surface is fitted to a logarithmic profile by the method of least squares. The fit is carried out employing four vertical values of θ_v calculated from measurements in La Herrería at the surface, and at 3, 6 and 10 m. The skin temperature is calculated from the upward longwave radiation. The fitting is carried out as follows:

$$\theta_v(z,t) = \alpha(t) + \beta(t)\ln(z) + \gamma(t)\ln^2(z) + \delta(t)\ln^3(z). \tag{B1}$$

We find that from the value of $\delta(t)$, which provides information about the curvature of the profile in its lowest part, we can infer the static stability of the thermal profile. We illustrate the thermal profile at three different times of day in Fig. B1, each time associated with a different static stability for a moderate downslope event: 25 July. The use of four vertical levels allows the fit to a cubic polynomial, and as a consequence more realistic near-surface profiles. Given also the limited number of measurements, the fit is exact (note that $r^2 = 1$), which would not occur in case of having a greater number of vertical measurements.

From a careful inspection of $\delta(t)$ for different events at various times of day and employing θ_v in K and z in m, we classify the static stability of the lowest 10-m atmospheric layer into the three subsequent groups according to the value of $\delta(t)$:

$$\begin{aligned}
&\textit{Unstable}: \quad \delta(t) < -0.3, \\
&\textit{Neutral}: \quad -0.3 \leq \delta(t) \leq 0, \\
&\textit{Stable}: \quad \delta(t) > 0. \\
&\qquad\qquad\qquad tagB2
\end{aligned} \tag{B1}$$

Author contributions. CY, MS, CRC, GM and JAA assisted with the collection and validation of the quality data, CY lead the project and conducted the field experiment, CRC and MS contributed to the data treatment, JAA carried out the calculations and wrote the manuscript, and JVA and MAJ helped with the interpretation of results. All the authors have revised and commented on the manuscript.

Competing interests. We declare that not competing interests are present

Acknowledgements. This research has been funded by ATMOUNT-II project [Ref. CGL2015-65627-C3-3-R (MINECO/FEDER)] and the Project [Ref. CGL2016-81828-REDT/AEI] from the Spanish Government, and by the GuMNet (Guadarrama Monitoring Network, www.ucm.es/gumnet) observational network of CEI Moncloa campus of International Excellence. Jon A. Arrillaga is supported by the Predoctoral Training Program for No-Doctor Researchers of the Department of Education, Language Policy and Culture of the Basque Government (PRE_2017_2_0069, MOD = B). We thank the contribution of all the members of the GuMNet Team, especially Dr. J.F. González-Rouco, and *Patrimonio Nacional* for the facilities given during the installation of the meteorological tower.

References

AEMET: Summary of Summer 2017, Spanish Meteorological Agency, http://www.aemet.es/en/noticias/2017/09/Verano_2017, 2017.

Arrillaga, J. A., Yagüe, C., Sastre, M., Román-Cascón, C., Maqueda, G., Inclán, R., González-Roúco, J., Santolaria, E., Durán, L., and Navarro., J.: WRF simulations of upslope and downslope flows over the Guadarrama Mountain Range (Spain), in: 32nd Conference on Agricultural and Forest Meteorology, Salt Lake City (UT, USA), 2016.

Arrillaga, J. A., Vilà-Guerau de Arellano, J., Bosveld, F., Baltink, H. K., Yagüe, C., Sastre, M., and Román-Cascón, C.: Impacts of afternoon and evening sea-breeze fronts on local turbulence, and on CO2 and radon-222 transport, Q. J. R. Meteorol. Soc., pp. 1–22, https://doi.org/10.1002/qj.3252, 2018.

Atkinson, B.: Meso-Scale Atmospheric Circulations, Academic Press, London, 1981.

Banta, R. M. and Gannon, P. T.: Influence of soil moisture on simulations of katabatic flow, Theor. Appl. Climatol., 52, 85–94, https://doi.org/10.1007/BF00865509, 1995.

Barry, R. G.: Mountain Weather and Climate, Cambridge University Press, Cambridge, UK., Meteorol. Appl., 17, 506 pp., https://doi.org/10.1002/met.222, 2008.

Borge, R., Narros, A., Artíñano, B., Yagüe, C., Gómez-Moreno, F. J., de la Paz, D., Román-Cascón, C., Díaz, E., Maqueda, G., Sastre, M., Quaassdorff, C., Dimitroulopoulou, C., and Vardoulakis, S.: Assessment of microscale spatio-temporal variation of air pollution at an urban hotspot in Madrid (Spain) through an extensive field campaign, Atmos. Environ., 140, 432 – 445, https://doi.org/10.1016/j.atmosenv.2016.06.020, 2016.

Borge, R., Artíñano, B., Yagüe, C., Gomez-Moreno, F. J., Saiz-Lopez, A., Sastre, M., Narros, A., García-Nieto, D., Benavent, N., Maqueda, G., Barreiro, M., de Andrés, J. M., and Ángeles Cristóbal: Application of a short term air quality action plan in Madrid (Spain) under a high-pollution episode - Part I: Diagnostic and analysis from observations, Sci. Total Environ., 635, 1561 – 1573, https://doi.org/10.1016/j.scitotenv.2018.03.149, 2018.

Campbell-Scientific: EasyFlux DL Eddy-Covariance CR3000 Datalogger Program, https://s.campbellsci.com/documents/us/product-brochures/b_easyflux-dl.pdf, 2017.

Casso-Torralba, P., Vilà-Guerau de Arellano, J., Bosveld, F., Soler, M. R., Vermeulen, A., Werner, C., and Moors, E.: Diurnal and vertical variability of the sensible heat and carbon dioxide budgets in the atmospheric surface layer, J. Geophys. Res. Atmos., 113, n/a–n/a, https://doi.org/10.1029/2007JD009583, d12119, 2008.

Chrust, M. F., Whiteman, C. D., and Hoch, S. W.: Observations of Thermally Driven Wind Jets at the Exit of Weber Canyon, Utah, J. Appl. Meteorol. Clim., 52, 1187–1200, https://doi.org/10.1175/JAMC-D-12-0221.1, 2013.

Cristofanelli, P., Calzolari, F., Bonafè, U., Lanconelli, C., Lupi, A., Busetto, M., Vitale, V., Colombo, T., and Bonasoni, P.: Five-year analysis of background carbon dioxide and ozone variations during summer seasons at the Mario Zucchelli station (Antarctica), Tellus B, 63, 831–842, https://doi.org/10.1111/j.1600-0889.2011.00576.x, 2011.

Detto, M., Montaldo, N., Albertson, J. D., Mancini, M., and Katul, G.: Soil moisture and vegetation controls on evapotranspiration in a heterogeneous Mediterranean ecosystem on Sardinia, Italy, Water Resour. Res., 42, 1–16, https://doi.org/10.1029/2005WR004693, 2006.

Doran, J. C.: The effects of ambient winds on valley drainage flows, Boundary-Layer Meteorol., 55, 177–189, https://doi.org/10.1007/BF00119333, 1991.

Durán, L., Sánchez, E., and Yagüe, C.: Climatology of precipitation over the Iberian Central System mountain range, Int. J. Climatol., 33, 2260–2273, https://doi.org/10.1002/joc.3602, 2013.

Durán, L., Rodríguez-Muñoz, I., and Sánchez, E.: The Peñalara Mountain Meteorological Network (1999–2014): Description, Preliminary Results and Lessons Learned, Atmosphere, 8, 203, https://doi.org/10.3390/atmos8100203, 2018.

Fitzjarrald, D. R.: Katabatic Wind in Opposing Flow, J. Atmos. Sci., 41, 1143–1158, https://doi.org/10.1175/1520-0469(1984)041<1143:KWIOF>2.0.CO;2, 1984.

Flocas, H. A., Helmis, C. G., Blikas, S. N., Asimakopoulos, D. N., Bartzis, J. G., and Deligiorgi, D. G.: Mean Characteristics of the Katabatic Flow of a 1024 m High Knife Edge Mountain, Theor. Appl. Climatol., 59, 237–249, https://doi.org/10.1007/s007040050027, 1998.

Grachev, A. A., Leo, L. S., Di Sabatino, S., Fernando, H. J. S., Pardyjak, E. R., and Fairall, C. W.: Structure of Turbulence in Katabatic Flows Below and Above the Wind-Speed Maximum, Boundary-Layer Meteorol., 159, 469–494, https://doi.org/10.1007/s10546-015-0034-8, 2016.

GuMNet: www.ucm.es/gumnet/, 2018.

Hang, C., Nadeau, D. F., Gultepe, I., Hoch, S. W., Román-Cascón, C., Pryor, K., Fernando, H. J. S., Creegan, E. D., Leo, L. S., Silver, Z., and Pardyjak, E. R.: A Case Study of the Mechanisms Modulating the Evolution of Valley Fog, Pure Appl. Geophys., 173, 3011–3030, https://doi.org/10.1007/s00024-016-1370-4, 2016.

Högström, U.: Review of some basic characteristics of the atmospheric surface layer, Boundary-Layer Meteorol., 78, 215–246, https://doi.org/10.1007/BF00120937, 1996.

Horst, T. W. and Doran, J. C.: Nocturnal drainage flow on simple slopes, Boundary-Layer Meteorol., 34, 263–286, https://doi.org/10.1007/BF00122382, 1986.

Hsieh, C. I., Katul, G., and Chi, T.-w.: An approximate analytical model for footprint estimation of scalar fluxes in thermally stratified atmospheric flows, Adv. Water Resour., 23, 765 – 772, https://doi.org/10.1016/S0309-1708(99)00042-1, 2000.

Jacobs, A. F. G., Heusinkveld, B. G., and Holtslag, A. A. M.: Seasonal and interannual variability of carbon dioxide and water balances of a grassland, Climatic Change, 82, 163–177, https://doi.org/10.1007/s10584-006-9182-7, 2007a.

Jacobs, C. M. J., Jacobs, A. F. G., Bosveld, F. C., Hendriks, D. M. D., Hensen, A., Kroon, P. S., Moors, E. J., Nol, L., Schrier-Uijl, A., and Veenendaal, E. M.: Variability of annual CO_2 exchange from Dutch grasslands, Biogeosciences, 4, 803–816, https://doi.org/10.5194/bg-4-803-2007, 2007b.

Jensen, D., Nadeau, D. F., Hoch, S. W., and Pardyjak, E. R.: The evolution and sensitivity of katabatic flow dynamics to external influences through the evening transition, Q. J. R. Meteorol. Soc., 143, 423–438, https://doi.org/10.1002/qj.2932, 2017.

Jiménez, M. A., Cuxart, J., and Martínez-Villagrasa, D.: Influence of a valley exit jet on the nocturnal atmospheric boundary layer at the foothills of the Pyrenees, Q. J. R. Meteorol. Soc., 145, 356–375, https://doi.org/10.1002/qj.3437, 2019.

Kaimal, J. and Finnigan, J.: Atmospheric Boundary Layer Flows: Their Structure and Measurements, 289 pp., Oxford University Press, 1994.

Kaimal, J. C., Clifford, S. F., and Lataitis, R. J.: Effect of finite sampling on atmospheric spectra, Boundary-Layer Meteorol., 47, 337–347, https://doi.org/10.1007/BF00122338, 1989.

Legrand, M., Preunkert, S., Savarino, J., Frey, M. M., Kukui, A., Helmig, D., Jourdain, B., Jones, A. E., Weller, R., Brough, N., and Gallée, H.: Inter-annual variability of surface ozone at coastal (Dumont d'Urville, 2004–2014) and inland (Concordia, 2007–2014) sites in East Antarctica, Atmos. Chem. Phys., 16, 8053–8069, https://doi.org/10.5194/acp-16-8053-2016, 2016.

Lehner, M., Whiteman, C. D., Hoch, S. W., Jensen, D., Pardyjak, E. R., Leo, L. S., Di Sabatino, S., and Fernando, H. J. S.: A Case Study of the Nocturnal Boundary Layer Evolution on a Slope at the Foot of a Desert Mountain, J. Appl. Meteorol. Clim., 54, 732–751, https://doi.org/10.1175/JAMC-D-14-0223.1, 2015.

Li, J., Sun, J., Zhou, M., Cheng, Z., Li, Q., Cao, X., and Zhang, J.: Observational analyses of dramatic developments of a severe air pollution event in the Beijing area, Atmos. Chem. Phys., 18, 3919–3935, https://doi.org/10.5194/acp-18-3919-2018, 2018.

Lloyd, J. and Taylor, J.: On the Temperature Dependence of Soil Respiration, Funct. Ecol., 8, 315–323, https://doi.org/10.2307/2389824, 1994.

Lothon, M., Lohou, F., Pino, D., Couvreux, F., Pardyjak, E. R., Reuder, J., Vilà-Guerau de Arellano, J., Durand, P., Hartogensis, O., Legain, D., Augustin, P., Gioli, B., Lenschow, D. H., Faloona, I., Yagüe, C., Alexander, D. C., Angevine, W. M., Bargain, E., Barrié, J., Bazile, E., Bezombes, Y., Blay-Carreras, E., van de Boer, A., Boichard, J. L., Bourdon, A., Butet, A., Campistron, B., de Coster, O., Cuxart, J., Dabas, A., Darbieu, C., Deboudt, K., Delbarre, H., Derrien, S., Flament, P., Fourmentin, M., Garai, A., Gibert, F., Graf, A., Groebner, J., Guichard, F., Jiménez, M. A., Jonassen, M., van den Kroonenberg, A., Magliulo, V., Martin, S., Martinez, D., Mastrorillo, L., Moene, A. F., Molinos, F., Moulin, E., Pietersen, H. P., Piguet, B., Pique, E., Román-Cascón, C., Rufin-Soler, C., Saïd, F., Sastre-Marugán, M., Seity, Y., Steeneveld, G. J., Toscano, P., Traullé, O., Tzanos, D., Wacker, S., Wildmann, N., and Zaldei, A.: The BLLAST field experiment: Boundary-Layer Late Afternoon and Sunset Turbulence, Atmos. Chem. Phys., 14, 10 931–10 960, https://7doi.org/10.5194/acp-14-10931-2014, 2014.

Mahrt, L.: Nocturnal Boundary-Layer Regimes, Boundary-Layer Meteorol., 88, 255–278, https://doi.org/10.1023/A:1001171313493, 1998.

Mahrt, L.: Stably Stratified Atmospheric Boundary Layers, Annu. Rev. Fluid Mech., 46, 23–45, https://doi.org/10.1146/annurev-fluid-010313-141354, 2014.

Mahrt, L. and Larsen, S.: Relation of slope winds to the ambient flow over gentle terrain, Boundary-Layer Meteorol., 53, 93–102, https://doi.org/10.1007/BF00122465, 1990.

Mahrt, L., Vickers, D., Nakamura, R., Soler, M. R., Sun, J., Burns, S., and Lenschow, D.: Shallow Drainage Flows, Boundary-Layer Meteorol., 101, 243–260, https://doi.org/10.1023/A:1019273314378, 2001.

Manins, P. C. and Sawford, B. L.: A Model of Katabatic Winds, J. Atmos. Sci., 36, 619–630, https://doi.org/10.1175/1520-0469(1979)036<0619:AMOKW>2.0.CO;2, 1979.

Mauritsen, T. and Svensson, G.: Observations of Stably Stratified Shear-Driven Atmospheric Turbulence at Low and High Richardson Numbers, J. Atmos. Sci., 64, 645–655, https://doi.org/10.1175/JAS3856.1, 2007.

Nadeau, D., Pardyjak, E. R., Higgins, C. W., Huwald, H., and Parlange, M. B.: Flow during the evening transition over steep Alpine slopes, Q. J. R. Meteorol. Soc., 139, 607–624, https://doi.org/10.1002/qj.1985, 2013.

Oldroyd, H. J., Pardyjak, E. R., Higgins, C. W., and Parlange, M. B.: Buoyant Turbulent Kinetic Energy Production in Steep-Slope Katabatic Flow, Boundary-Layer Meteorol., 161, 405–416, https://doi.org/10.1007/s10546-016-0184-3, 2016.

Papadopoulos, K. H. and Helmis, C. G.: Evening and Morning Transition of Katabatic Flows, Boundary-Layer Meteorol., 92, 195–227, https://doi.org/10.1023/A:1002070526425, 1999.

Pardyjak, E. R., Fernando, H. J. S., Hunt, J. C., Grachev, A. A., and Anderson, J. A.: A case study of the development of nocturnal slope flows in a wide open valley and associated air quality implications, Meteorol. Z., 18, 85–100, https://doi.org/10.1127/0941-2948/2009/362, 2009.

Plaza, J., Pujadas, M., and Artíñano, B.: Formation and Transport of the Madrid Ozone Plume, J. Air Waste Manag. Assoc., 47, 766–774, https://doi.org/10.1080/10473289.1997.10463938, 1997.

Poulos, G. and Zhong, S.: An Observational History of Small-Scale Katabatic Winds in Mid-Latitudes, Geogr. Compass, 2, 1798–1821, https://doi.org/10.1111/j.1749-8198.2008.00166.x, 2008.

Poulos, G. S., Blumen, W., Fritts, D. C., Lundquist, J. K., Sun, J., Burns, S. P., Nappo, C., Banta, R., Newsom, R., Cuxart, J., Terradellas, E., Balsley, B., and Jensen, M.: CASES-99: A Comprehensive Investigation of the Stable Nocturnal Boundary Layer, Bull. Am. Meteor. Soc., 83, 555–582, https://doi.org/10.1175/1520-0477(2002)083<0555:CACIOT>2.3.CO;2, 2002.

Román-Cascón, C., Yagüe, C., Mahrt, L., Sastre, M., Steeneveld, G.-J., Pardyjak, E., van de Boer, A., and Hartogensis, O.: Interactions among drainage flows, gravity waves and turbulence: a BLLAST case study, Atmos. Chem. Phys., 15, 9031–9047, https://doi.org/10.5194/acp-15-9031-2015, 2015.

Román-Cascón, C., Yagüe, C., Arrillaga, J., Lothon, M., Pardyjak, E., Lohou, F., Inclán, R., Sastre, M., Maqueda, G., Derrien, S., Meyerfeld, Y., Hang, C., Campargue-Rodríguez, P., and Turki, I.: Comparing mountain breezes and their impacts on CO2 mixing ratios at three contrasting areas, Atmos. Res., 221, 111 – 126, https://doi.org/10.1016/j.atmosres.2019.01.019, 2019.

Rotach, M. W., Wohlfahrt, G., Hansel, A., Reif, M., Wagner, J., and Gohm, A.: The World is Not Flat: Implications for the Global Carbon Balance, Bull. Am. Meteor. Soc., 95, 1021–1028, https://doi.org/10.1175/BAMS-D-13-00109.1, 2014.

Sastre, M., Yagüe, C., Román-Cascón, C., and Maqueda, G.: Atmospheric Boundary-Layer Evening Transitions: A Comparison Between Two Different Experimental Sites., Boundary-Layer Meteorol., 157, 375 – 399, https://doi.org/10.1007/s10546-015-0065-1, 2015.

Schotanus, P., Nieuwstadt, F., and de Bruin, H.: Temperature-Measurement with a Sonic Anemometer and Its Application to Heat and Moisture Fluxes, Boundary-Layer Meteorol., 26, 81–93, https://doi.org/10.1007/BF00164332, 1983.

Soler, M., Infante, C., Buenestado, P., and Mahrt, L.: Observations Of Nocturnal Drainage Flow In A Shallow Gully, Boundary-Layer Meteorol., 105, 253–273, https://doi.org/10.1023/A:1019910622806, 2002.

Steeneveld, G. J., Wokke, M. J. J., Groot Zwaaftink, C. D., Pijlman, S., Heusinkveld, B. G., Jacobs, A. F. G., and Holtslag, A. A. M.: Observations of the radiation divergence in the surface layer and its implication for its parameterization in numerical weather prediction models, J. Geophys. Res. Atmos., 115, 1–13, https://doi.org/10.1029/2009JD013074, 2010.

Stiperski, I. and Rotach, M. W.: On the Measurement of Turbulence Over Complex Mountainous Terrain, Boundary-Layer Meteorol., 159, 97–121, https://doi.org/10.1007/s10546-015-0103-z, 2016.

Stull, R. B.: An Introduction to Boundary Layer Meteorology, Kluwer Academic Publishers, 1988.

Sun, H., Clark, T. L., Stull, R. B., and Black, T. A.: Two-dimensional simulation of airflow and carbon dioxide transport over a forested mountain: Part II. Carbon dioxide budget analysis and advection effects, Agric. For. Meteorol., 140, 352 – 364, https://doi.org/10.1016/j.agrformet.2006.03.016, the Fluxnet-Canada Research Network: Influence of Climate and Disturbance on Carbon Cycling in Forests and Peatlands, 2006.

Sun, J., Burns, S. P., Delany, A. C., Oncley, S. P., Turnipseed, A. A., Stephens, B. B., Lenschow, D. H., LeMone, M. A., Monson, R. K., and Anderson, D. E.: CO2 transport over complex terrain, Agric. For. Meteorol., 145, 1 – 21, https://doi.org/10.1016/j.agrformet.2007.02.007, 2007.

Sun, J., Mahrt, L., Banta, R. M., and Pichugina, Y. L.: Turbulence Regimes and Turbulence Intermittency in the Stable Boundary Layer during CASES-99, J. Atmos. Sci., 69, 338–351, https://doi.org/10.1175/JAS-D-11-082.1, 2012.

Sun, J., Mahrt, L., Nappo, C., and Lenschow, D. H.: Wind and Temperature Oscillations Generated by Wave–Turbulence Interactions in the Stably Stratified Boundary Layer, J. Atmos. Sci., 72, 1484–1503, https://doi.org/10.1175/JAS-D-14-0129.1, 2015.

Sun, J., Lenschow, D. H., LeMone, M. A., and Mahrt, L.: The Role of Large-Coherent-Eddy Transport in the Atmospheric Surface Layer Based on CASES-99 Observations, Boundary-Layer Meteorol., 160, 83–111, https://doi.org/10.1007/s10546-016-0134-0, 2016.

Terradellas, E. and Cano, D.: Implementation of a Single-Column Model for Fog and Low Cloud Forecasting at Central-Spanish Airports, Pure Appl. Geophys., 164, 1327–1345, https://doi.org/10.1007/s00024-007-0221-8, 2007.

Van de Wiel, B. J. H., Moene, A. F., Steeneveld, G., Baas, P., Bosveld, F., and Holtslag, A. A. M.: Intermittent Turbulence and Oscillations in the Stable Boundary Layer over Land. Part III: A classification for observations during CASES-99, J. Atmos. Sci., 60, 2509–2522, https://doi.org/10.1175/1520-0469(2002)059<2567:ITAOIT>2.0.CO;2, 2003.

Van de Wiel, B. J. H., Moene, A. F., and Jonker, H. J. J.: The Cessation of Continuous Turbulence as Precursor of the Very Stable Nocturnal Boundary Layer, J. Atmos. Sci., 69, 3097–3115, https://doi.org/10.1175/JAS-D-12-064.1, 2012a.

Van de Wiel, B. J. H., Moene, A. F., Jonker, H. J. J., Baas, P., Basu, S., Donda, J. M. M., Sun, J., and Holtslag, A. A. M.: The Minimum Wind Speed for Sustainable Turbulence in the Nocturnal Boundary Layer, J. Atmos. Sci., 69, 3116–3127, https://doi.org/10.1175/JAS-D-12-0107.1, 2012b.

Van der Linden, S. J. A., Baas, P., Antoon van Hooft, J., van Hooijdonk, I. G. S., Bosveld, F. C., and van de Wiel, B. J. H.: Local Characteristics of the Nocturnal Boundary Layer in Response to External Pressure Forcing, J. Appl. Meteorol. Clim., 56, 3035–3047, https://doi.org/10.1175/JAMC-D-17-0011.1, 2017.

Van Hooijdonk, I. G. S., Donda, J. M. M., Clercx, H. J. H., Bosveld, F. C., and van de Wiel, B. J. H.: Shear Capacity as Prognostic for Nocturnal Boundary Layer Regimes, J. Atmos. Sci., 72, 1518–1532, https://doi.org/10.1175/JAS-D-14-0140.1, 2015.

Webb, E. K., Pearman, G. I., and Leuning, R.: Correction of flux measurements for density effects due to heat and water vapour transfer, Q. J. R. Meteorol. Soc., 106, 85–100, https://doi.org/10.1002/qj.49710644707, 1980.

Whiteman, C.: Mountain Meteorology: Fundamentals and Applications, Oxford University Press, 2000.

Whiteman, C. D.: Breakup of Temperature Inversions in Deep Mountain Valleys: Part I. Observations, J. Appl. Meteorol., 21, 270–289, https://doi.org/10.1175/1520-0450(1982)021<0270:BOTIID>2.0.CO;2, 1982.

Zardi, D. and Whiteman, C.: Mountain Weather Research and Forecasting: Recent Progress and Current Challenges, vol. XIII of *Springer Atmospheric Sciences*, chap. Diurnal Mountain WInd Systems., pp. 35–119, Springer Netherlands, 1 edn., 2013.

Zhou, F.-H., Zhang, R.-W., Shi, R., Chen, J., He, Y.-K., and Xie, Q.: Processing of Turbulent Data and Flux Quality Control of Observed Data from Yongxing Island in Spring 2016, J. Coast. Res., 84, 114 – 124, https://doi.org/10.2112/SI84-017.1, 2018.

Table 1. ~~Technical specifications~~ Specifications about the variables measured and the devices employed in this study over the intensive summer 2017 campaign [22/06–26/09].

Variable	Height (m, agl)	Sampling rate	Instrument
Air ~~Temperature*~~ temperature	3, 6, 10	1 Hz	Aspirated thermometer
Relative humidity	2	1 Hz	T/RH probe
Wind speed	3, 6, 10	1 Hz	Cup anemometer
Wind direction	10	1 Hz	Wind vane
Turbulent ~~fluxes**~~ parameters	4, 8	~~IRGASON***~~ 10 Hz	IRGASON
Rain	surface	-	Pluviometer
Soil ~~moisture****~~ moisture	-0.04	10 min	Reflectometer
~~Soil heat flux -0.04 Heat-flux plate Hukseflux HFP01SC~~ Radiation components	1, 2	1 Hz	4-component radiometer
CO_2 concentration	4, 8	10 Hz	IRGASON
Water-vapour concentration	4, 8	10 Hz	IRGASON

Table 2. Algorithm for ~~katabatic~~ thermally-driven downslope criteria. First column indicates the filter number; second column the physical description of the filter; and third column, the criteria to be fulfilled in order to pass each of the filters.

Filter	Criteria	Description
1	Weak large-scale winds	$V_{850} < 6$ m s^{-1}
2	Days without synoptic cold fronts	$(\Delta\theta_{e,850}/\Delta t) > -1.5\,^{\circ}$C / 6h
3	Non-rainy events	$pp < 0.5$ mm/day
4	Minimum persistence in the ~~katabatic~~ downslope direction	$WD \in [250^{\circ}\text{–}340^{\circ}]_{2h}$

Table 3. Classification of ~~katabatic types~~ the downslope events according to their maximum 10-min averaged wind speed at 6 m from the onset until ~~24~~ 2400 UTC.

Type	Definition	Number of events
Weak	$U_{max} < 1.5$ m s^{-1}	14
Moderate	1.5 m s^{-1} $\leq U_{max} \leq$ 3.5 m s^{-1}	23
Intense	$U_{max} > 3.5$ m s^{-1}	3

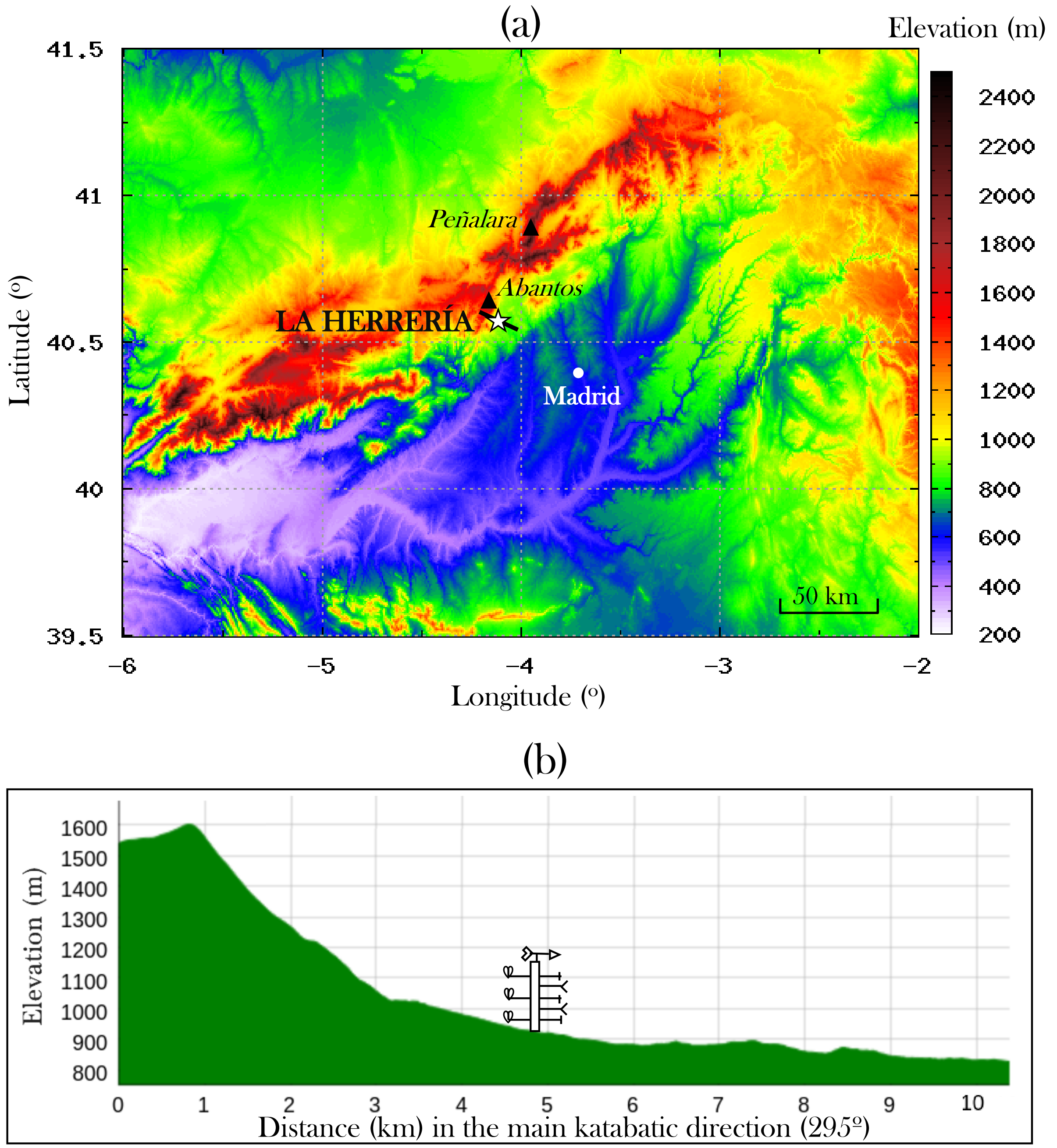

Figure 1. (a) Topography of the area surrounding La Herrería site, which is indicated with a star. ~~Additionally, the~~ The position of the city of Madrid, and Abantos (1763 m) and Peñalara peaks (2420 m) are additionally pointed out. The black line points the cross-section along the main downslope direction from La Herrería, represented below. The source of topography data is ~~ASTER GDEM, which is a product of NASA and METI~~SRTM 90 m DEM (http://srtm.csi.cgiar.org/). (b) Topographical profile ~~in~~ along the ~~main katabatic direction from La Herrería, depicted ∼5 km around in both directions~~cross-section indicated by the black line. ~~It is obtained~~ Obtained from ~~the~~ *Geocontext-Profiler*~~tool~~.

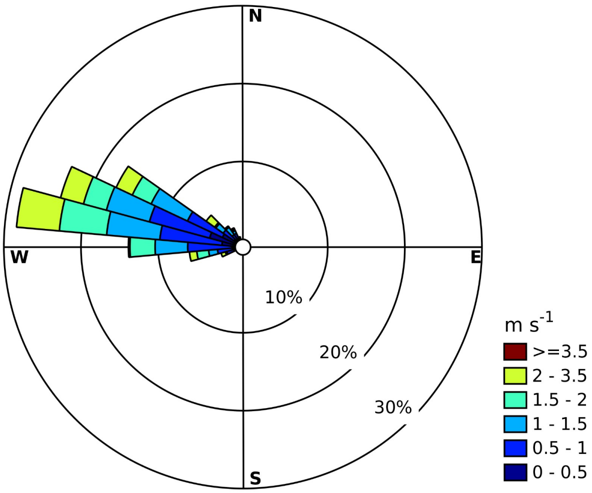

Figure 2. Wind rose at 6 m over the 2 h after the onset of the ~~katabatic~~ downslope flow for the 40 selected events.

(a) Onset

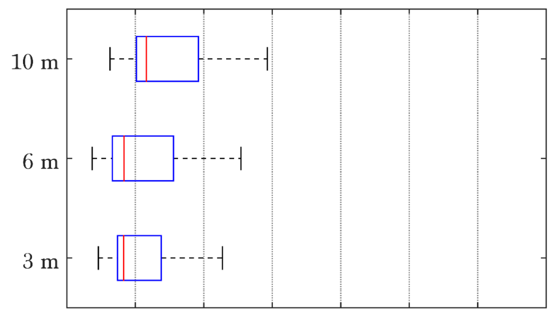

(b) Maximum intensity (considering values at 6 m).

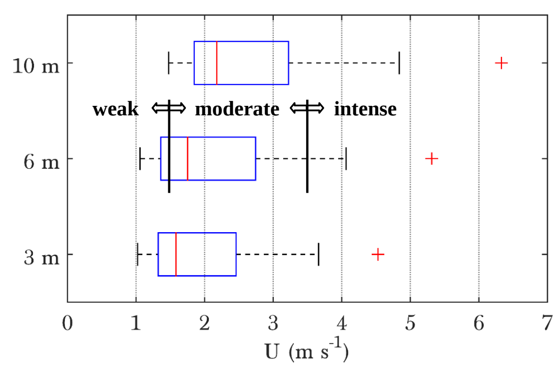

Figure 3. Box plots of the wind speed profile at 3, 6 and 10 m for the ~~katabatic~~ downslope events, (a) at the time of the onset and (b) ~~for~~ at the time of the maximum value at 6 m (from the onset till 2400 UTC) for each ~~level~~event. The red vertical line within blue boxes represents the median, the blue box delimits first and third quartiles, and whiskers delimit the most extreme points not considered outliers (red crosses). Black vertical lines and arrows pinpoint the limits for the wind speed at 6 m that separate weak, moderate and intense ~~of katabatics~~downslope events.

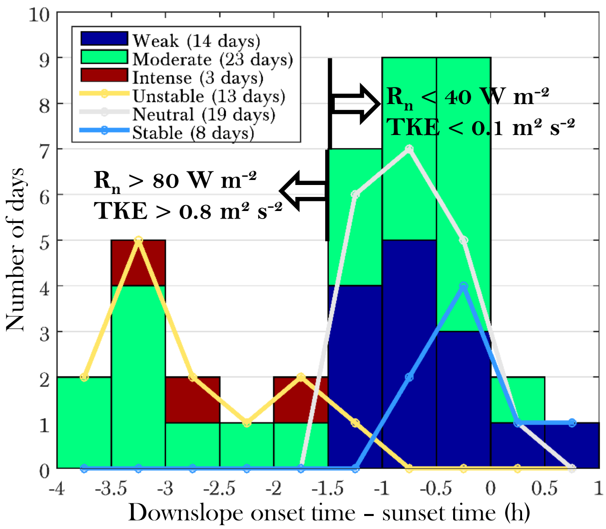

Figure 4. Histograms of the difference between the ~~katabatic~~ downslope onset time and sunset time, for the three groups of intensities (bars) and for different ~~thermal stratification~~ static stabilities at the moment of the onset (lines). Values of the net radiation (R_n) and turbulent kinetic energy (TKE) are also indicated on both sides from the -1.5 h time difference.

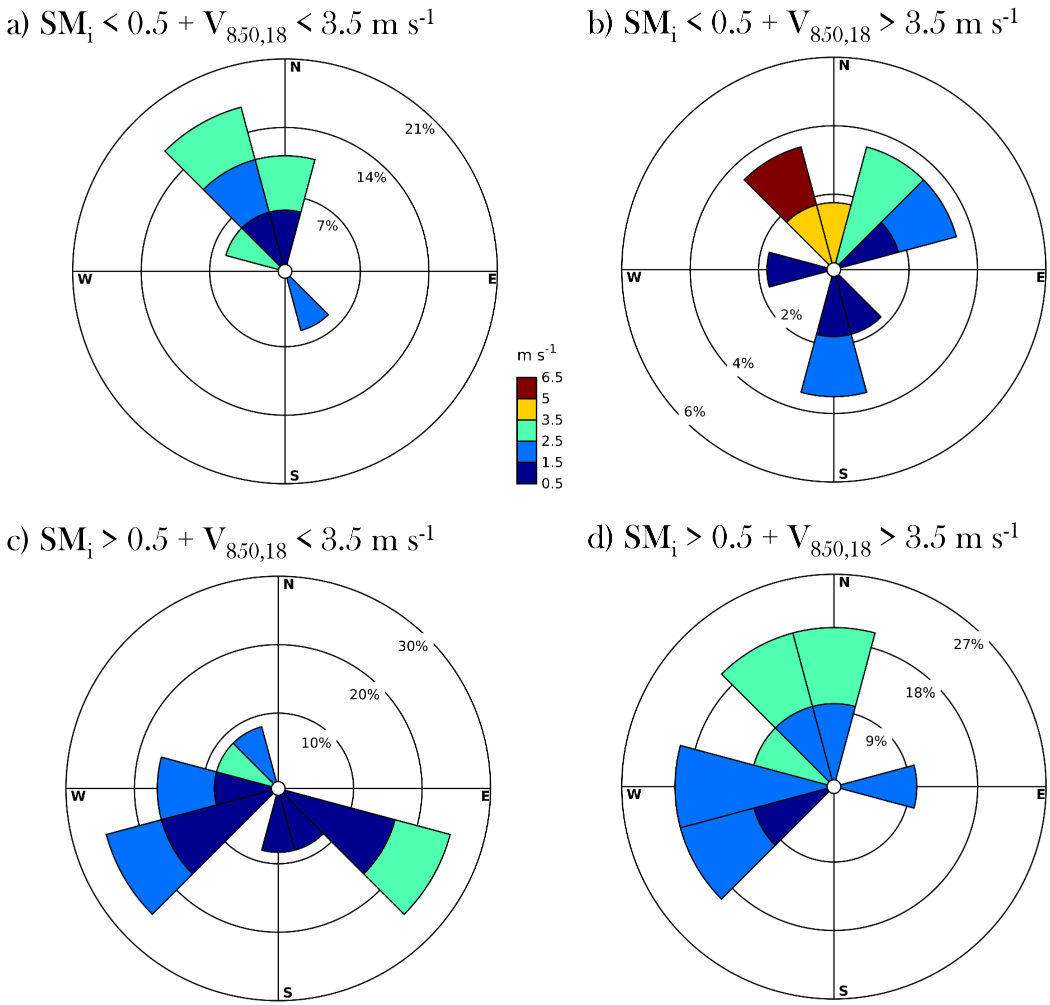

Figure 5. Wind roses representing the maximum ~~katabatic~~ downslope wind speed at 6 m in colours, for different directions from the NCEP-reanalysis wind at 850 hPa, at the closest grid point ~~to~~ from La Herrería (40.5° N, 4° W) at 18 UTC. Wind roses are shown for different values of the soil-moisture index (SM_i) and the reanalysis wind speed ($V_{850,18}$) (a-d). Note that the frequency scale of the wind roses is variable.

~~Maximum wind speed (U_{max}) at 6 m for each katabatic event versus TKE at 8 m at the moment of the katabatic onset. Note that the moderate katabatics are divided into two subgroups.~~

~~(a) Average soil-heat flux (*G*) and (b) average longwave-radiative loss (*LWU-LWD*) during the katabatic stage (from the onset until 2400 UTC) *vs* the soil-moisture index (SM_i). The grey line represents the 4-th order polynomial fitting of the data.~~

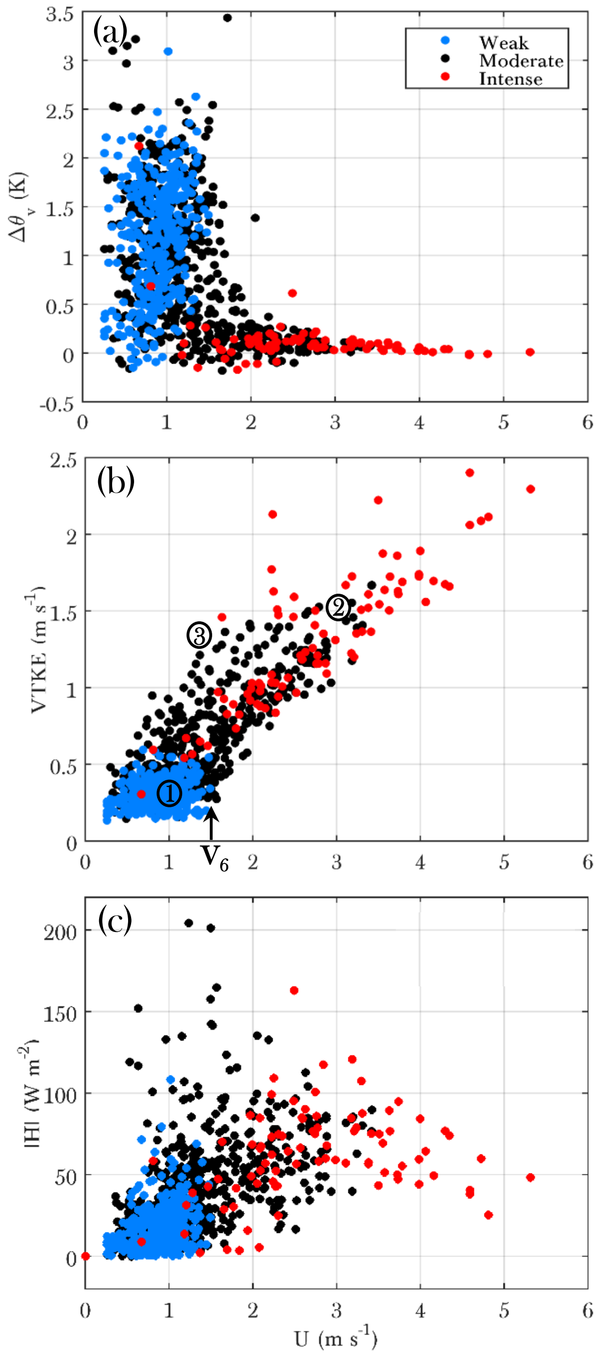

Figure 6. (a) ~~Temperature~~ Thermal stratification ~~($\Delta\theta_v$) and~~ $\left(\Delta\theta_v = \theta_v(10m) - \theta_v(3m)\right)$, (b) turbulence velocity scale (~~V_{TKE}~~ V_{TKE}), and (c) the absolute value of the sensible-heat flux (H) at 8 m ~~versus~~ *vs* wind speed (U) at 6 m. The numbers in (b) pinpoint the SBL regimes defined in Sun et al. (2012): (1) weak turbulence driven by local instabilities, (2) intense turbulence driven by the bulk shear, and (3) moderate turbulence driven by top-down events. The threshold wind-speed (V_6) at which the HOST transition occurs is indicated too.

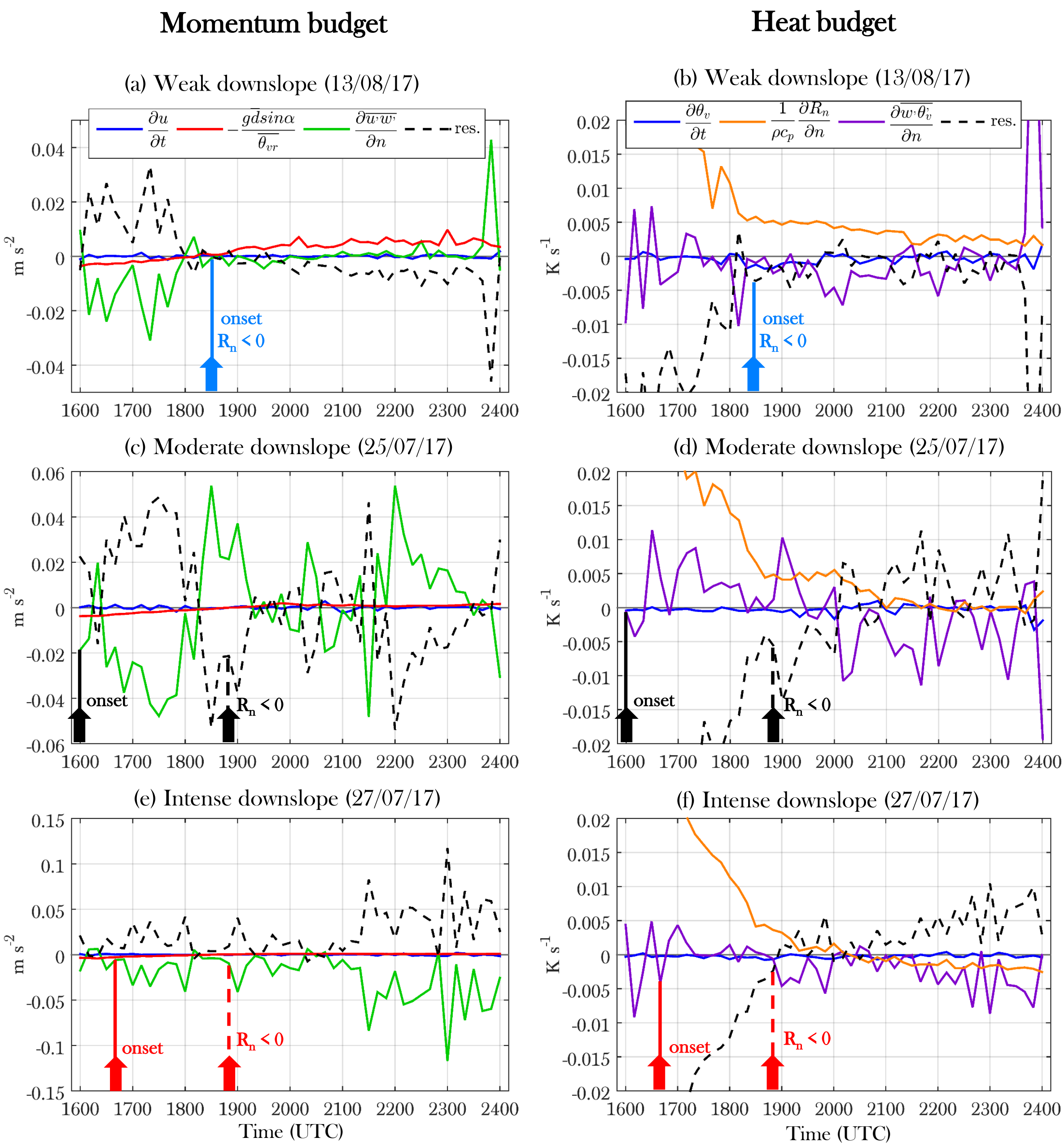

Figure 7. ~~Absolute value~~ Time evolution of the ~~sensible-heat flux~~ different terms from the momentum (~~*H*~~a,c,e) ~~*vs* wind speed~~ and heat budget (~~*U*~~b,d,f) ~~at 6 m.~~

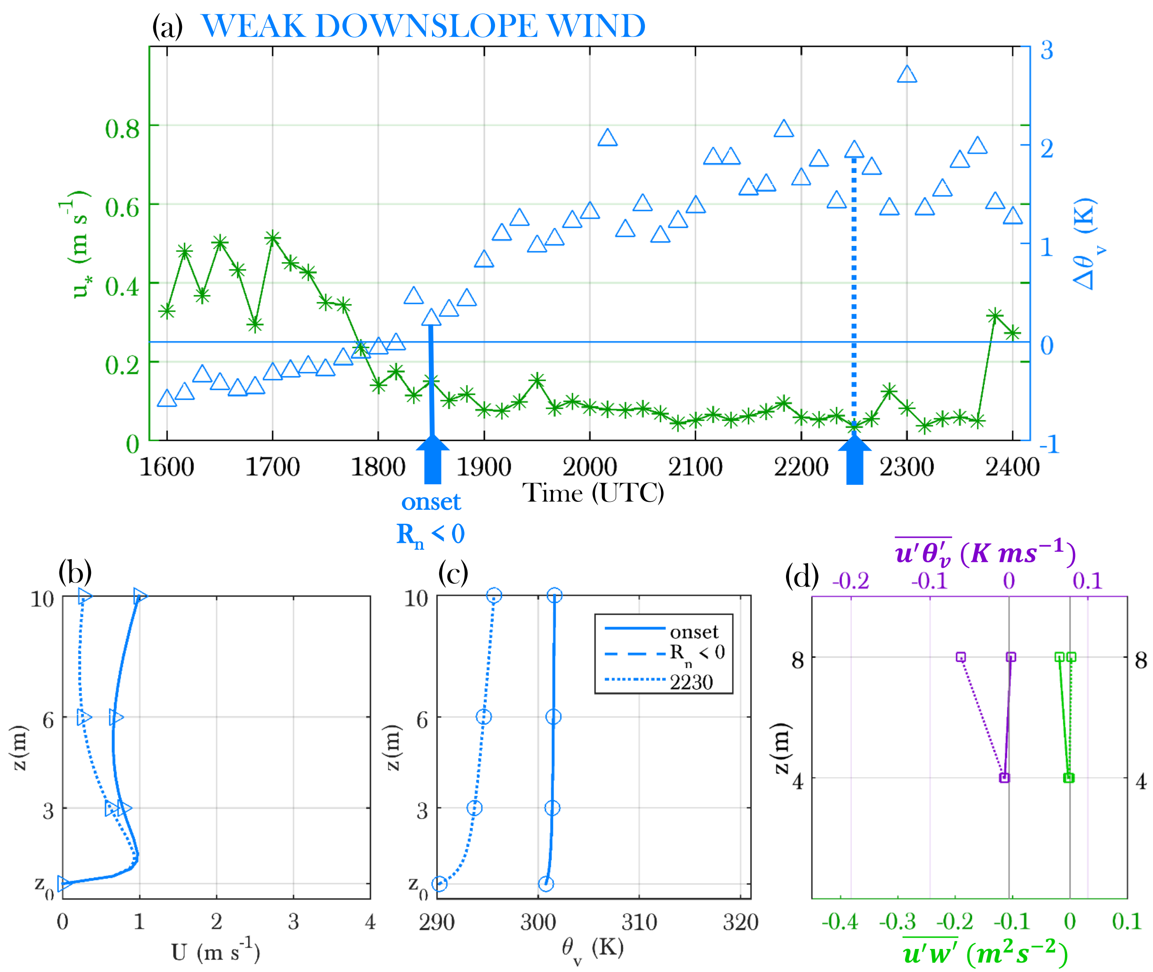

Figure 8. (a) Time evolution of the friction velocity (u_*) ~~at 4~~ and ~~8 m for a weak-katabatic~~ thermal stratification (~~13/08/2017~~$\Delta\theta_v = \theta_v(10m) - \theta_v(3m)$) ~~and an intense-katabatic~~ for the weak downslope event (~~27~~13/~~07~~08/2017). The ~~coloured arrows and~~ horizontal line represents $\Delta\theta_v = 0$. The solid arrow with the tied ~~dashed~~ vertical lines ~~indicate~~ point three times of interest: the solid line indicates the ~~respective~~ onset ~~times~~time, the ~~red pointed~~ dashed line the time at which ~~R_{net}~~ R_n turns negative~~for the intense event~~, and the ~~dashed black vertical~~ dotted line is ~~represented~~ depicted at ~~2100~~ 2230 UTC when the SBL is already well developed~~for both events~~. ~~(b-g)~~ Vertical profiles of (b) the wind speed (U)~~and~~, (c) virtual potential temperature (θ_v) ~~at the onset time (b,c), when R_{net} turns negative~~ and (d~~,e~~) ~~,~~ $\overline{u'w'}$ and $\overline{u'\theta_v'}$ turbulent fluxes at ~~2100 UTC (f,g). Note that~~ the ~~horizontal scales~~ three times of interest are ~~variable~~shown below.

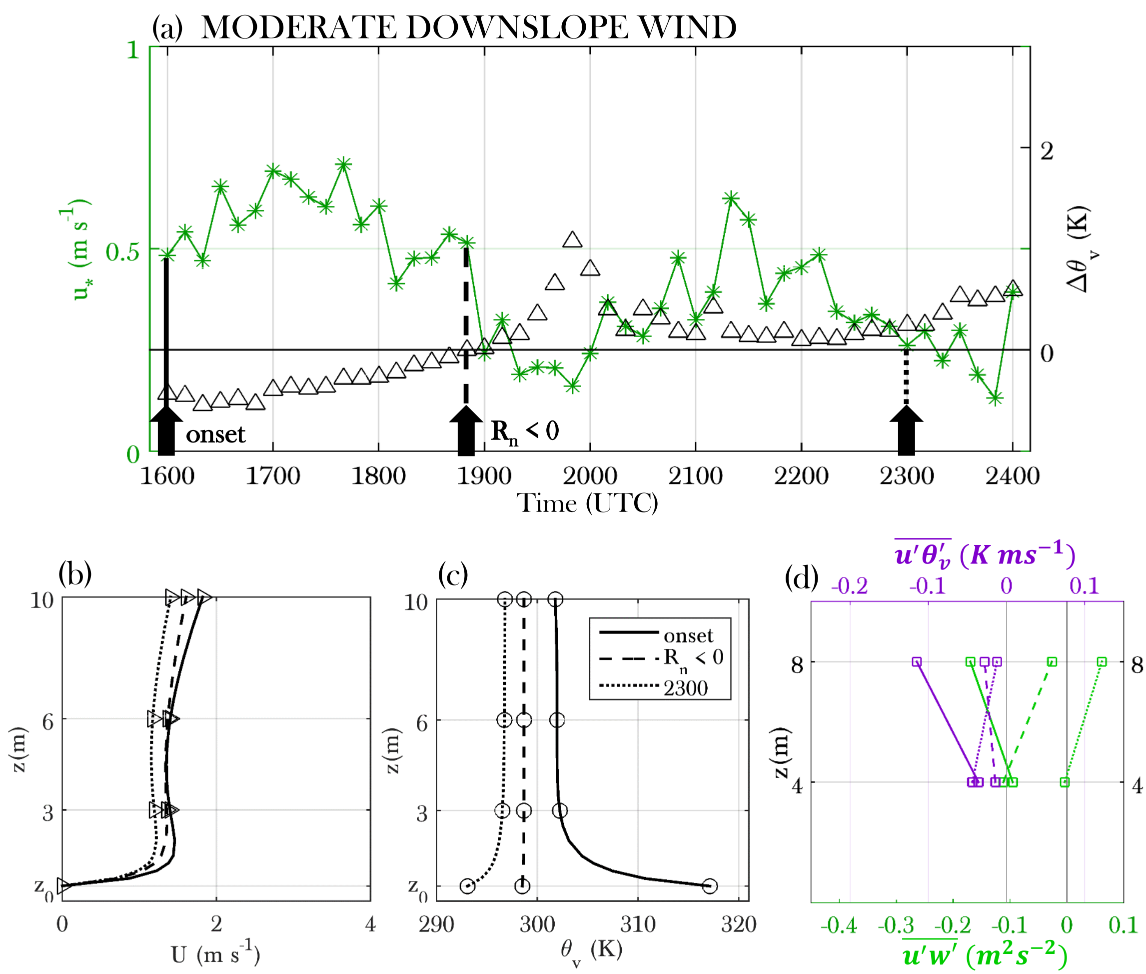

Figure 9. ~~Time evolution of~~ (a) *Idem* from Fig. 8 for the ~~wind shear at 4 and 8 m, thermal stratification~~ moderate downslope event (~~$\Delta\theta_v$~~ 25/07/2017)~~and~~ , except the ~~surface-energy balance for~~ change of the ~~weak~~ last time of interest from 2230 to 2300 UTC.

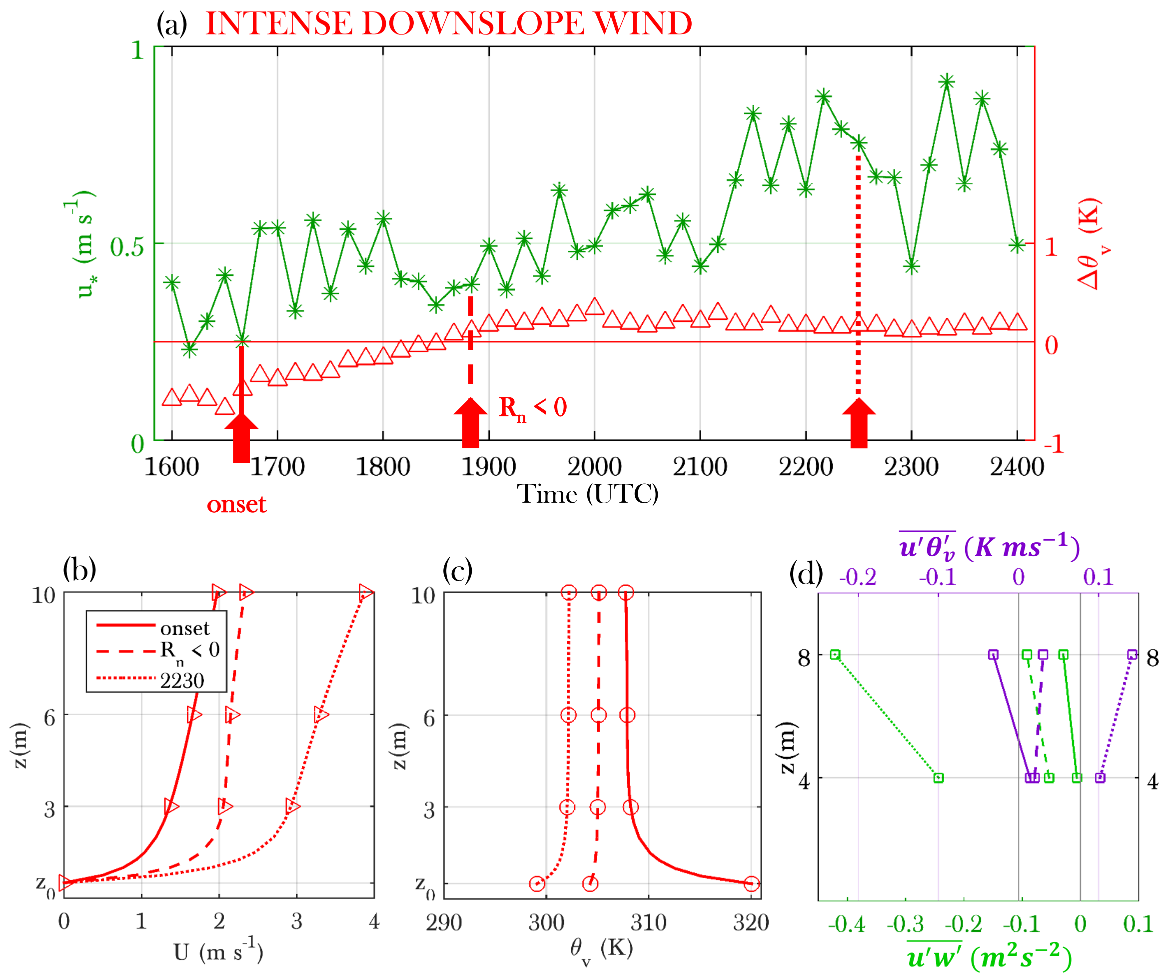

Figure 10. (a) ~~and~~ *Idem* from Fig. 8 for the intense downslope event (~~b~~27/07/2017)~~events. The vertical dashed line indicates the onset time of the katabatic flow~~.

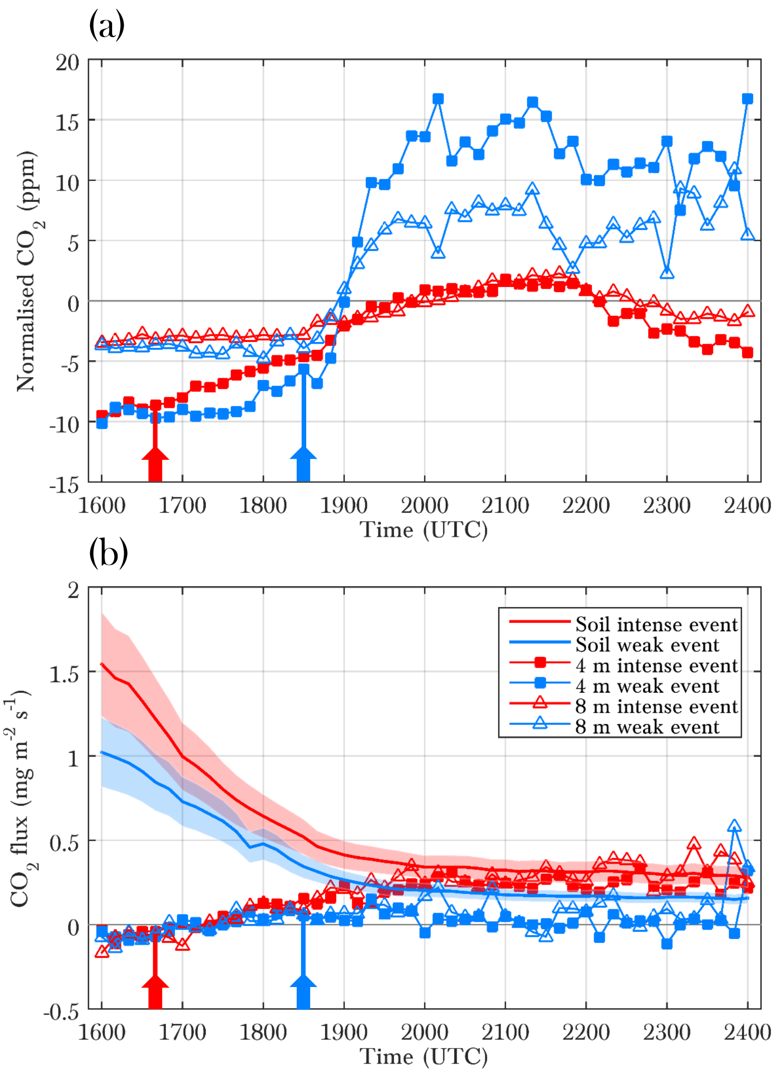

Figure 11. Time evolution of the normalised CO_2 mixing ratio (a) and vertical turbulent fluxes (b) at 4 and 8 m agl for the weak (blue) and intense (red) events. In (b) we include in solid lines the soil-respiration estimation and the 20% uncertainty of R_{10} (see Eq.3) in shaded. The onset of the ~~katabatic~~ downslope flow is indicated from faced arrows of respective colours.

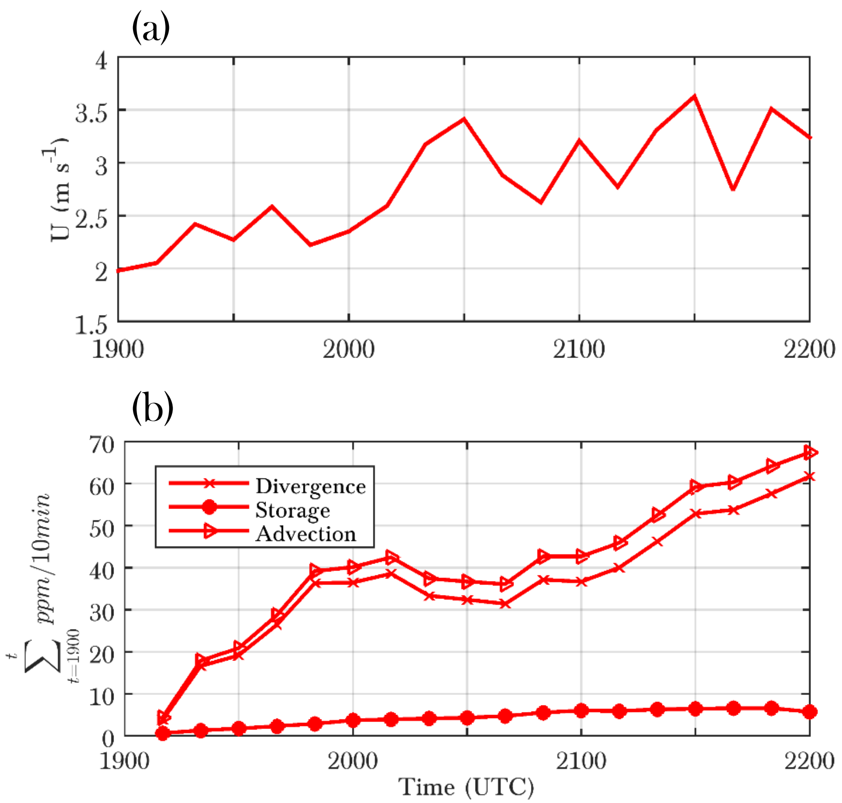

Figure 12. Time evolution between 1900 and 2200 UTC for the intense ~~katabatic~~ downslope event, of (a) the wind speed (U) at 6 m, and (b) the different terms of the CO_2 budget from Eq. 5. Note that the cumulative sum from 1900 UTC is represented in (b), and that the advection term, which is negative, is shown in absolute values.

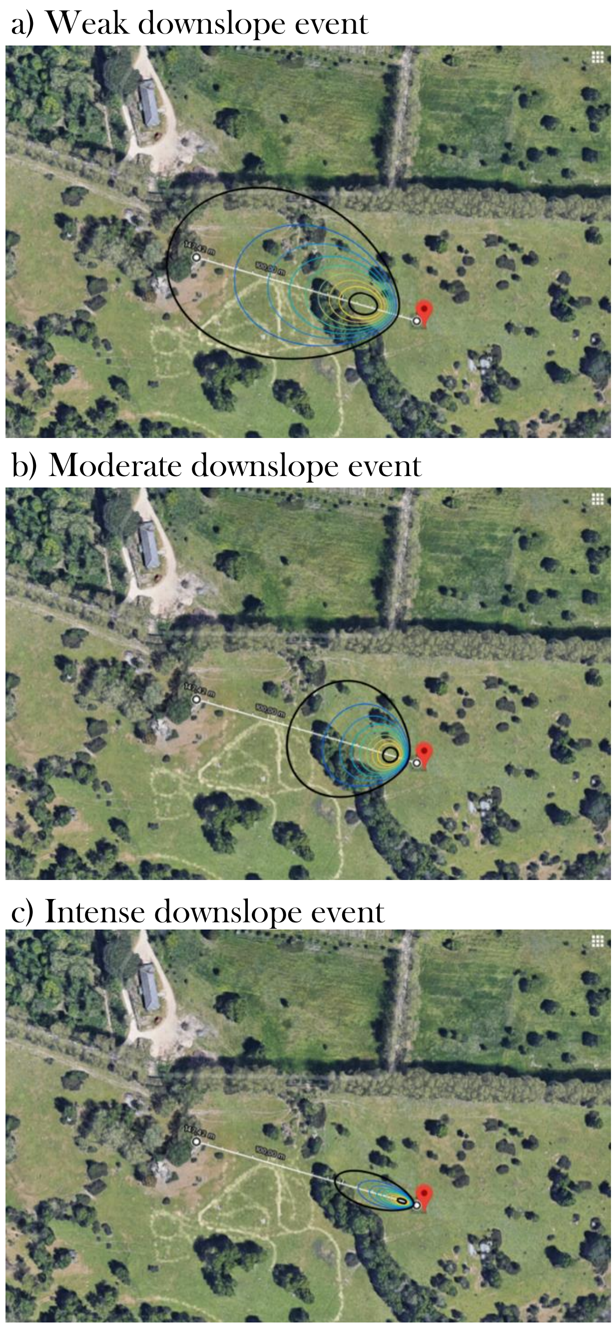

Figure A1. Estimation of the footprint area for the turbulent fluxes at 8 m in the mean local downslope direction (295º) in La Herrería for (a) a weak (13/08/2017), (b) a moderate (25/07/2017) and (c) an intense (27/07/2017) downslope event. Black contour lines delimit 90% and 10% of the total flux footprint. Map data ©2019 Google, Inst. Geogr. Nacional (Spain), *accessed 19 February 2019*.

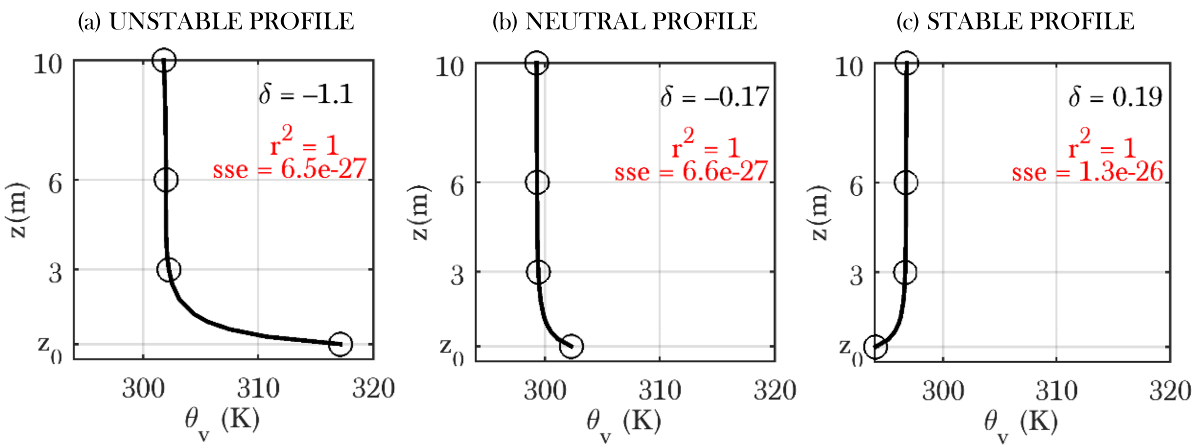

Figure B1. Vertical profiles of the virtual potential temperature (θ_v) for different static stabilities. Values are taken from a moderate downslope event (25 July) at (a) 1600 UTC, (b) 1830 UTC and (c) 2130 UTC. The value of δ is shown in black, and the square of the multiple correlation coefficient (r^2) and the sum of the squares due to error (*sse*) are shown in red, as a measure of the goodness of fit.